U.S. DEPARTMENT OF ENERGY

PNNL-13528

Prepared for the U.S. Department of Energy
under Contract DE-AC05-76RL01830

Trawsfynydd Plutonium Estimate

Bruce D. Reid
Patrick G. Heasler
David C. Gerlach
Jim Livingston

11/20/2009

Pacific Northwest
NATIONAL LABORATORY

Proudly Operated by **Battelle** *Since 1965*

DISCLAIMER

PACIFIC NORTHWEST NATIONAL LABORATORY
operated by
BATTELLE
for the
UNITED STATES DEPARTMENT OF ENERGY
under Contract DE-AC05-76RL01830

Printed in the United States of America

Available to DOE and DOE contractors from the
Office of Scientific and Technical Information,
P.O. Box 62, Oak Ridge, TN 37831-0062;
ph: (865) 576-8401
fax: (865) 576-5728
email: reports@adonis.osti.gov

Available to the public from the National Technical Information Service,
U.S. Department of Commerce, 5285 Port Royal Rd., Springfield, VA 22161
ph: (800) 553-6847
fax: (703) 605-6900
email: orders@ntis.fedworld.gov
online ordering: http://www.ntis.gov/ordering.htm

This document was printed on recycled paper.
(9/2003)

Trawsfynydd Plutonium Estimate

BD Reid
Dave Gerlach
Pat Heasler
Jim Livingston

September 1997

Prepared for the
U.S. Department of Energy

Pacific Northwest National Laboratory
Richland, Washington 99352

Authorized Derivative Classifier

E. F. Love, Jr.
Senior Development Engineer
Pacific Northwest National Laboratory
Date 9/25/97

UNCLASSIFIED

1.0 Introduction and Summar

Objective

This report serves to document an estimate of the cumulative plutonium production of the Trawsfynydd Unit II reactor (Traws II) over its operating life that was made using the Graphite Isotope Ratio Method (GIRM). The estimate of the plutonium production in Traws II provided in this report has been generated under blind conditions. In other words, the estimate of the Traws II plutonium production has been generated without the knowledge of the plutonium production declared by the reactor operator (Nuclear Electric). The objective of this report is to demonstrate that the GIRM can be employed to serve as an accurate tool to verify weapons materials production declarations.

Background and Report Summary

The ability to estimate the cumulative quantity of plutonium produced by a reactor is important for establishing a basis for weapons materials accountability. The GIRM has been developed for this purpose at the Pacific Northwest National Laboratory (PNNL), under the sponsorship of the U.S. Department of Energy. A detailed discussion of the GIRM concept is provided in Reference 1, however a brief summary is provided in the following paragraph.

The graphite used as a moderator in natural uranium fueled reactors must be extensively purified prior to use. In practice, however, many elements typically remain as trace impurities at the part-per-million level. Hanford production reactor graphite, for example, has measurable (although widely variable) concentrations of Al, B, Ba, Ca, Cr, Fe, Li, Ni, S, Si, Sr, Ti, V, and Zn. Some of these impurities have sufficiently large and well known neutron cross sections to undergo significant and predictable isotopic transmutation in a reactor. Since the initial concentrations of impurities are highly variable, even within a small region of the graphite, the absolute quantity of a particular impurity element found in irradiated graphite is not a good indicator of the extent of neutron irradiation. The ratios of isotopes within a given element, however, do not depend on these initial concentrations, and can thus be used as indicators of cumulative neutron irradiation. A measurement of isotope ratios, in combination with knowledge of a reactor's design and operational history, can allow accurate estimation of plutonium production. Since the GIRM relies on measurement of the graphite moderator, which remains in the reactor over its entire life, it provides a inherent advantage over other methods used to determine cumulative production that are based on examination of discharged fuel.

The basic proof of principal experiment for GIRM was conducted at PNNL during 1994, using archived graphite samples that had been previously irradiated in the Hanford C-Reactor and the French G-2 Reactor. The results of these experiments were encouraging. These experiments used a series of chemical separations, radiochemistry, and mass spectrometry techniques to isolate elements of interest from bulk samples and to measure several isotopic ratios. These measurements were interpreted using reactor physics calculations based on the design of these

reactors, yielding estimates of neutron fluence. These estimates were then compared with the known irradiation histories of the sample graphite.

Following the encouraging results from the initial proof of principal experiment, a detailed assessment was performed on the potential accuracy of the GIRM in estimating cumulative plutonium production from measurements of isotope ratios. This detailed assessment of the GIRM accuracy is documented in Reference 1. The accuracy assessment accounts for uncertainties that may be present in knowledge about the reactor parameters and measurement uncertainties. The accuracy assessment documented in Reference 1 concluded that with sufficient number of samples (~30) the achievable accuracy of GIRM to estimate cumulative plutonium production was within approximately 7%. The accuracy assessment withstood the scrutiny of an in depth independent technical peer review in 1995. The technical peer review panel recommended that a full reactor scale experiment be performed to validate the capabilities of GIRM to estimate plutonium production.

A review of the potential reactor sites upon which to perform the full scale experiment identified the Traws II reactor in Wales as an ideal candidate. The Traws II is a commercial, gas cooled, graphite moderated power reactor that, at the time of the proposed experiment, was undergoing preliminary decommissioning activities. As a consequence, the reactor still retained much of its operating staff and the experiment would not conflict with power production objectives. Further, the detailed operating records and fuel management data for Traws II were available. Since Nuclear Electric, the plant operator, routinely engaged in graphite sampling activities at their commercial reactors the proposed graphite sampling activity was a well understood technology. As a result of the above factors the full scale experiment could be performed more cost effectively in the U.K. at Traws II than any U.S. option. The U.K. Department of Trade and Industry and Nuclear Electric also demonstrated a willingness to collaborate on the project. A A graphite sampling plan was devised at PNNL and carried out by Nuclear Electric at the Traws II reactor in 1995. The graphite sampling activities were performed in a very competent fashion by Nuclear Electric and a full compliment of 90 samples were obtained. The samples, which are approximately 1 gram in size, were obtained from 11 different fuel channels from three different planes in the reactor. The details of the Nuclear Electric sampling activities and the data acquired during the sampling are documented in Reference 2. In addition to the sample data, Reference 2 also provides the reactor specific information for detailed reactor physics calculations. The reactor specific information includes the Traws II fuel management history, reactor geometry and materials, fuel geometry and materials, and operating conditions such as temperature. Nuclear Electric provided Issue 1 of the graphite sampling report to PNNL and Issue 2 of the graphite sampling report to the U.S. DOE. Issue 2 of the graphite sampling report differs from Issue 1 in that it also provides the tabulated cumulative plutonium produced at Traws II based on Nuclear Electric records. The Nuclear Electric records of plutonium production at Traws II have been withheld from the PNNL analysts to ensure there is no technical prejudice in reporting results.

Once received at PNNL, the graphite samples were machined in a glove box to clean potential sources of contamination and generate sample materials for analysis. In many instances multiple

subsamples were generated for each individual graphite sample. The sample materials received from the machining activities were subjected to microwave dissolution, chemical separations, and mass spectrometric analysis. Chapter 2 describes sample preparation and laboratory analysis. As recommended in Reference 1, the mass spectrometric analysis focused on measurement of titanium isotopic ratios due to this element's sensitivity in supporting GIRM objectives. With the exception of one sample, which was severely fractured, one or more titanium isotopic measurements were obtained for each graphite sample. A detailed discussion of the machining and sample measurement activities are provided in the following sections of this report. As means to further ensure a blind experiment, the analyst performing the mass spectrometry was not provided with the location in the reactor from which the sample was obtained until the results from the measurements were formally reported.

Using the reactor and fuel parameters provided in Reference 2, a reactor physics model was developed that could be used to estimate titanium isotope ratios as a function of exposure. Using this reactor physics model, the estimated titanium isotope ratios were calculated for each location in the core from which a sample was obtained. A comparison between the estimated titanium isotopic ratios, based on the reactor physics calculations, and the measured titanium isotope ratios, using mass spectrometry, was made and is documented in this report. In most cases, the comparison between measured and predicted titanium ratios is good.

As described in Chapter 3, a reactor physics model was further employed to estimate the cumulative plutonium production in the fuel assemblies located next to each sample location. Therefore, for each sample location and using the measured titanium isotope ratios, an estimate was calculated of the cumulative plutonium produced in the fuel assemblies that were adjacent to the sample. A statistical aggregation scheme was then employed to translate estimates of local plutonium production to an estimate of cumulative plutonium production for the reactor as a whole. A detailed description is provided in this report of the reactor physics model and the statistical aggregation scheme used to make the estimate of the cumulative plutonium production at Traws II.

Results and Conclusions

The estimated cumulative plutonium production in the Traws II reactor over its operating life is 3.63 MT a 2 sigma bound of 10.4%. This production estimate is based on the application of the Graphite Isotope Ratio Methodology described in this report. A later comparison will be made to the plutonium production declared by Nuclear Electric, the reactor operator.

The results of this work indicate that the GIRM is a viable means of estimating plutonium production in a graphite moderated reactor providing sufficient graphite samples (~30) can be obtained from the active core region. An analytical means of measuring the altered isotopic ratios of titanium in the graphite moderator was developed and documented in this report. An important conclusion reached in this analytical work is that there is apparently a substantial degree of heterogeneity in the concentrations of titanium impurities in the reactor grade graphite on both a macroscopic and microscopic scale. Due to this heterogeneity, there exists the

potential for only very small quantities of titanium to be present in any given sample. Therefore, every effort must be made to control the blank levels in the analytical process.

2.0 Sample Processing and Analytical Methods

2.1 Sample Machining

The samples as received from Trawsfynydd reactor Unit 2 were packaged in small plastic vials as the innermost container. These were moved, a few at a time, into a specially prepared glove box under DOE radiological control guidelines. The glove box contained a lathe which was used to first machine the outer surfaces of each sample to both remove surface contamination and then to fabricate the sample into a more ideal cylindrical shape for further processing. This was required because the samples obtained by the reactor trepanning sampling operation were somewhat curved and could not be directly clamped into a chuck or holder for shaping and machining. Thus, each sample had a slightly different diameter after preparation, as noted in Table 2-1. The end of each sample furthest from the fuel channel was recognizable, having been broken off upon removal from the fuel channel. The sample end nearest the fuel channel was relatively smooth and was used as a reference point in the glove box machining and shaping operation at PNNL. This end was machined to obtain a flat surface and the amount of material removed is referred to as the 'face-off' in Table 2-1.

Each sample was prepared for subsampling analyses to assess small intra-sample differences or trends in isotope ratios relative to distance from the fuel channel. The first two sets of subsamples, obtained from samples 42 and 77, spatially adjacent duplicates taken from fuel channel 09J10-4, were prepared as solid wafers. For the remainder of the samples, each subsample was prepared by progressively shaving the face of the sample cylinder to a precisely measured length along the sample cylinder and producing a powder and the powder was collected in a plastic vial. Due to some waste in cutting the wafers, the thicknesses of the wafers prepared from samples 42 and 77 are less than the length of cylinder section typically used to prepare powders. As a result, samples 42 and 77 contained less material than subsequent powdered samples, however in some cases, small amounts of sample powder were lost during machining early on, though this effect was improved and minimized. The graphite samples displayed some variations in hardness, granularity, and characteristics of powder produced, and each sample required careful observation and attention during the machining and powdering process. For some samples, the trepanned sample was shorter than average, and yielded only 1 or 2 subsamples. Sample 62 fractured in the chuck during machining and yielded only one small subsample. Sample 85 broke into two small pieces either during the trepanning in the fuel channel or during retrieval, and both of these pieces were too small to process in the glove box lathe (Table 2-1).

Table 2-1. Machining Data for the 90 TRAWS Graphite Samples

First Half-Plane Channel's 08J07, 01J08, 02J07, 09J10, 06J06, 04J07								
Sample #	Channel ID	Dia.	Face-off	-1	-2	-3	-4	Comments
86	06J06-4	.350	.150	.125	.125	.120		
26	06J06-8	.450	.092	.120	.120			
2	06J06-4	.400	.054	.120	.120	.120		
12	06J06-3	.407	.066	.120	.120	.120	.120	
75	06J06-2	.440	.060	.120	.120			
19	06J06-1	.420	.130	.120	.120	.130		
14	06J06-7	.462	.090	.120	.120	.120	.120	
34	06J06-5	.420	.065	.120	.120	.120	.120	
60	06J06-6	.360	.062	.120	.120	.120		
24	01J08-3	.445	.090	.120	.120	.120	.120	
48	01J08-5	.465	.105	.120	.120	.120		
30	01J08-7	.470	.090	.120	.120	.120	.120	
27	01J08-6	.480	.100	.120	.120	.120		
11	01J08-1	.450	.080	.120	.120	.120	.120	
3	01J08-8	.450	.090	.120	.120	.120		
68	01J08-4	.430	.085	.120	.120	.120		
70	01J08-2	.420	.070	.120	.120	.120		
71	01J08-4	.450	.130	.120	.120			
50	02J07-2	.435	.155	.120	.120			
18	02J07-7	.465	.100	.120	.120	.120		
84	02J07-1	.445	.080	.120	.120	.120		
32	02J07-6	.445	.100	.120	.120	.120	.080	
15	02J07-3	.375	.060	.120	.120	.120	.120	
13	02J07-4	.420	.080	.120	.120	.120	.120	
51	02J07-8	.455	.090	.120	.120	.120	.120	
21	02J07-5	.445	.090	.120	.120	.120	.090	Face-off -0
1	01J08-1	.445	.100	.120	.120	.070		Face-off -0
25	04J07-4	.440	.070	.120	.120	.120	.120	Face-off -0
46	04J07-7	.475	.075	.120	.120	.120	.120	Face-off -0
83	04J07-3	.455	.075	.120	.120	.120	.080	Face-off -0

First Half-Plane Channel's 08J07, 01J08, 02J07, 09J10, 06J06, 04J07								
Sample #	**Channel ID**	**Dia.**	**Face-off**	**-1**	**-2**	**-3**	**-4**	**Comments**
6	04J07-2	.465	.140	.120	.120	.120		Face-off -0
9	04J07-8	.470	.095	.120	.120	.120	.120	Face-off -0
79	04J07-4	.450	.105	.120	.120	.120	.120	Face-off -0
17	04J07-1	.450	.085	.120	.120	.120	.120	Face-off -0
55	04J07-5	.455	.100	.120	.120			Face-off -0
23	09J10-7	.435	.055	.120	.120	.120	.120	
10	09J10-6	.460	.120	.120	.120	.120		
4	09J10-2	.440	.080	.120	.120	.120	.120	
7	09J10-3	.450	.070	.120	.120	.120	.120	
37	09J10-5	.385	.025	.120	.120	.120	.120	
72	09J10-8	.415	.070	.120	.110			
76	09J10-1	.435	.200	.120	.120	.120	.120	
42	09J10-4	.400	.058					Machine Disk .080 Thick X .400 Dia
77	09J10-4	.400	.048					Machine Disk .080 Thick X .400 Dia.
52	08J07-5	.465	.100	.120	.120	.120		Face-off -0
80	08J07-6	.465	.100	.120	.120			Face-off -0
59	08J07-8	.465	.090	.120	.120	.120		Face-off -0
74	08J07-7	.475	0.75	.120	.120	.120		Face-off -0

Second Half-Plane Channel's 10G06, 11E07, 12C06								
Sample #	**Channel ID**	**Dia.**	**Face-off**	**-1**	**-2**	**-3**	**-4**	**Comments**
67	11E07-7	.470	.090	.120	.120	.120	.120	Face-off -0
56	10G06-8	.445	.100	.120	.120	.075		Face-off -0
35	11E07-3	.475	.110	.120	.120	.120		Face-off -0
38	11E07-5	.470	.115	.120	.120			Face-off -0
62	11E07-1	.460	.085					Face-off -0 Sample Fractured In Chuck-Partial Sample on -1
5	11E07-4	.460	.115	.120	.120	.120		Face-off -0
8	11E07-2	.475	.100	.120	.120	.050		Face-off -0
54	11E07-6	.460	.105	.120	.120	.120		Face-off -0
33	12C06-3	.440	.095	.120	.120	.120		Face-off -0
89	12C06-4	.475	.115	.120	.100			Face-off -0
78	12C06-5	.465	.085	.120	.120	.120	.105	Face-off -0
58	12C06-4	.465	.090	.120	.120	.120		Face-off -0
28	12C06-6	.475	.080	.120	.120	.120	.120	Face-off -0
29	12C06-7	.465	.100	.120	.120	.120	.080	Face-off -0
65	12C06-2	.450	.085	.120	.120	.120		Face-off -0
31	12C06-8	.480	.070	.120	.120	.070		Face-off -0
22	12C06-1	.450	.085	.120	.120	.120	.100	Face-off -0
49	10G06-8	???	???	.120	.120	.120		Face-off -0
88	10G06-5	.460	.100	.120	.120	.100		Face-off -0
20	10G06-1	.450	.150	.120	.120	.080		Face-off -0
47	10G06-4	.420	.100	.120	.095			Face-off -0
81	10G06-7	.450	.090	.120	.120	.120		Face-off -0
85	10G06-2							Face-off -0 Sample in two pieces - to small to hold in Chuck
16	10G06-6	.475	.100	.120	.120	.120		Face-off -0
43	10G06-3	.470	.065	.120				Face-off -0

Third Half-Plane Channel's 11N11, 12Q06								
Sample #	Channel ID	Dia.	Face-off	-1	-2	-3	-4	Comments
40	11N11-1	.450	.080	.120	.120	.120	.120	Face-off -0
44	11N11-4	.470	.090	.120	.120	.120		Face-off -0
90	11N11-5	.475	.100	.120	.120	.120		Face-off -0
69	11N11-7	.475	.080	.120	.120	.120		Face-off -0
66	11N11-2	.460	.085	.120	.120	.120	.120	Face-off -0
41	11N11-3	.460	.090	.120	.120	.120	.120	Face-off -0
61	11N11-8	.470	.065	.120	.120	.120	.095	Face-off -0
82	11N11-6	.470	.085	.120	.120	.120	.078	Face-off -0
45	12Q06-1	.450	.110	.120	.120	.120		Face-off -0
53	12Q06-4	.445	.070	.120	.120	.120	.100	Face-off -0
87	12Q06-4	.430	.070	.120	.120	.120	.120	Face-off -0
63	12Q06-7	.450	.090	.120	.120	.120		Face-off -0
73	12Q06-5	.440	.080	.120	.120	.120	.100	Face-off -0
39	12Q06-2	.435	.105	.120	.120	.050?		Face-off -0
36	12Q06-3	.460	.105	.120	.120	.110		Face-off -0
64	12Q06-6	.445	.075	.120	.120	.120		Face-off -0
57	12Q06-8	.470	.075	.120	.120	.120		Face-off -0

2.2 Sample Digestion Experiments

A relatively new microwave sample digestion system was purchased due to the stated capability of achieving higher pressures and digesting semi-conducting and conductive or metallic samples. The microwave was furnished with accessories to monitor internal pressures and temperatures in a specially configured digestion vessel. These features helped in developing digestion procedures for this study. The microwave digestion system can be programmed for any length of operation while monitoring pressure and temperature, and the microwave power is shut off temporarily when temperature and pressure limits are achieved and resumed when the levels drop slightly. Thus, a specific peak internal pressure and temperature can be maintained for a length of time which is conducive to digesting specific sample matrices, and venting of digestion vessels and release or radioactive material onto the inner walls of the microwave oven can be avoided. The microwave can be programmed for unattended operation and cooling steps, however it was found that occasionally, the cables connecting the pressure sensor and thermocouple to the monitor vessel would become slightly kinked or experience some resistance or drag during the partial rotation and reversals of the sample vessel carousel. A safety interlock

feature would then shut off the power and cease operation, in order to prevent the possibility of disconnecting the cables and venting the acid mixture in the monitor vessel. This occurred with enough frequency to affect sample turnaround times and productivity, and we therefore purchased and installed an external infrared temperature sensor which instead monitored external vessel temperatures and regulated power and microwave application so as not to exceed desired internal vessel temperatures and pressures for a particular acid mixture.

While waiting for approval of procedures and radiological safety-mandated permits, we conducted experiments on 'cold' or unirradiated graphite samples. Our initial desire was to be able to digest and dissolve a solid wafer of graphite, rather than a powdered sample, to minimize possible contamination from natural Ti during the machining process. Early experiments utilized nitric acid (HNO_3), hydrogen peroxide (H_2O_2), and especially hydrofluoric acid (HF), since forming a fluoride complex is the only way to assure Ti remaining in solution. Combinations of these reagents only succeeded in leaching part of the Ti and other elemental impurities out of the graphite wafer, as detected by analysis of the supernatant leachate solution by inductively coupled plasma mass spectrometry (ICPMS) analysis. We also performed experiments on powdered, unirradiated graphite samples and found an improved yield of leached impurity elements including Ti.

Complete digestion and solution of each graphite sample was seen as the best way in improve yield and to be certain that we were attacking Ti impurities in more than one type of site, i.e., intra crystalline atomic scale substitutional vs. intergranular Ti-bearing mineral phase impurities, even though each should be equally affected by neutron fluence exposure and yield the same altered Ti isotope ratios. A clear, complete solution resulting from complete digestion is also desirable for ion exchange separation procedures. Graphite is especially difficult to dissolve in any acid reagents except perchloric acid, $HClO_4$, and we purchased a special acid scrubber accessory to collect and neutralize perchloric acid vapors to prevent venting into the laboratory fume hood. Initial experiments resulted in clear solutions in perchloric acid obtained from solid graphite wafers only after several hours of microwave digestion or up to two days' time. An additional disadvantage of the perchloric acid was the high boiling point and the excessive length of time required to evaporate the perchloric acid from the digested sample prior to separation chemistry using ion exchange procedures. Some loss of Ti in the form of volatile $TiCl_4$ (boiling point ~135° C) from the sample + acid mixture could also occur during digestion or hotplate evaporation steps with perchloric acid. During initial digestion experiments on 'cold' graphite samples, we also ran digestion 'blank' experiments by adding only the acid digestion mixtures to the microwave vessels. After microwaving, these were analyzed using ICPMS to try to determine the levels of impurity elements in the high-purity acids alone, and to assess how much 'blank' or natural unirradiated Ti may be added to the graphite samples during digestions.

The high boiling point of perchloric acid was potentially the slowest part of the digestion procedure and we investigated the use of a rapid evaporation method using a commercial drying carousel in the microwave oven. The original inner microwave vessels containing the sample digestate and solution were removed from the outer high-pressure casings and fitted into a different type of carousel designed to rotate in the microwave oven while the samples are heated

and the vapors were pumped out and filtered through the special acid vapor neutralization module described earlier. The goal was to evaporate off the perchloric acid, which adversely affects the ion exchange separation procedures described later, and to obtain a nearly dry residue which would then be redissolved in HF. Most samples would be suitable for this process, however, graphite, which is a semiconducting material, was found to intensely focus and absorb microwave energy when dried. This led in one case to ignition and limited combustion of the graphite residue in the microwave vessel cavity. To avoid this hazard, especially with irradiated samples, and to minimize digestion blanks, we decided to perform intensive microwave leaching of powdered graphite samples only in high-purity HF as described below.

Subsample wafers taken from samples 42 and 77 were digested in the microwave using a mixture of nitric, perchloric, and hydrofluoric acids, and required several cycles, or a total of several hours, to produce effects ranging from a completely clear solution to a suspension of fine particles. The latter were judged usable and centrifuged prior to ion exchange separation, because we were interested in the isotopic compositions of Ti, and not necessarily an accurate measurement of bulk Ti contents in the irradiated graphite samples. As we describe below, the isotope ratios measured in each of the subsamples taken from samples 42 and 77 showed unexpected variability beyond instrument accuracy and run precision values. This variability was typically in the form of ratios being biased in one direction toward values typical of natural, unirradiated Ti. Results of acid blank analyses by ICPMS had earlier revealed relative blank levels of the various acids in use, and perchloric acid was observed to have the highest levels of Ti, i.e., several hundred parts-per-trillion or picograms/ml, while nitric acid and hydrofluoric acid had levels lower by a factor of 10. Furthermore, it was possible to further pre-clean the high-purity hydrofluoric acid as purchased by employing the same ion exchange method as outlined below for separation of Ti from other impurity elements in the sample solution. Thus, we adopted a modified partial digestion or leaching procedure using only hydrofluoric acid, HF, in the vessels during microwave digestions, and performed this leaching procedure on samples which were powdered to maximize surface areas attacked by the HF and to increase Ti yields in the resulting sample leachate solutions. This new procedure appeared to reduce the number of measurements of isotope ratio values biased toward natural Ti by reducing the amount of blank Ti added during microwave digestions.

2.3 Preparation and Calibration of Ti Isotopic Spike

A high-purity (quoted as 94%) amount of ^{46}Ti was purchased from Oak Ridge Isotopes to use as a 'spike' in blank determinations and possibly in analysis of bulk Ti contents by isotope dilution mass spectrometric analysis. The Ti isotopic spike was supplied as TiO_2, which is relatively insoluble, and required a lengthy, difficult dissolution in sulfuric acid (H_2SO_4). The final ^{46}Ti spike solution was made up in dilute HF with a trace of sulfuric acid and contained a bulk concentration of approximately 40 micrograms/ml. For isotope dilution analysis and blank determinations, this concentration had to be measured more precisely by calibration against a normal Ti solution with a precisely known concentration. This latter solution was made by obtaining a small amount of highly refined, 99.9999% purity Ti metal from the Alta Group. The 2 g portion of metal was weighed multiple times on several occasions on an analytical balance to

within 0.1 mg, dissolved in dilute HF, and diluted to a solution volume which was weighed as precisely as possible to obtain an accurate figure for the Ti concentration.

Several aliquots of the Ti calibration solution were precisely weighed and portions of the ^{46}Ti spike solution were also precisely weighed and added to each. The mixtures were varied to obtain a range of measured isotope ratio values. These mixtures were of sufficient purity to load directly onto filaments for mass spectrometric analysis, and the ^{46}Ti spike solution was also analyzed alone. The high purity normal Ti calibration solution was also used throughout this study as a Ti mass spectrometric reference standard to assess both accuracy and reproducibility of Ti isotope ratio measurements in the graphite samples.

Results of mass spectrometric analysis of three standard+spike mixtures and replicate analyses of the spike solution are shown in Figure 2.3-1 below. Since the spike is almost pure ^{46}Ti, and ^{48}Ti is the most abundant natural isotope of titanium, the measured ratios of $^{46}Ti/^{48}Ti$ are the most useful in determining the bulk concentration of Ti in the spike solution. The mixed $^{46}Ti/^{48}Ti$ ratio R_m can be expressed as a mixture

$$R_m=(A^{46}{}_N N + A^{46}{}_S S)/(A^{48}{}_N N + A^{48}{}_S S)$$

where N is the number of atoms of the normal element and S is the number of atoms of the spike present in the mixture, and $A^x{}_N$ or $A^x{}_S$ refer to the specific abundances of isotope x in the normal element and the spike respectively. This mixing equation is easily solved for the number of Ti atoms in a given amount of spike solution by measuring the mixed ratio. The three replicate determinations of the spike sample mixtures yielded an average concentration of Ti in the spike of 40.80 +/- 1% micrograms (10^{-6} g)/ml and an average abundance of 96.76% ^{46}Ti, slightly more enriched than the value given by the vendor.

Table 2-2. Comparison of Results for Fuel Channel Duplicate Samples

Ti Isotope Ratios (Corrected)									
Sample	Channel	46/48	error	47/48	error	49/48	error	50/48	error
86-1	06J06-4	0.11608	0.00092	0.10303	0.00077	0.12285	0.00097	0.08515	0.00384
86-1, rep	06J06-4	0.11575	0.00074	0.10304	0.00053	0.12532	0.00057	0.07972	0.00099
86-2	06J06-4	0.11606	0.00075	0.10416	0.00057	0.12736	0.00068	0.09236	0.00333
86-2, rep	06J06-4	0.11577	0.00082	0.10369	0.00049	0.12794	0.00067	0.08628	0.00129
86-2, rep	06J06-4	0.11367	0.00096	0.10274	0.00025	0.12617	0.00126	0.08704	0.00098
86-3	06J06-4	0.11691	0.00068	0.10393	0.00037	0.13301	0.0052	0.08439	0..00199
86-3, rep	06J06-4	0.11543	0.00161	0..10291	0.00067	0.13098	0.00182	0.09292	0.00108
2-1	06J06-4	0.11761	0.00074	0.10482	0.00043	0.14047	0.00066	0.08309	0.00117

Ti Isotope Ratios (Corrected)									
Sample	Channel	46/48	error	47/48	error	49/48	error	50/48	error
2-2	06J06-4	0.11551	0.00056	0.10322	0.00041	0.12314	0.00060	0.08107	0.00105
2-3	06J06-4	0.11771	0.00031	0.10473	0.00031	0.14153	0.00053	0.08780	0.00189
42-1	09J10-4	0.11840	0.00121	0.10502	0.00085	0.16248	0.00118	0.08748	0.00115
42-2	09J10-4	0.10939	0.00192	0.10000	0.00129	0.10626	0.00121	0.09105	0.00364
42-3	09J10-4	0.11997	0.00134	0.10586	0.00106	0.17211	0.00123	0.08467	0.00088
42-3, rep	09J10-4	0.12012	0.00087	0.10590	0.00097	0.17094	0.00128	0.08476	0.00100
42-4	09J10-4	0.11876	0.00097	0.10596	0.00114	0.16783	0.00067	0.08554	0.00113
42-5	09J10-4	0.1163/6	0.00137	0.10429	0.00091	0.14896	0.00119	0.08507	0.00077
42-5, rep	09J10-4	0.11719	0.00089	0.10425	0.00083	0.14874	0.00104	0.08243	0.00064
77-1	09J10-4	0.12152	0.00035	0.10699	0.00051	0.17379	0.00083	0.08569	0.00068
77-2	09J10-4	0.12125	0.00063	0.10643	0.00053	0.17105	0.00061	0.08598	0.00094
77-3	09J10-4	0.12245	0.00047	0.10736	0.00046	0.17665	0.00043	0.08910	0.00155
77-4	09J10-4	0.12227	0.00068	0.10714	0.00036	0.17861	0.00138	0.09008	0.00097
77-5	09J10-4	0.12141	0.00055	0.10654	0.00058	0.17138	0.00061	0.08800	0.00065
71-2	01J08-4	0.11172	0.00071	0.10089	0.00059	0.10008	0.00034	0.08393	0.00070
68-2	01J08-4	0.11369	0.00065	0.10257	0.00057	0.11576	0.00049	0.09120	0.00293
68-3	01J08-4	0.11268	0.00071	0.10182	0.00072	0.11484	0.00067	0.08793	0.00114
25-2	04J07-4	0.11909	0.00060	0.10539	0.00057	0.15486	0.00047	0.08187	0.00026
25-3	04J07-4	0.12372	0.00069	0.10820	0.00056	0.18683	0.00070	0.08630	0.00054
25-3, rep	04J07-4	0.12309	0.00091	0.10802	0.00081	0.18728	0.00132	0.08598	0.00081
25-4	04J07-4	0.12359	0.00062	0.10828	0.00055	0.18788	0.00079	0.08615	0.00069
79-2	04J07-4	0.12089	0.00055	0.10668	0.00059	0.16384	0.00073	0.08701	0.00072
79-3	04J07-4	0.12287	0.00052	0.10735	0.00040	0.17788	0.00051	0.08843	0.00118
79-4	04J07-4	0.12101	0.00062	0.10676	0.00040	0.16666	0.00069	0.08519	0.00058
89	12C06-4	0.11388	0.00071	0.10349	0.00058	0.13677	0.00067	0.07988	0.00113
58	12Q06-4	0.11445	0.00098	0.10370	0.00075	0.13789	0.00066	0.07988	0.00100
53	12Q06-4	0.11362	0.00044	0.10307	0.00041	0.12893	0.00049	0.08011	0.00067
87	12Q06-4	0.11827	0.00052	0.10611	0.00036	0.15817	0.00042	0.08142	0.00050

Cr Isotope Ratios							
Sample	Channel ID	50/52	error	53/52	error	54/42	error
86-1	06J06-4	0.03028	0.00014	0.06745	0.00047	0.02021	0.00035
86-1, rep	06J06-4	0.03044	0.00021	0.06803	0.00044	0.02069	0.00021
86-2	06J06-4	0.04808	0.00029	0.10279	0.00049	0.02575	0.00028
86-3	06J06-4	0.02503	0.00018	0.05714	0.00022	0.01779	0.00016
86-3, rep	06J06-4	0.02515	0.00016	0.05723	0.00014	0.01796	0.00015

2.4 Laboratory Protocols and Blank Determinations

The choice of materials and apparatus used in all stages of preparations, including machining of samples to final ion exchange separation of Ti for mass spectrometric analysis, was governed by our need to minimize contamination by natural or blank Ti. Since Ti is a relatively common element, this required avoidance of metallic containers, for example. The tool bit used to both shape and powder the samples in the gloveboxed lathe was composed of tungsten carbide, which contains very low levels of impurities and is much harder than the graphite samples. During machining, the powdered sample material was directed into small polystyrene plastic vials and were tightly capped until transferred into the microwave vessels for acid digestion, thus minimizing transfer steps and containers.

Most laboratory ware used in sample digestions and ion exchange separations was composed of various types of Teflon, a group of fluoropolymer plastics which provide the most chemically inert materials available, and thus, the lowest potential for blank contributions. The microwave digestion vessels and caps were composed of a special Teflon able to withstand high pressures (to 1560 psi) and high temperatures (to 270°C). These were precleaned before use, and cleaned between uses, by subjecting them to the same acid digestion mixture and two cycles of the same pressure-temperature regulated digestion program sequence as that used for sample digestions. All other labware, including capped Teflon vials and polyethylene disposable transfer pipets, was first precleaned by soaking in a solution of ~ 50% ammonium hydroxide for several days, rinsing thoroughly in deionized water, and then soaking in a solution of ~30% nitric acid + 5% HF for several days, followed by final rinsing in water which was filtered, deionized, and distilled in a four-cartridge Milli-Q system. Ion exchange columns designed to hold about 0.5cc of anion exchange resin were fabricated from disposable polyethylene transfer pipets fitted with semipermeable frit material, and were also precleaned in the above manner. Columns, sample vials, and transfer pipets were not recycled during this study: a new set of labware was used for each graphite sample. This practice was adopted to prevent cross-contamination of trace impurity elements and to allow archiving of all sample residues and unused fractions collected from ion exchange procedures for possible further study.

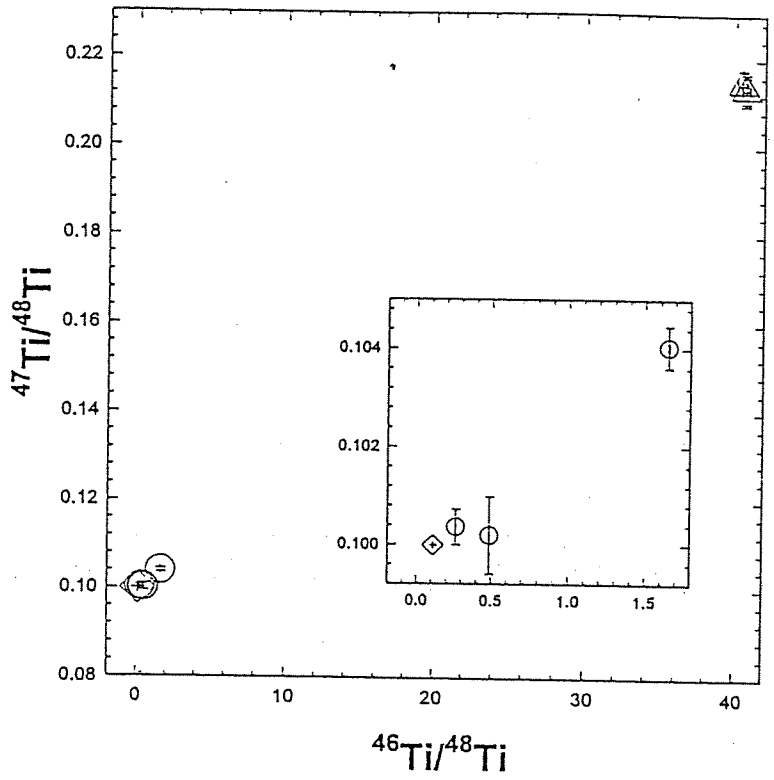

Figure 2.3-1. Analyses of Ti isotope ratios in a calibration of ^{46}Ti spike; diamond symbol refers to isotopic composition of natural titanium, triangle symbol refers to results of spike analyses, the circles are spike-standard mixtures.

The high purity acids used in all parts of this study were purified by the vendor by sub-boiling distillation in all-Teflon systems and are shipped in double-bagged Teflon bottles with a specific certificate of analysis. The impurity levels in these high-grade acids are typically in the sub-ppb (parts-per-billion) range or may be as high as a few ppb for some elements. The certified analytical values supplied by the vendor for each lot varied by the type of acid. Perchloric acid was highest in impurity elements of interest (375 ppt Ti, 150 ppt Cr, 6 ppb Fe, <25 ppt V), and nitric acid (96 ppt Ti, 37 ppt Cr, <25 ppt Fe, <25 ppt V) and hydrofluoric acid (<20 ppt Ti, <5 ppt Cr, <500 ppt Fe, <10 ppt V) contained lower amounts of these elements. The concentrated (~30N) hydrofluoric acid was further purified by first diluting to 5 N with Milli-Q water and passing it through anion exchange resin in a similar manner for the separation of Ti from the sample leachate as described below.

2.5 Elemental Separations via Ion Exchange Methods

Samples or analytes consisting of elemental separates prepared for analysis of isotopic compositions by thermal ionization mass spectrometry (TIMS) must be separated from the sample matrix, graphite in this study, and also from other elements close in atomic number which may have isotopes of overlapping masses. These overlapping isotopes are referred to as isobaric interferences and if not adequately eliminated, can prevent accurate determination of the isotopic composition of the impurity element of interest. Separation from the sample matrix also improves thermal emission and ionization and enhances the ion yield and run quality during mass spectrometric measurement. For sample preparation and measurement of Ti, the isobaric interferences included ^{48}Ca, ^{50}V, and ^{50}Cr, and for Cr, the interferences included ^{50}Ti, ^{50}V, and ^{54}Fe and we derived or modified separation procedures to eliminate these interferences.

A method for Ti separation and purification was adapted from methods developed for Ti and Hf extraction from various types of meteorites for the study of primordial Ti isotopic variations from the formation of the solar system (Patchett and Tatsumoto, 1980; Niederer et al, 1980; Niemeyer and Lugmair, 1981). Titanium and other related metals referred to as 'high field strength elements' (Zr, Nb, Hf, Ta) readily form anionic complexes with fluorine and this is often the best way to retain these elements in solution. Other elements such as Cr and Fe do not form such complexes, and anion exchange resin (BioRad AD1X4, 400 mesh size) was used to effectively separate Ti from all other elements in solution. The resin was converted or conditioned to fluoride form by passing 5N HF through the column prepared with 0.5 cc resin resting on a semipermeable frit fitted at one end of the plastic pipet. The Ti from each graphite sample solution or leachate was selectively held on specific sites in the resin as TiF_6^{-2} while other elements passed through. The Ti from the sample was removed or eluted from the resin with dilute nitric acid, which effectively destroyed the fluoride form of the resin and its capability to retain Ti.

The microwave leaching in this study, used after the first few attempts with a perchloric acid mixture, employed 5N strength precleaned HF. After microwave leaching and cooling of the samples, the resulting sample slurry was transferred to a capped Teflon vial and allowed to settle, or in some cases was centrifuged. The earlier samples processed with perchloric acid were

evaporated on a hot plate to remove the perchloric acid. This step was followed by the addition of a small amount of HF and further evaporation to convert all sample Ti to fluoride and to evaporate the remainder of the perchloric acid. This sample residue was redissolved as much as possible in 5N HF and centrifuged to separate insoluble or undissolved sample material by settling. For both types of sample digestions, the supernatant clear HF solution was loaded onto the column of anion resin which had been previously conditioned with 5N HF. For many samples, some finely suspended undissolved graphite was added unavoidably with the sample solution and eventually settled onto the top of the resin column, but this did not appear to effect the separation. This was followed by several additions of precleaned 5N HF to ensure that all sample solution had passed through and equilibrated with the resin. This first column fraction contained most of the sample impurity elements, including Cr, and was collected in a Teflon vial and evaporated to dryness. Approximately one milliliter of 5N nitric acid was added and allowed to flow through. This fraction contained the Ti from the sample solution and was collected, dried, and used directly for mass spectrometric analysis. Elution fractions designated for mass spectrometric analysis were collected in special conical Teflon capped vials which concentrated the sample into a small pinpoint for better concentration and visibility, and loading onto mass spectrometer filaments.

Several ion exchange separation methods for chromium were attempted, but none appeared to have any particular advantages over another. Chromium readily exists in at least two oxidation states, Cr(II) and Cr(III), and sometimes Cr(VI). This tendency affects the yield of Cr from ion exchange separations, which as for Ti, largely rely on the formation of a single cationic or anionic species or complex that will be either selectively held or removed from the ion exchange resin relative to other matrix and impurity elements. An extraction method also developed for meteoritical studies (Birck and Allegre, 1984; Papanastassiou, 1986) was adapted for use in this study. An initial step of the published method involved oxidation of all Cr in the sample solution to Cr(III) using cerium(IV) ammonium nitrate, a very effective oxidant. However, this did not appear to be as effective as described, since two Cr-bearing elution fractions continued to occur in the ion exchange procedure, and addition of this compound to the solution appeared to increase the Cr blank significantly.

A cation exchange procedure for Cr was adopted in this study for its simplicity, although a yield less than 100% was also typical for this method like many others. The Cr-bearing elution fraction in 5N HF from the Ti anion exchange procedure was evaporated to near dryness and 0.5 ml of concentrated high-purity hydrochloric acid (HCl) was added, to convert all transition metals to chloride cation complexes. The fraction was again evaporated on a hotplate to dryness and redissolved in a small amount of 0.2 M HCl. A cation exchange column was prepared with 0.5 cc of BioRad AG50X8 cation exchange resin (400 mesh size), precleaned by passing several ml of concentrated HCl through the resin, rinsed with Milli-Q water, and then preconditioned with 0.2 M HCl. Ideally, the transition metals are adsorbed as chloride complexes and differentially desorbed according to their ionic radius and affinity for the resin substitutional sites. The expected result was that several sequential fractions would each contain a different transition metal, and that calibration of this sequence should result in a reproducible elution peak to collect a Cr fraction separated from Fe, V, and Ca. An early elution peak or Cr-bearing, Fe-

free fraction was observed, followed by a sequence of alkaline elements and transition metals, and a later, less-intense Cr peak occurred very close to that for Fe. This indicated that Cr was occurring in two oxidation states, and the later peak was probably due to a Cr(III) chloride complex. The early elution peak typically contained more Cr, as evidenced by ICPMS analysis, and probably resulted from a Cr fluoride complex, because Ti was also observed to elute immediately in test cases. We concluded that residual fluorine from the first anion exchange separation for Ti caused this effect and decided to make use of it for sample separations. Thus, the very first fraction after loading the sample solution in 0.2M HCl onto a cation bed conditioned with 0.2 M HCl was collected as the desired Cr-bearing fraction in a cone-shaped Teflon capped vial. Later results of mass spectrometric analysis indicated that this fraction was sufficiently low in Ti and Fe to permit Cr isotopic measurements. The remaining sample solution containing Fe and other matrix elements were collected, dried, and archived.

2.6 Mass Spectrometry

The quality of results in thermal ionization mass spectrometric (TIMS) analysis depends on several factors, including (1) an available amount of the isolated, separated elemental sample, (2) first ionization potential of the element, (3) efficiency of ionization from the MS filament on which the sample is loaded, and (4) detection sensitivity and ion transmission efficiency of the mass spectrometer. Except for (2), each of these factors was evaluated, and modified and improved where possible during this study.

a. Filament Loading Methods

In thermal ionization mass spectrometry, samples are typically mounted or pipetted as a solution onto a narrow ribbon (< 1mm) of high-purity, zone-refined metal, typically tantalum (Ta), tungsten (W), or rhenium (Re). Sample filaments are made for the mass spectrometer by welding small measured pieces of the ribbon onto a reusable holder which has been precisely machined for the source, or front end, of the mass spectrometer. These are made up in large batches and resistively heated at a current of several amps under a high vacuum to remove or 'bake out' impurities before use. While under a high vacuum, a second step is performed at lower current to diffuse carbon into the filament by bleeding a small amount of propane into the vacuum chamber. This carburization process has been found to greatly increase the ion yield by thermal emission of many elements, especially actinide and transuranic elements.

We found a relatively improved ion emission for Ti on carburized Re filaments after attempting other types of filament materials, both carburized and noncarburized. We also modified the shape of the filament for enhanced ion emission by constructing a precisely machined forming jig to bend and form a small depression in the center of the filament ribbon before welding onto the filament assembly. This served to better concentrate the emission of ions by reducing the angular dispersion immediately from the filament. In preparation for mass spec analysis, elution fractions containing Ti in this study were redissolved in a few microliters of dilute nitric and hydrofluoric acid prior to loading on the sample filament. In many cases, a small amount of white (possibly Ca-bearing) or brown (Fe-bearing) precipitate remained, and this was allowed to

settle out before attempting to load 1 microliter fractions onto a sample filament. The sample solution was dried in air by applying a low current (~0.5 amp) across the filament before mounting in the source of the mass spectrometer, pumping down to high vacuum, and beginning analysis.

Carburized Re filaments were also used for Cr analyses after trying out alternatives. Chromium thermal emission was improved by adopting and modifying a method also used earlier in meteorite studies. Prior to loading the Cr samples, microliter amounts of dilute, high-purity boric acid (H_2BO_3) and a suspension of high-purity silica gel (SiO_2) were loaded onto the sample filament and dried at a low applied current. The Cr elution fraction was dissolved in dilute high-purity nitric acid and loaded in one microliter fractions onto the filament. This mixture was dried and the filament current increased slowly until a barely visible dull red glow was achieved in air, at which point the mixture on the filament had partially fused. This practice, as described in previous work, lowers the 'work function' of the Re filament material and as a result, selectively lowers the ionization temperature, and required filament current, of Cr during the mass spec analysis. This also improves the quality of the analysis because the Cr emission is improved relative to small amounts of Ca, and Ti, and Fe sometimes remaining in the sample after ion exchange separations.

Sample filament loading procedures were tested thoroughly using high-purity standard solutions of Ti and Cr. This also allowed calibration of the instrument settings for each mass, or isotope, of interest without utilizing sample material, and to also determine the small amount of instrument bias and accuracy of measurements. As discussed below, most instruments yield isotope ratio measurements for standards that may be slightly different from the accepted or certified reference values for isotope abundances, and a small correction for bias based on numerous standard measurements is then applied to results from each sample measurement. The instrument bias may be based on specific ion optics design features of the instrument, but is usually mostly due to subtle within-run thermal fractionation of the lighter isotopes of an element relative to heavier isotopes. This may be controlled by ensuring that all samples and standards are loaded and run in the same manner, including the beginning and within-run range of applied filament current and ionization temperature. Measurements of Cr samples and standards were very similar in run conditions, probably because the special filament loading procedure adopted tended to induce more uniform run conditions. In contrast to Cr, the Ti samples and standards achieved desired thermal ionization yields at different temperatures and filament currents. The high-purity Ti standard ran at filament currents typically 0.5-0.8 amp lower than sample Ti, because Ti ionization in the latter was partly retarded or suppressed by the presence of small amounts of matrix elements that were not completely removed and also organic residue from the ion exchange resin.

Titanium samples thus ran differently from the standard Ti, but differences were also observed between sample runs. Even though uniform digestion and ion exchange separation procedures were applied to all samples, the mass spectrometer runs often differed in the amounts of isobaric interferences present or in the initial ionization temperature for Ti. This indicated variability in the abundances of impurity elements from one sample to the next, and this was even observed to

some degree between adjacent subsamples taken from the same sample core. Thus, each sample was unique and care was taken at the start of, and during, each mass spec analysis. For example, Ca and Cr have lower first ionization potentials and the mass spectrometer was alternately tuned to ^{44}Ca, ^{48}Ti, and ^{52}Cr at the beginning of each Ti isotopic analysis. Data acquisition for Ti isotope ratios was begun only after ^{44}Ca and ^{52}Cr emissions were at a sufficiently low level to avoid significant ^{48}Ca and ^{50}Cr isobaric interferences on ^{48}Ti and ^{50}Ti, respectively. Chromium analyses were rarely affected by any isobaric interference because the filament loading method effectively produced an additional chemical separation by lowering the ionization temperature of the Cr on the filament.

b. Comparison of Instruments

Two different mass spectrometer instruments differing in design and detection sensitivity were compared for use in this study. One instrument is a 3-stage instrument offering unusually high detection sensitivity resulting from efficient ion transmission and an ion pulse counting detection system. The first two stages are electromagnets typical of most mass spectrometers and these are followed by an electrostatic analyzer which offers further mass filtering and improved resolution by further reducing tailing between adjacent ion beam peaks. In general, the large spatial dispersion via magnetic separation of ions in the Ti-Cr mass range does not require the high resolution and abundance sensitivity provided by a 3-stage instrument. Titanium and Cr samples were prepared on filaments as above and loaded into the 3-stage instrument. The desired maximum count rate of 10^6 cts/sec, in the linear range of the electron multiplier detector and below the saturation level, was observed for amounts of Ti and Cr standards as low as 5 ng (10^{-9} g), and this showed much promise for the study, suggesting that successful analyses could be obtained for relatively small samples of graphite, or for samples of graphite possessing extremely low levels of Ti and Cr impurities. However, the run precision and reproducibility of Ti and Cr isotopic ratios measured on the 3-stage instrument was surprisingly poor, about 5-8% (1 SE). Some aspects of the design of the instrument may be the cause, specifically the mechanism of switching the ion accelerating voltage, rather than magnet current, to jump from one mass to another, and also the electron multiplier is off-axis with respect to the final ion beam, requiring a deflector plate and applied voltage to deflect ions into the detector. As a result of these findings, some modifications of this relatively new 3-stage instrument are planned.

All analyses in this study were thus conducted on a single-stage mass spectrometer with electromagnetic switching of masses and an electron multiplier detector, though lacking the gain provided by a pulse counting system. Since this same instrument was used two years in a proof-of-principle demonstration project leading up the present study, a few minor modifications, including reconditioning the electron multiplier and a new improved magnet regulator, have led to enhanced detection sensitivity and stability. Previously, samples consisting of more than 100 ng of Ti were required for an adequate analysis, and 500 ng preferred. Titanium standard solution amounts of 10 to 50 ng run on this instrument now appear to yield good results and run precision. Most samples may have been loaded and analyzed in this range, though without prior knowledge of initial impurity contents in the graphite samples nor of the yields from ion exchange separation, it is difficult to estimate the amounts utilized for each sample analysis.

c. Results for Ti and Cr Standards

During development of sample digestion and ion exchange separation methods, and before work on the actual irradiated graphite samples, replicate analyses of the Ti standard solution were performed on the single-stage mass spectrometer to evaluate run precision, accuracy, and the amount of instrument mass bias. The results are illustrated in Figure 2.6-1, wherein accepted values of each Ti isotope ratio are shown for comparison. Shortly before commencing analyses of Ti extracted from irradiated graphite samples, some small changes in filament loading and the amount of Ti standard loaded were adopted, and this corresponds to a change in measured values relative to the accepted values; all sample analysis results were corrected for instrument bias using correction factors based on these later measurements. Results of analyses of a Cr standard solution are shown in Figure 2.6-2. No further measurements were made after determining that Cr isotope ratios would be less useful due to uncertainties arising from V both in the graphite samples and in Ti and Cr elution separates.

Correction factors for instrument mass bias were calculated from the average of all analyses of Ti and Cr standards acquired during sample analyses. In general, one analysis of the Ti standard solution was conducted each day, or one for about every 5 or 6 sample analyses. The apparent instrument bias is the opposite to that expected for relative thermal fractionation of light vs. heavy isotopes. This is shown by measured $^{47}Ti/^{48}$ and $^{46}Ti/^{48}Ti$ values which are higher than, and $^{49}Ti/^{48}Ti$ and $^{50}Ti/^{48}Ti$ which are lower than accepted values (Figure 2.6-1). This same result is seen in the measured values for a Cr standard solution (Figure 2.6-2), suggesting that for both Ti and Cr, within-run relative thermal fractionation may be negligible, and the instrument bias arises from specific design features.

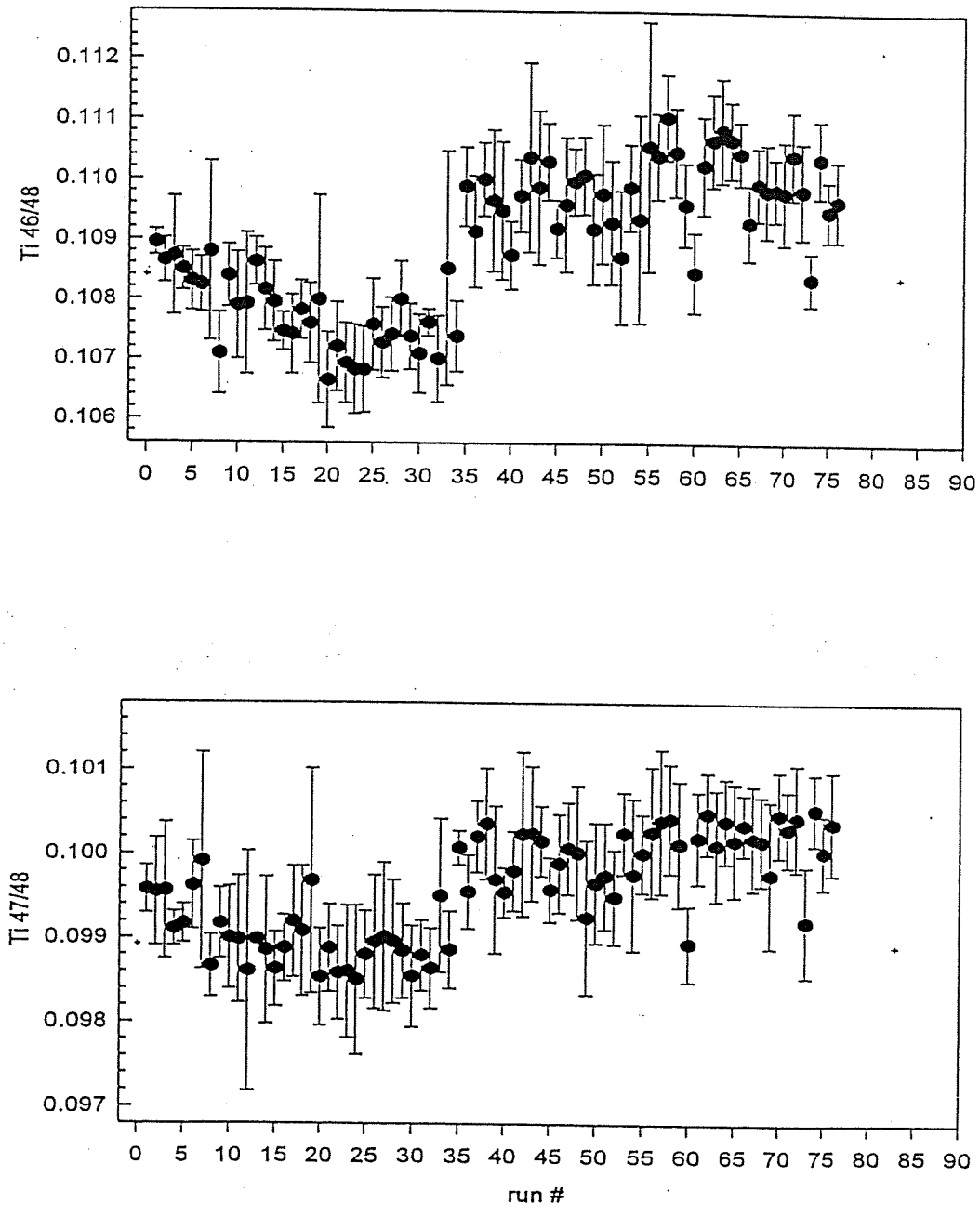

Figure 2.6-1. Results of mass spectrometric analyses of a Ti standard solution. Accepted values are shown by plus symbols in each plot. Error bars represent one standard error.

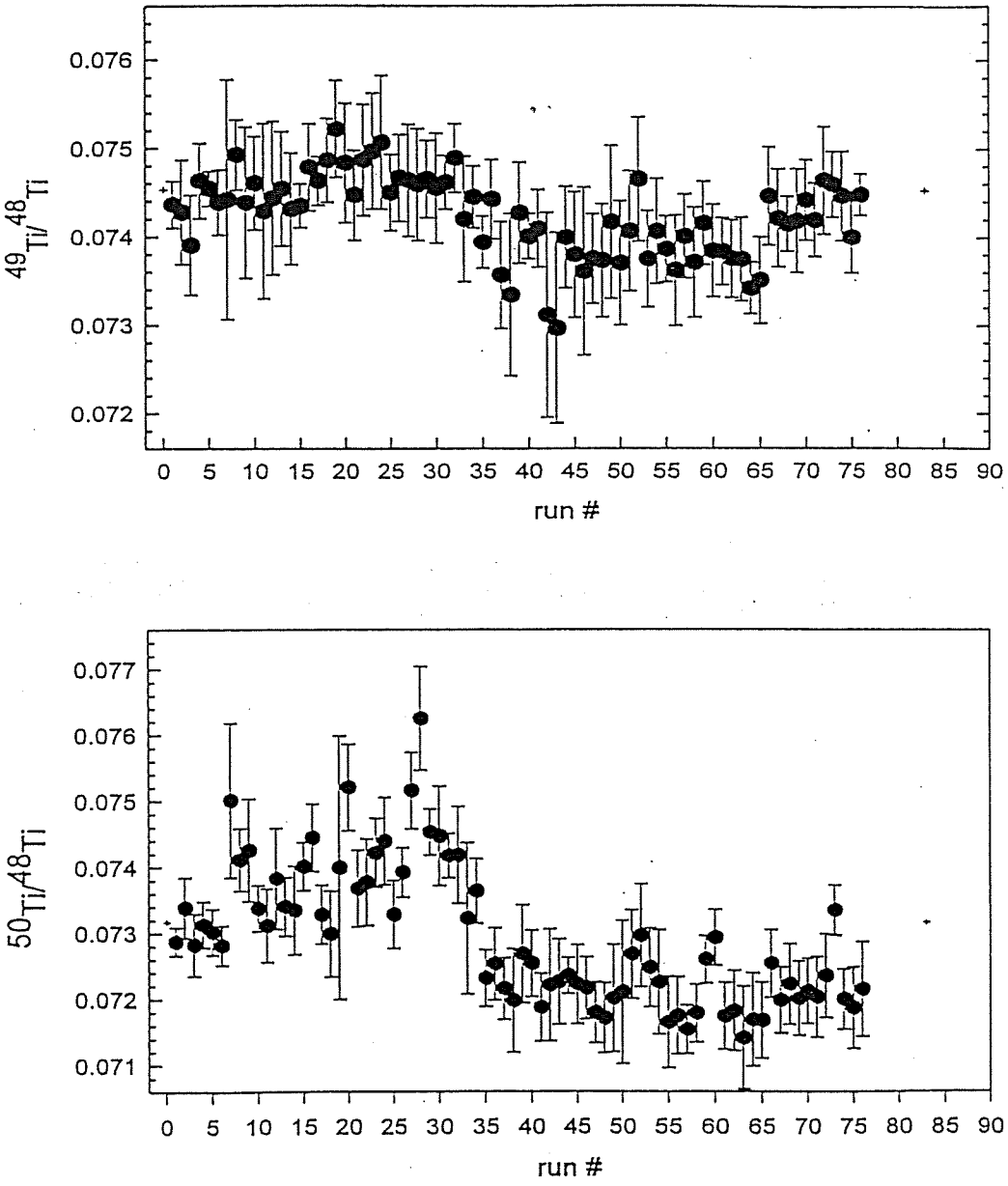

Figure 2.6-1 (con't). Results of mass spectrometric analysis of a Ti standard solution.

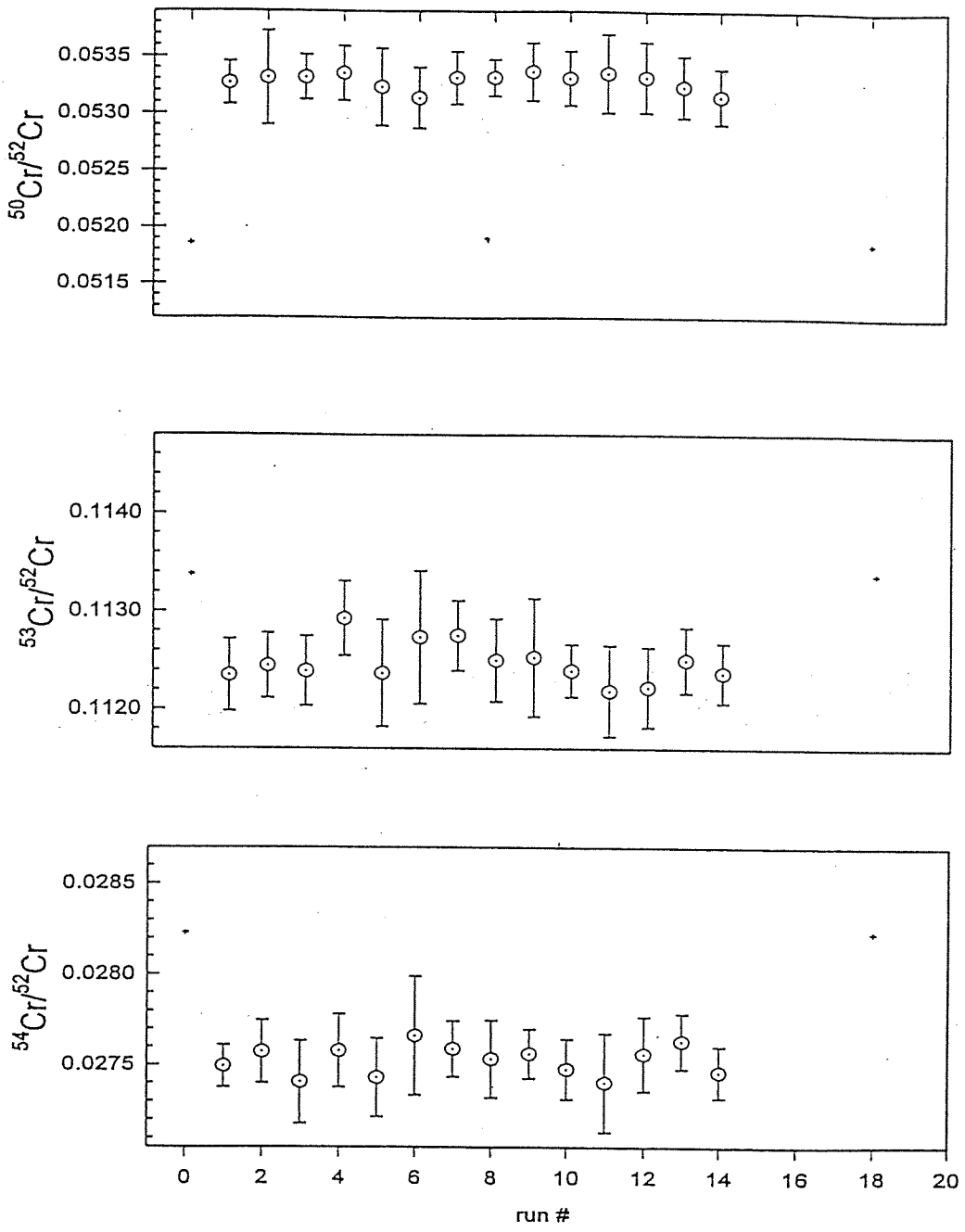

Figure 2.6-2. Results of mass spectrometric analysis of a Cr standard solution. Accepted values are shown as plus symbols. Error bars represent one standard error.

2.7 Initial Results for Irradiated Trawsfynydd Graphite Samples

a. Samples 42 and 77

Subsamples taken from the two core samples 42 and 77 were digested in a mixture which included perchloric acid as described earlier, and were revealed later in this study to be closely adjacent samples taken from the same level in the same fuel channel, and therefore should have experienced the same degree of neutron fluence exposure. Results of mass spectrometric analyses of Ti isotope ratios in these samples and their groups of subsamples are listed in Table 2-2. The $^{49}Ti/^{48}Ti$ ratios are the most affected by neutron fluence, and vary greatly in the subsamples from #42, with the highest values overlapping the lowest values measured in subsamples taken from #77. The subsample variability in #77 is markedly less, but still does not display a coherent trend or variation in isotope ratios along the sample.

b. Samples 2 and 86

Results from 42 and 77 above, and ICPMS measurements of perchloric acid digestion vs. hydrofluoric acid (HF) leaching experiments suggested changing to a method whereby lower amounts of blank, or natural unirradiated Ti would be contributed during processing, as described earlier. Samples 2 and 86, also adjacent samples from a single position in the same fuel channel, were the first samples to be machined as powders and leached in the microwave oven with only HF. Results for subsamples from 86, especially the replicate analyses with better run precision, were encouraging and appeared to display a trend along the sample from subsample 86-1 to 86-3. Subsamples from #2, however, with the exception of the middle subsample 2-2, were characterized by higher $^{49}Ti/^{48}Ti$ ratios, or more altered Ti isotope ratios, and did not display any clear trend. Significant blank Ti contributions mixed with the sample Ti will only bias the irradiated, altered Ti isotope ratios toward those characteristic of natural Ti. Thus, all of the 86 subsamples may be affected by blank Ti, since two of the #2 subsamples displayed more altered Ti isotope ratios, a difference far greater than could be accounted for by run precision and analytical uncertainty.

An intermediate conclusion based on these results was that the blank Ti contribution even from HF leaching was larger than anticipated, and that small-scale heterogeneity, or at least on the scale of the subsamples, in the distribution of Ti-bearing inclusions or domains was more significant than expected. To further address this problem, and to possibly find other samples which could better display subsample isotopic variations with neutron fluence along the sample length, all remaining graphite samples were prepared as powdered subsamples. This approximately tripled the number of required sample digestions and mass spectrometric analyses.

2.8 Analytical Results for the Remainder of Samples From 1st Half-Plane

All remaining samples from the first half plane, or 'J' plane, were prepared as powdered subsamples and strongly leached in the microwave oven to minimize blanks and continue to search for subsample trends in Ti isotope ratios. Chromium isotope ratios were not analyzed

(yet) in any remaining samples, due to complications and uncertainties posed by the presence of vanadium, but a few analyses to further evaluate or solve this problem could be carried out in the future, since all sample materials and elution fractions have been archived. Data from this analysis is reported in Table 2-3.

Measured Ti isotope ratios trend between those for natural Ti and some maximum value produced by neutron fluence exposure, though due to the 'blind' approach taken in the early stage of this study, this maximum was not known in advance. The $^{49}Ti/^{48}Ti$ is the most variable, due to a larger cross section relative to the other isotopes of Ti, and therefore measured ratios vary from near natural ^{48}Ti values (0.074) to a high of >0.18. The trend between natural Ti and a maximum value is expected, since it is assumed that isotopic compositions in Ti impurities in the graphite moderator material were characteristic of natural, unirradiated material. This trend is displayed by all the data in Figure 2.8-1 on the following pages. The scatter in $^{50}Ti/^{48}Ti$ ratios was surprising at first, but later was attributed to significant amounts of vanadium, rather than ^{50}Cr, still present in the Ti elution separate which contributed ^{50}V to the ^{50}Ti peak. Vanadium is close in thermal emission characteristics and was more persistent during the analysis than either Ca or Cr remaining in the Ti fraction. As mentioned above, it was possible to 'burn off' Ca, which interferes and adds to mass 48, and Cr (interfering at mass 50) to an acceptably low level, but V remained to the extent that the measured $^{50}Ti/^{48}Ti$ ratios decreased steadily throughout the run, thus accounting for the scatter in values and the larger errors on this ratio as measured compared to the other Ti isotope ratios. The trend of $^{46}Ti/^{48}Ti$ vs. $^{49}Ti/^{48}Ti$ is good, though the range in measured $^{46}Ti/^{48}Ti$ ratios is both different and greater than expected, and is affected by the presence of Sc which after neutron fluence exposure is an interference at mass 46. The most useful Ti isotope ratios for neutronics calculations thus involve ^{47}Ti, ^{48}Ti, and ^{49}Ti.

The variation plots in Figure 2.8-1 also allowed recognition of possible problematic analyses and several replicate analyses were conducted for samples appearing to fall off of the main trend or which had larger errors from initial analyses. In most cases, the replicate analyses were an improvement or at least reduced the apparent scatter to some degree.

Table 2-3a. Measured Isotope Ratios

sample	channel ID	44/48	error	46/48	error	47/48	error
86-1	06J06-4	0.0035	0.0019	0.1175	0.0009	0.1041	0.0008
86-1,rep	06J06-4	0.0005	0.0003	0.1172	0.0008	0.1042	0.0005
86-2	06J06-4	0.0409	0.0045	0.1171	0.0008	0.1049	0.0006
86-2,rep	06J06-4	0.0285	0.0023	0.1169	0.0008	0.1045	0.0005
86-2,rep	06J06-4	0.0001	0.0000	0.1151	0.0010	0.1038	0.0003
86-3	06J06-4	0.0121	0.0054	0.1182	0.0007	0.1049	0.0004
86-3,rep	06J06-4	0.0017	0.0004	0.1168	0.0016	0.1040	0.0007
2-1	06J06-4	0.0198	0.0088	0.1189	0.0008	0.1058	0.0004

Table 2-3a. Measured Isotope Ratios (con't)							
sample	channel ID	44/48	error	46/48	error	47/48	error
2-2	06J06-4	0.0146	0.0065	0.1168	0.0006	0.1042	0.0004
2-3	06J06-4	0.0042	0.0016	0.1191	0.0003	0.1058	0.0003
26-1	06J06-8	0.0034	0.0019	0.1131	0.0003	0.1025	0.0003
26-2	06J06-8	0.0068	0.0018	0.1129	0.0006	0.1019	0.0005
34-1	06J06-5	0.0029	0.0025	0.1212	0.0005	0.1072	0.0004
34-2	06J06-5	0.0014	0.0002	0.1164	0.0010	0.1048	0.0008
34-2,rep	06J06-5	0.0008	0.0002	0.1164	0.0010	0.1046	0.0006
34-3	06J06-5	0.0007	0.0004	0.1191	0.0005	0.1060	0.0005
34-4	06J06-5	0.0003	0.0001	0.1208	0.0004	0.1071	0.0004
34-4,rep	06J06-5	0.0041	0.0038	0.1214	0.0004	0.1075	0.0005
60-1	06J06-6	0.0006	0.0004	0.1183	0.0006	0.1058	0.0005
60-2	06J06-6	0.0005	0.0004	0.1179	0.0007	0.1059	0.0007
60-3	06J06-6	0.0029	0.0020	0.1147	0.0005	0.1030	0.0006
60-3,rep	06J06-6	0.0007	0.0005	0.1145	0.0006	0.1032	0.0006
14-1	06J06-7	0.0010	0.0010	0.1160	0.0004	0.1040	0.0003
14-2	06J06-7	0.0032	0.0018	0.1138	0.0012	0.1016	0.0009
14-2,rep	06J06-7	0.0007	0.0002	0.1169	0.0016	0.1047	0.0011
14-3	06J06-7	0.0017	0.0010	0.1139	0.0018	0.1025	0.0007
14-3,rep	06J06-7	0.0002	0.0001	0.1126	0.0007	0.1021	0.0005
14-4	06J06-7	0.0017	0.0015	0.1168	0.0007	0.1040	0.0006
72-1	09J10-8	0.0031	0.0013	0.1135	0.0018	0.1022	0.0008
72-1, rep	09J10-8	0.0000	0.0000	0.1125	0.0008	0.1019	0.0006
72-2	09J10-8	0.0008	0.0001	0.1123	0.0006	0.1015	0.0007
75-1	06J06-2	0.0009	0.0003	0.1134	0.0008	0.1025	0.0006
75-2	06J06-2	0.0022	0.0013	0.1173	0.0008	0.1048	0.0007
75-3	06J06-2	0.0079	0.0042	0.1111	0.0004	0.1004	0.0007
19-1	06J06-1	0.0075	0.0011	0.1115	0.0010	0.1011	0.0009
19-2	06J06-1	0.0061	0.0016	0.1140	0.0006	0.1026	0.0004
19-3	06J06-1	0.0057	0.0019	0.1120	0.0003	0.1018	0.0003
76-1	09J10-1	0.0029	0.0009	0.1106	0.0008	0.1003	0.0005
76-2	09J10-1	0.0126	0.0024	0.1134	0.0010	0.1020	0.0004
76-2,rep	09J10-1	0.0055	0.0011	0.1119	0.0026	0.1005	0.0027

Table 2-3a. Measured Isotope Ratios (con't)							
sample	channel ID	44/48	error	46/48	error	47/48	error
76-3	09J10-1	0.0037	0.0027	0.1145	0.0005	0.1030	0.0005
76-3,rep	09J10-1	0.0253	0.0049	0.1149	0.0004	0.1030	0.0003
76-4	09J10-1	0.0067	0.0003	0.1134	0.0006	0.1024	0.0006
7-1	09J10-3	0.0036	0.0025	0.1167	0.0006	0.1046	0.0006
7-2	09J10-3	0.0050	0.0024	0.1098	0.0025	0.1004	0.0025
7-2,rep	09J10-3	0.0002	0.0002	0.1109	0.0014	0.1007	0.0010
7-3	09J10-3	0.0114	0.0047	0.1180	0.0011	0.1051	0.0009
7-4	09J10-3	0.0008	0.0004	0.1120	0.0006	0.1015	0.0008
7-4,rep	09J10-3	0.0001	0.0000	0.1115	0.0007	0.1014	0.0005
12-1	06J06-3	0.0224	0.0070	0.1118	0.0072	0.1009	0.0015
12-2	06J06-3	0.0041	0.0017	0.1125	0.0004	0.1016	0.0005
12-3	06J06-3	0.0012	0.0007	0.1114	0.0005	0.1004	0.0007
12-3,rep	06J06-3	0.0007	0.0002	0.1117	0.0007	0.1012	0.0006
12-4	06J06-3	0.0033	0.0018	0.1140	0.0003	0.1027	0.0004
37-2	09J10-5	0.0009	0.0006	0.1218	0.0005	0.1079	0.0004
37-3	09J10-5	0.0004	0.0006	0.1219	0.0006	0.1082	0.0005
37-4	09J10-5	0.0001	0.0001	0.1212	0.0008	0.1077	0.0004
10-2	09J10-6	0.0007	0.0007	0.1207	0.0004	0.1070	0.0004
10-3	09J10-6	0.0022	0.0024	0.1208	0.0004	0.1072	0.0003
4-2	09J10-2	0.0044	0.0011	0.1106	0.0006	0.1005	0.0006
4-3	09J10-2	0.0030	0.0020	0.1115	0.0010	0.1011	0.0006
4-4	09J10-2	0.0049	0.0025	0.1082	0.0020	0.0972	0.0016
4-4,rep	09J10-2	0.0144	0.0027	0.1132	0.0007	0.1023	0.0008
70-2	01J08-2	0.0009	0.0005	0.1134	0.0006	0.1024	0.0002
70-3	01J08-2	0.0120	0.0047	0.1139	0.0009	0.1034	0.0008
70-4	01J08-2	0.0011	0.0007	0.1128	0.0005	0.1020	0.0010
3-2	01J08-8	0.0034	0.0020	0.1128	0.0009	0.1020	0.0008
3-3	01J08-8	0.0077	0.0059	0.1120	0.0007	0.1017	0.0007
11-2	01J08-1	0.0006	0.0002	0.1114	0.0007	0.1011	0.0007
11-3	01J08-1	0.0018	0.0004	0.1112	0.0006	0.1011	0.0004
11-4	01J08-1	0.0115	0.0213	0.1121	0.0006	0.1014	0.0004
51-2	02J07-8	0.0002	0.0001	0.1130	0.0007	0.1024	0.0007

Table 2-3a. Measured Isotope Ratios (con't)							
sample	channel ID	44/48	error	46/48	error	47/48	error
51-3	02J07-8	0.0002	0.0001	0.1129	0.0008	0.1025	0.0007
51-4	02J07-8	0.0004	0.0001	0.1128	0.0004	0.1023	0.0006
23-2	09J10-7	0.0040	0.0035	0.1175	0.0006	0.1049	0.0004
23-3	09J10-7	0.0037	0.0031	0.1170	0.0008	0.1046	0.0006
23-4	09J10-7	0.0031	0.0020	0.1165	0.0007	0.1043	0.0005
27-2	01J08-6	0.0006	0.0001	0.1141	0.0010	0.1032	0.0006
27-3	01J08-6	0.0005	0.0003	0.1145	0.0003	0.1031	0.0004
48-2	11N11-1	0.0010	0.0008	0.1147	0.0005	0.1040	0.0005
48-3	11N11-1	0.0001	0.0000	0.1154	0.0005	0.1040	0.0006
74-2	08J07-7	0.0001	0.0001	0.1162	0.0006	0.1045	0.0006
74-3	08J07-7	0.0003	0.0003	0.1166	0.0005	0.1049	0.0004
18-2	09J10-6	0.0004	0.0002	0.1153	0.0007	0.1038	0.0003
18-3	09J10-6	0.0003	0.0001	0.1152	0.0007	0.1037	0.0005
24-2	01J08-3	0.0007	0.0002	0.1124	0.0004	0.1018	0.0003
24-3	01J08-3	0.0094	0.0017	0.1131	0.0008	0.1023	0.0006
24-4	01J08-3	0.0002	0.0001	0.1142	0.0012	0.1025	0.0007
21-2	02J07-5	0.0006	0.0039	0.1207	0.0006	0.1068	0.0004
21-3	02J07-5	0.0009	0.0002	0.1156	0.0006	0.1035	0.0006
21-4	02J07-5	0.0037	0.0011	0.1126	0.0005	0.1020	0.0005
52-2	08J07-5	0.0003	0.0001	0.1234	0.0007	0.1093	0.0005
52-3	08J07-5	0.0002	0.0001	0.1229	0.0008	0.1090	0.0006
15-2	02J07-3	0.0049	0.0022	0.1166	0.0007	0.1042	0.0004
15-3	02J07-3	0.0024	0.0007	0.1183	0.0004	0.1055	0.0006
15-4	02J07-3	0.0007	0.0002	0.1179	0.0007	0.1054	0.0006
13-2	02J07-4	0.0003	0.0001	0.1146	0.0005	0.1033	0.0005
13-3	02J07-4	0.0085	0.0006	0.1190	0.0005	0.1065	0.0005
13-4	02J07-4	0.0023	0.0007	0.1193	0.0004	0.1066	0.0007
84-2	02J07-1	0.0003	0.0001	0.1130	0.0004	0.1021	0.0007
84-3	02J07-1	0.0000	0.0000	0.1127	0.0005	0.1025	0.0006
32-2	02J07-6	0.0001	0.0000	0.1184	0.0004	0.1057	0.0004
32-3	02J07-6	0.0019	0.0005	0.1188	0.0005	0.1059	0.0005
32-4	02J07-6	0.0009	0.0006	0.1186	0.0004	0.1053	0.0004

Table 2-3a. Measured Isotope Ratios (con't)							
sample	channel ID	44/48	error	46/48	error	47/48	error
59-2	08J07-8	0.0002	0.0001	0.1138	0.0005	0.1025	0.0006
59-3	08J07-8	0.0002	0.0000	0.1087	0.0005	0.0994	0.0005
50-2	02J07-2	0.0004	0.0002	0.1159	0.0007	0.1040	0.0007
68-2	06J06-6	0.0023	0.0014	0.1151	0.0007	0.1037	0.0006
68-3	06J06-6	0.0001	0.0000	0.1141	0.0007	0.1029	0.0007
30-2	01J08-7	0.0006	0.0004	0.1132	0.0005	0.1021	0.0006
30-3	01J08-7	0.0000	0.0000	0.1101	0.0005	0.1006	0.0004
30-4	01J08-7	0.0032	0.0005	0.1130	0.0008	0.1023	0.0009
80-2	08J07-6	0.0010	0.0006	0.1192	0.0011	0.1063	0.0009
9-2	04J07-8	0.0000	0.0000	0.1131	0.0004	0.1025	0.0007
9-3	04J07-8	0.0000	0.0000	0.1127	0.0003	0.1022	0.0005
9-4	04J07-8	0.0001	0.0001	0.1144	0.0007	0.1031	0.0005
46-2	04J07-7	0.0020	0.0011	0.1167	0.0002	0.1042	0.0006
46-3	04J07-7	0.0002	0.0001	0.1177	0.0004	0.1050	0.0006
46-4	04J07-7	0.0002	0.0000	0.1174	0.0006	0.1050	0.0007
1-2	04J07-6	0.0002	0.0001	0.1179	0.0007	0.1055	0.0005
1-3	04J07-6	0.0001	0.0001	0.1181	0.0005	0.1053	0.0006
17-2	04J07-1	0.0004	0.0001	0.1147	0.0006	0.1030	0.0004
17-3	04J07-1	0.0001	0.0000	0.1146	0.0010	0.1030	0.0012
17-4	04J07-1	0.0012	0.0004	0.1150	0.0008	0.1033	0.0005
25-2	04J07-4	0.0002	0.0000	0.1206	0.0006	0.1065	0.0006
25-3	04J07-4	0.0004	0.0001	0.1253	0.0007	0.1094	0.0006
25-3,rep	04J07-4	0.0006	0.0001	0.1246	0.0009	0.1092	0.0008
25-4	04J07-4	0.0005	0.0001	0.1251	0.0006	0.1094	0.0006
83-2	04J07-3	0.0002	0.0000	0.1207	0.0006	0.1073	0.0005
83-3	04J07-3	0.0017	0.0005	0.1224	0.0008	0.1079	0.0005
83-4	04J07-3	0.0001	0.0000	0.1196	0.0008	0.1062	0.0004
6-2	04J07-2	0.0002	0.0001	0.1164	0.0015	0.1042	0.0014
6-3	04J07-2	0.0006	0.0004	0.1186	0.0007	0.1054	0.0004
55-2	04J07-5	0.0001	0.0000	0.1212	0.0007	0.1079	0.0006
55-3	04J07-5	0.0001	0.0001	0.1204	0.0004	0.1068	0.0007

Table 2-3a. Measured Isotope Ratios (con't)							
sample	channel ID	44/48	error	46/48	error	47/48	error
71-2	01J08-4	0.0003	0.0001	0.1131	0.0007	0.1020	0.0006
79-2	04J07-4	0.0030	0.0020	0.1224	0.0006	0.1078	0.0006
79-3	04J07-4	0.0014	0.0006	0.1244	0.0005	0.1085	0.0004
79-4	04J07-4	0.0000	0.0000	0.1225	0.0006	0.1079	0.0004
42-1	09J10-4			0.1199	0.0012	0.1062	0.0009
42-2	09J10-4			0.1107	0.0019	0.1011	0.0013
42-3	09J10-4			0.1215	0.0014	0.1070	0.0011
42-3,rep	09J10-4			0.1216	0.0009	0.1071	0.0010
42-4	09J10-4			0.1202	0.0010	0.1071	0.0012
42-5	09J10-4			0.1178	0.0014	0.1054	0.0009
42-5,rep	09J10-4			0.1186	0.0009	0.1054	0.0008
77-1	09J10-4			0.1230	0.0004	0.1081	0.0005
77-2	09J10-4			0.1228	0.0006	0.1076	0.0005
77-3	09J10-4			0.1240	0.0005	0.1085	0.0005
77-4	09J10-4			0.1238	0.0007	0.1083	0.0004
77-5	09J10-4			0.1229	0.0006	0.1077	0.0006
Second Half-plane, channels 10G06, 11E07, 12C06							
67	11E07-7	0.0001	0.0000	0.1138	0.0007	0.1037	0.0005
56	11E07-8	0.0002	0.0000	0.1136	0.0004	0.1029	0.0005
35	11E07-3	0.0002	0.0001	0.1199	0.0006	0.1069	0.0005
38	11E07-5	0.0006	0.0002	0.1213	0.0005	0.1079	0.0005
62	11E07-1	0.0001	0.0000	0.1096	0.0012	0.1005	0.0009
5	11E07-4	0.0002	0.0000	0.1211	0.0005	0.1083	0.0003
8	11E07-2	0.0002	0.0001	0.1167	0.0005	0.1047	0.0005
54	11E07-6	0.0003	0.0002	0.1167	0.0007	0.1053	0.0006
33	12C06-3	0.0003	0.0001	0.1170	0.0004	0.1052	0.0004
89	12C06-4	0.0008	0.0003	0.1153	0.0007	0.1046	0.0006
78	12C06-5	0.0010	0.0007	0.1156	0.0009	0.1048	0.0006
58	12C06-4	0.0006	0.0003	0.1159	0.0010	0.1048	0.0008
28	12C06-6	0.0002	0.0002	0.1167	0.0006	0.1052	0.0006
29	12C06-7	0.0018	0.0002	0.1147	0.0005	0.1038	0.0004
65	12C06-2	0.0003	0.0001	0.1160	0.0004	0.1046	0.0005

Table 2-3a. Measured Isotope Ratios (con't)							
sample	channel ID	44/48	error	46/48	error	47/48	error
31	12C06-8	0.0006	0.0001	0.1127	0.0007	0.1017	0.0010
22	12C06-1	0.0107	0.0033	0.1137	0.0005	0.1027	0.0004
49	10G06-8	0.0002	0.0001	0.1128	0.0004	0.1024	0.0004
88	10G06-5	0.0027	0.0009	0.1217	0.0004	0.1084	0.0003
20	10G06-1	0.0003	0.0001	0.1139	0.0005	0.1032	0.0004
47	10G06-4	0.0010	0.0002	0.1212	0.0004	0.1079	0.0004
81	10G06-7	0.0088	0.0026	0.1144	0.0006	0.1035	0.0004
16	10G06-6	0.0042	0.0027	0.1179	0.0013	0.1068	0.0008
43	10G06-3	0.0021	0.0032	0.1153	0.0005	0.1046	0.0005
Third Half-plane, channels 11N11, 12Q06							
40	11N11-1	0.0004	0.0001	0.1138	0.0004	0.1030	0.0003
44	11N11-4	0.0002	0.0000	0.1218	0.0007	0.1083	0.0005
90	11N11-9	0.0003	0.0001	0.1172	0.0005	0.1055	0.0005
69	11N11-7	0.0006	0.0003	0.1153	0.0008	0.1042	0.0005
66	11N11-2	0.0000	0.0000	0.1162	0.0006	0.1052	0.0005
41	11N11-3	0.0011	0.0004	0.1126	0.0007	0.1021	0.0005
61	11N11-8	0.0010	0.0001	0.1111	0.0004	0.1012	0.0005
82	11N11-6	0.0002	0.0001	0.1187	0.0005	0.1066	0.0005
45	12Q06-1	0.0008	0.0002	0.1128	0.0005	0.1024	0.0002
53	12Q06-4	0.0009	0.0002	0.1150	0.0004	0.1042	0.0004
87	12Q06-4	0.0015	0.0002	0.1197	0.0005	0.1072	0.0004
63	12Q06-7	0.0003	0.0001	0.1138	0.0008	0.1032	0.0006
73	12Q06-5	0.0011	0.0002	0.1199	0.0004	0.1073	0.0005
39	12Q06-2	0.0002	0.0001	0.1134	0.0005	0.1029	0.0004
36	12Q06-3	0.0002	0.0001	0.1151	0.0004	0.1041	0.0003
64	12Q06-6	0.0013	0.0005	0.1144	0.0004	0.1036	0.0005
57	12Q06-8	0.0001	0.0000	0.1124	0.0008	0.1023	0.0005

Table 2-3a. Measured Isotope Ratios (con't)							
Sample	channel ID	49/48	error	50/48	error	52/48	error
86-1	06J06-4	0.1219	0.0010	0.0852	0.0038	0.0233	0.0148
86-1, rep	06J06-4	0.1244	0.0006	0.0796	0.0010	0.0177	0.0042
86-2	06J06-4	0.1260	0.0007	0.0919	0.0033	0.0217	0.0069
86-2, rep	06J06-4	0.1267	0.0007	0.0852	0.0013	0.0050	0.0016
86-2, rep	06J06-4	0.1252	0.0013	0.0879	0.0010	0.0386	0.0128
86-3	06J06-4	0.1319	0.0005	0.0832	0.0020	0.0007	0.0004
86-3, rep	06J06-4	0.1300	0.0018	0.0993	0.0012	0.1471	0.1269
2-1	06J06-4	0.1392	0.0007	0.0819	0.0012	0.0005	0.0004
2-2	06J06-4	0.1221	0.0006	0.0800	0.0010	0.0012	0.0005
2-3	06J06-4	0.1404	0.0005	0.0867	0.0019	0.0016	0.0006
26-1	06J06-8	0.1039	0.0003	0.0765	0.0005	0.0033	0.0017
26-2	06J06-8	0.1042	0.0007	0.0761	0.0003	0.0025	0.0015
34-1	06J06-5	0.1569	0.0006	0.0801	0.0004	0.0004	0.0001
34-2	06J06-5	0.1306	0.0016	0.0771	0.0006	0.0113	0.0081
34-2, rep	06J06-5	0.1312	0.0015	0.0776	0.0008	0.0152	0.0054
34-3	06J06-5	0.1438	0.0007	0.0788	0.0003	0.0002	0.0000
34-4	06J06-5	0.1591	0.0006	0.0802	0.0004	0.0001	0.0000
34-4, rep	06J06-5	0.1597	0.0007	0.0808	0.0006	0.0002	0.0001
60-1	06J06-6	0.1436	0.0005	0.0810	0.0009	0.0012	0.0001
60-2	06J06-6	0.1485	0.0009	0.0815	0.0011	0.0032	0.0011
60-3	06J06-6	0.1103	0.0007	0.0777	0.0008	0.0018	0.0004
60-3, rep	06J06-6	0.1112	0.0006	0.0787	0.0014	0.0350	0.0166
14-1	06J06-7	0.1143	0.0005	0.0858	0.0010	0.0033	0.0016
14-2	06J06-7	0.1237	0.0014	0.0803	0.0022	0.0029	0.0006
14-2, rep	06J06-7	0.1265	0.0013	0.0773	0.0028	0.0617	0.0383
14-3	06J06-7	0.0943	0.0022	0.0772	0.0007	0.0005	0.0001
14-3, rep	06J06-7	0.0965	0.0005	0.0764	0.0009	0.0151	0.0038
14-4	06J06-7	0.1279	0.0015	0.0860	0.0026	0.0001	0.0001
72-1	09J10-8	0.0989	0.0019	0.0849	0.0006	0.0020	0.0014
72-1, rep	09J10-8	0.1016	0.0006	0.0883	0.0034	0.0100	0.0064
72-2	09J10-8	0.0982	0.0007	0.0802	0.0010	0.0003	0.0000
75-1	06J06-2	0.1098	0.0008	0.0769	0.0012	0.0003	0.0001

Table 2-3a. Measured Isotope Ratios (con't)							
Sample	channel ID	49/48	error	50/48	error	52/48	error
75-2	06J06-2	0.1302	0.0005	0.0832	0.0007	0.0011	0.0002
75-3	06J06-2	0.0790	0.0006	0.0734	0.0007	0.0084	0.0055
19-1	06J06-1	0.0924	0.0005	0.0764	0.0005	0.0022	0.0003
19-2	06J06-1	0.1033	0.0005	0.0816	0.0013	0.0010	0.0003
19-3	06J06-1	0.0937	0.0004	0.0772	0.0004	0.0005	0.0001
76-1	09J10-1	0.0789	0.0004	0.0726	0.0003	0.0011	0.0002
76-2	09J10-1	0.1038	0.0004	0.0817	0.0013	0.0044	0.0008
76-2, rep	09J10-1	0.1004	0.0020	0.0799	0.0027	0.0047	0.0009
76-3	09J10-1	0.1083	0.0003	0.0811	0.0007	0.0029	0.0002
76-3, rep	09J10-1	0.1083	0.0005	0.0816	0.0002	0.0022	0.0010
76-4	09J10-1	0.1069	0.0006	0.0774	0.0005	0.0032	0.0006
7-1	09J10-3	0.1279	0.0007	0.0790	0.0006	0.0078	0.0013
7-2	09J10-3	0.0908	0.0015	0.0799	0.0035	0.0424	0.0186
7-2, rep	09J10-3	0.0896	0.0009	0.0753	0.0020	0.0287	0.0029
7-3	09J10-3	0.1541	0.0009	0.0827	0.0009	0.0066	0.0010
7-4	09J10-3	0.0941	0.0004	0.0745	0.0004	0.0054	0.0010
7-4, rep	09J10-3	0.0937	0.0009	0.0749	0.0006	0.0112	0.0034
12-1	06J06-3	0.0929	0.0013	0.0768	0.0022	0.0072	0.0014
12-2	06J06-3	0.0916	0.0009	0.0759	0.0004	0.0002	0.0000
12-3	06J06-3	0.0849	0.0004	0.0743	0.0004	0.0049	0.0031
12-3, rep	06J06-3	0.0856	0.0004	0.0737	0.0005	0.0037	0.0008
12-4	06J06-3	0.1010	0.0005	0.0781	0.0005	0.0029	0.0007
37-2	09J10-5	0.1699	0.0005	0.0882	0.0008	0.0048	0.0013
37-3	09J10-5	0.1789	0.0005	0.0872	0.0025	0.0007	0.0004
37-4	09J10-5	0.1689	0.0003	0.0858	0.0012	0.0057	0.0016
10-2	09J10-6	0.1601	0.0006	0.0850	0.0011	0.0035	0.0012
10-3	09J10-6	0.1579	0.0004	0.0840	0.0011	0.0059	0.0027
4-2	09J10-2	0.0881	0.0005	0.0750	0.0011	0.0187	0.0077
4-3	09J10-2	0.0999	0.0007	0.0786	0.0008	0.0083	0.0026
4-4	09J10-2	0.0945	0.0018	0.0739	0.0016	0.0154	0.0074
4-4, rep	09J10-2	0.0986	0.0005	0.0771	0.0011	0.0240	0.0075
70-2	01J08-2	0.1000	0.0004	0.0835	0.0010	0.0027	0.0005

Table 2-3a. Measured Isotope Ratios (con't)							
Sample	channel ID	49/48	error	50/48	error	52/48	error
70-3	01J08-2	0.1001	0.0008	0.0837	0.0010	0.0080	0.0022
70-4	01J08-2	0.0988	0.0008	0.0849	0.0018	0.0061	0.0014
3-2	01J08-8	0.0880	0.0007	0.0852	0.0013	0.0046	0.0007
3-3	01J08-8	0.0846	0.0008	0.0798	0.0016	0.0092	0.0042
11-2	01J08-1	0.0863	0.0007	0.0810	0.0006	0.0045	0.0010
11-3	01J08-1	0.0850	0.0005	0.0795	0.0005	0.0066	0.0021
11-4	01J08-1	0.0868	0.0005	0.0866	0.0034	0.0101	0.0129
51-2	02J07-8	0.0981	0.0006	0.0827	0.0025	0.0062	0.0018
51-3	02J07-8	0.0996	0.0005	0.0866	0.0024	0.0061	0.0018
51-4	02J07-8	0.0949	0.0003	0.0870	0.0007	0.0046	0.0012
23-2	09J10-7	0.1287	0.0004	0.0798	0.0009	0.0023	0.0009
23-3	09J10-7	0.1269	0.0012	0.0795	0.0009	0.0019	0.0010
23-4	09J10-7	0.1264	0.0007	0.0795	0.0005	0.0055	0.0019
27-2	01J08-6	0.1094	0.0007	0.0783	0.0014	0.0030	0.0016
27-3	01J08-6	0.1100	0.0006	0.0792	0.0006	0.0003	0.0005
48-2	11N11-1	0.1171	0.0006	0.0840	0.0007	0.0048	0.0008
48-3	11N11-1	0.1179	0.0010	0.0873	0.0010	0.0079	0.0017
74-2	08J07-7	0.1281	0.0008	0.0827	0.0010	0.0068	0.0027
74-3	08J07-7	0.1304	0.0007	0.0856	0.0015	0.0078	0.0031
18-2	09J10-6	0.1208	0.0006	0.0779	0.0005	0.0046	0.0017
18-3	09J10-6	0.1197	0.0007	0.0789	0.0006	0.0109	0.0015
24-2	01J08-3	0.0934	0.0004	0.0798	0.0006	0.0035	0.0014
24-3	01J08-3	0.1000	0.0007	0.0829	0.0006	0.0095	0.0024
24-4	01J08-3	0.1087	0.0007	0.0834	0.0020	0.0038	0.0034
21-2	02J07-5	0.1521	0.0005	0.0879	0.0007	0.0018	0.0004
21-3	02J07-5	0.1186	0.0004	0.0807	0.0006	0.0026	0.0011
21-4	02J07-5	0.0982	0.0005	0.0784	0.0006	0.0173	0.0035
52-2	08J07-5	0.1862	0.0004	0.0882	0.0009	0.0113	0.0049
52-3	08J07-5	0.1850	0.0007	0.0852	0.0007	0.0054	0.0020
15-2	02J07-3	0.1246	0.0009	0.0815	0.0009	0.0088	0.0033
15-3	02J07-3	0.1416	0.0007	0.0866	0.0009	0.0008	0.0001
15-4	02J07-3	0.1377	0.0006	0.0822	0.0008	0.0027	0.0008

Table 2-3a. Measured Isotope Ratios (con't)							
Sample	channel ID	49/48	error	50/48	error	52/48	error
13-2	02J07-4	0.1139	0.0006	0.0778	0.0004	0.0109	0.0021
13-3	02J07-4	0.1492	0.0009	0.0824	0.0006	0.0023	0.0005
13-4	02J07-4	0.1551	0.0008	0.0831	0.0005	0.0037	0.0011
84-2	02J07-1	0.1010	0.0004	0.0847	0.0011	0.0067	0.0013
84-3	02J07-1	0.1010	0.0004	0.0845	0.0008	0.0020	0.0003
32-2	02J07-6	0.1409	0.0005	0.0824	0.0006	0.0077	0.0031
32-3	02J07-6	0.1409	0.0006	0.0836	0.0008	0.0041	0.0013
32-4	02J07-6	0.1348	0.0004	0.0824	0.0006	0.0109	0.0034
59-2	08J07-8	0.1009	0.0007	0.0827	0.0012	0.0048	0.0019
59-3	08J07-8	0.0752	0.0005	0.0733	0.0005	0.0001	0.0000
50-2	02J07-2	0.1206	0.0005	0.0777	0.0007	0.0031	0.0018
68-2	06J06-6	0.1149	0.0005	0.0902	0.0029	0.0035	0.0017
68-3	06J06-6	0.1140	0.0007	0.0870	0.0011	0.0034	0.0013
30-2	01J08-7	0.0953	0.0005	0.0775	0.0007	0.0035	0.0010
30-3	01J08-7	0.0794	0.0006	0.0740	0.0005	0.0064	0.0013
30-4	01J08-7	0.0992	0.0011	0.0780	0.0008	0.0054	0.0007
80-2	08J07-6	0.1539	0.0010	0.0814	0.0003	0.0052	0.0021
9-2	04J07-8	0.1060	0.0005	0.0817	0.0006	0.0040	0.0006
9-3	04J07-8	0.0956	0.0004	0.0814	0.0012	0.0100	0.0028
9-4	04J07-8	0.1073	0.0006	0.0854	0.0005	0.0080	0.0019
46-2	04J07-7	0.1239	0.0008	0.0864	0.0012	0.0026	0.0005
46-3	04J07-7	0.1301	0.0005	0.0848	0.0005	0.0068	0.0011
46-4	04J07-7	0.1315	0.0007	0.0850	0.0006	0.0041	0.0008
1-2	04J07-6	0.1411	0.0007	0.0868	0.0009	0.0024	0.0025
1-3	04J07-6	0.1370	0.0004	0.0873	0.0012	0.0042	0.0012
17-2	04J07-1	0.1108	0.0006	0.0825	0.0004	0.0018	0.0007
17-3	04J07-1	0.1129	0.0008	0.0852	0.0013	0.0030	0.0007
17-4	04J07-1	0.1107	0.0007	0.0829	0.0006	0.0075	0.0017
25-2	04J07-4	0.1537	0.0005	0.0812	0.0003	0.0068	0.0009
25-3	04J07-4	0.1854	0.0007	0.0855	0.0005	0.0063	0.0012
25-3, rep	04J07-4	0.1859	0.0013	0.0857	0.0008	0.0155	0.0017
25-4	04J07-4	0.1865	0.0008	0.0858	0.0007	0.0142	0.0047

Table 2-3a. Measured Isotope Ratios (con't)							
Sample	channel ID	49/48	error	50/48	error	52/48	error
83-2	04J07-3	0.1627	0.0008	0.0823	0.0004	0.0066	0.0011
83-3	04J07-3	0.1701	0.0007	0.0867	0.0012	0.0041	0.0013
83-4	04J07-3	0.1572	0.0007	0.0817	0.0003	0.0058	0.0017
6-2	04J07-2	0.1371	0.0013	0.0905	0.0033	0.0187	0.0116
6-3	04J07-2	0.1379	0.0007	0.0832	0.0016	0.0012	0.0006
55-2	04J07-5	0.1665	0.0008	0.0856	0.0010	0.0114	0.0034
55-3	04J07-5	0.1558	0.0009	0.0843	0.0009	0.0102	0.0035
71-2	01J08-4	0.0993	0.0003	0.0833	0.0007	0.0094	0.0022
79-2	04J07-4	0.1626	0.0007	0.0861	0.0007	0.0053	0.0020
79-3	04J07-4	0.1765	0.0005	0.0877	0.0012	0.0080	0.0025
79-4	04J07-4	0.1654	0.0007	0.0842	0.0006	0.0016	0.0005
42-1	09J10-4	0.1613	0.0012	0.0863	0.0011		
42-2	09J10-4	0.1055	0.0012	0.0899	0.0036		
42-3	09J10-4	0.1708	0.0012	0.0836	0.0009		
42-3, rep	09J10-4	0.1697	0.0013	0.0837	0.0010		
42-4	09J10-4	0.1666	0.0007	0.0844	0.0011		
42-5	09J10-4	0.1479	0.0012	0.0840	0.0008		
42-5, rep	09J10-4	0.1476	0.0010	0.0814	0.0006		
77-1	09J10-4	0.1725	0.0008	0.0846	0.0007		
77-2	09J10-4	0.1698	0.0006	0.0849	0.0009		
77-3	09J10-4	0.1753	0.0004	0.0879	0.0015		
77-4	09J10-4	0.1773	0.0014	0.0889	0.0010		
77-5	09J10-4	0.1701	0.0006	0.0869	0.0006		
Second Half-plane, channels 10G06, 11E07, 12C06							
67	11E07-7	0.1300	0.0007	0.0795	0.0005	0.0030	0.0005
56	11E07-8	0.1063	0.0004	0.0752	0.0003	0.0017	0.0007
35	11E07-3	0.1571	0.0004	0.0814	0.0006	0.0056	0.0038
38	11E07-5	0.1695	0.0007	0.0817	0.0004	0.0025	0.0009
62	11E07-1	0.0789	0.0006	0.0828	0.0096	0.0025	0.0007
5	11E07-4	0.1777	0.0009	0.0828	0.0004	0.0049	0.0011
8	11E07-2	0.1322	0.0005	0.0789	0.0006	0.0023	0.0018
54	11E07-6	0.1406	0.0006	0.0794	0.0004	0.0001	0.0000

Table 2-3a. Measured Isotope Ratios (con't)							
Sample	channel ID	49/48	error	50/48	error	52/48	error
33	12C06-3	0.1395	0.0003	0.0786	0.0005	0.0023	0.0007
89	12C06-4	0.1357	0.0007	0.0805	0.0011	0.0317	0.0140
78	12C06-5	0.1358	0.0005	0.0841	0.0015	0.0054	0.0026
58	12C06-4	0.1369	0.0007	0.0798	0.0010	0.0181	0.0059
28	12C06-6	0.1412	0.0010	0.0797	0.0007	0.0033	0.0025
29	12C06-7	0.1205	0.0004	0.0774	0.0005	0.0006	0.0003
65	12C06-2	0.1260	0.0006	0.0770	0.0005	0.0060	0.0033
31	12C06-8	0.1049	0.0005	0.0763	0.0004	0.0047	0.0005
22	12C06-1	0.1014	0.0003	0.0749	0.0002	0.0022	0.0005
49	10G06-8	0.1018	0.0004	0.0747	0.0002	0.0007	0.0008
88	10G06-5	0.1809	0.0006	0.0835	0.0005	0.0151	0.0020
20	10G06-1	0.1127	0.0004	0.0757	0.0003	0.0001	0.0000
47	10G06-4	0.1687	0.0005	0.0880	0.0010	0.0126	0.0043
81	10G06-7	0.1272	0.0010	0.0816	0.0008	0.0430	0.0145
16	10G06-6	0.1597	0.0009	0.0827	0.0007	0.0531	0.0331
43	10G06-3	0.1345	0.0005	0.0790	0.0004	0.0013	0.0016
Third Half-plane, channels 11N11, 12Q06							
40	11N11-1	0.1050	0.0005	0.0749	0.0004	0.0068	0.0031
44	11N11-4	0.1754	0.0006	0.0813	0.0004	0.0058	0.0030
90	11N11-9	0.1413	0.0005	0.0788	0.0003	0.0049	0.0020
69	11N11-7	0.1314	0.0009	0.0815	0.0008	0.0270	0.0030
66	11N11-2	0.1356	0.0005	0.0781	0.0004	0.0007	0.0001
41	11N11-3	0.1002	0.0004	0.0770	0.0005	0.0092	0.0029
61	11N11-8	0.0888	0.0003	0.0768	0.0003	0.0059	0.0013
82	11N11-6	0.1536	0.0005	0.0798	0.0003	0.0105	0.0046
45	12Q06-1	0.0976	0.0003	0.0836	0.0016	0.0073	0.0039
53	12Q06-4	0.1280	0.0005	0.0798	0.0007	0.0144	0.0017
87	12Q06-4	0.1570	0.0004	0.0805	0.0005	0.0026	0.0012
63	12Q06-7	0.1174	0.0008	0.0783	0.0009	0.0024	0.0013
73	12Q06-5	0.1650	0.0008	0.0879	0.0014	0.0089	0.0040
39	12Q06-2	0.1075	0.0004	0.0749	0.0004	0.0043	0.0025
36	12Q06-3	0.1242	0.0004	0.0780	0.0003	0.0009	0.0003

Table 2-3a. Measured Isotope Ratios (con't)							
Sample	channel ID	49/48	error	50/48	error	52/48	error
64	12Q06-6	0.1167	0.0003	0.0782	0.0004	0.0087	0.0004
57	12Q06-8	0.1048	0.0005	0.0783	0.0012	0.0032	0.0034

Table 2-3b. Corrected Atom %						
sample	channel ID	46	47	48	49	50
86-1	06J06-4	8.231%	7.295%	70.046%	8.541%	5.886%
86-1,rep	06J06-4	8.226%	7.312%	70.205%	8.732%	5.524%
86-2	06J06-4	8.158%	7.310%	69.427%	8.777%	6.329%
86-2,rep	06J06-4	8.172%	7.308%	69.727%	8.854%	5.938%
86-2,rep	06J06-4	8.047%	7.262%	69.927%	8.757%	6.007%
86-3	06J06-4	8.227%	7.302%	69.506%	9.177%	5.789%
86-3,rep	06J06-4	8.100%	7.211%	69.320%	9.012%	6.357%
2-1	06J06-4	8.232%	7.325%	69.135%	9.639%	5.669%
2-2	06J06-4	8.215%	7.329%	70.249%	8.586%	5.621%
2-3	06J06-4	8.206%	7.290%	68.863%	9.674%	5.968%
26-1	06J06-8	8.104%	7.342%	71.639%	7.446%	5.469%
26-2	06J06-8	8.095%	7.306%	71.673%	7.474%	5.452%
34-1	06J06-5	8.273%	7.315%	68.239%	10.707%	5.466%
34-2	06J06-5	8.150%	7.336%	70.009%	9.147%	5.358%
34-2,rep	06J06-5	8.144%	7.322%	69.979%	9.181%	5.374%
34-3	06J06-5	8.228%	7.324%	69.074%	9.932%	5.442%
34-4	06J06-5	8.232%	7.302%	68.155%	10.841%	5.469%
34-4,rep	06J06-5	8.264%	7.317%	68.050%	10.870%	5.499%

Table 2-3b. Corrected Atom % (con't)						
sample	channel ID	46	47	48	49	50
60-1	06J06-6	8.164%	7.304%	69.032%	9.913%	5.588%
60-2	06J06-6	8.110%	7.284%	68.799%	10.214%	5.593%
60-3	06J06-6	8.164%	7.331%	71.135%	7.850%	5.520%
60-3,rep	06J06-6	8.145%	7.343%	71.130%	7.913%	5.469%
14-1	06J06-7	8.173%	7.327%	70.420%	8.049%	6.032%
14-2	06J06-7	8.022%	7.160%	70.450%	8.719%	5.650%
14-2,rep	06J06-7	8.222%	7.361%	70.312%	8.897%	5.208%
14-3	06J06-7	8.205%	7.383%	72.051%	6.796%	5.565%
14-3,rep	06J06-7	8.116%	7.359%	72.108%	6.961%	5.456%
14-4	06J06-7	8.142%	7.253%	69.700%	8.913%	5.992%
72-1	09J10-8	8.114%	7.308%	71.453%	7.066%	6.059%
72-1, rep	09J10-8	8.017%	7.259%	71.235%	7.235%	6.254%
72-2	09J10-8	8.065%	7.294%	71.825%	7.053%	5.762%
75-1	06J06-2	8.089%	7.306%	71.294%	7.828%	5.484%
75-2	06J06-2	8.173%	7.305%	69.659%	9.069%	5.794%
75-3	06J06-2	8.150%	7.365%	73.329%	5.799%	5.356%
19-1	06J06-1	8.079%	7.322%	72.386%	6.691%	5.522%
19-2	06J06-1	8.141%	7.321%	71.345%	7.372%	5.821%
19-3	06J06-1	8.093%	7.352%	72.208%	6.773%	5.574%
76-1	09J10-1	8.123%	7.366%	73.390%	5.794%	5.327%
76-2	09J10-1	8.101%	7.287%	71.376%	7.415%	5.820%
76-2,rep	09J10-1	8.039%	7.221%	71.803%	7.215%	5.722%
76-3	09J10-1	8.138%	7.326%	71.080%	7.700%	5.756%
76-3,rep	09J10-1	8.174%	7.332%	70.990%	7.706%	5.799%
76-4	09J10-1	8.103%	7.320%	71.418%	7.636%	5.523%
7-1	09J10-3	8.175%	7.326%	70.029%	8.961%	5.509%
7-2	09J10-3	7.970%	7.282%	72.523%	6.588%	5.637%
7-2,rep	09J10-3	8.063%	7.326%	72.727%	6.515%	5.369%
7-3	09J10-3	8.091%	7.206%	68.488%	10.567%	5.648%
7-4	09J10-3	8.104%	7.347%	72.373%	6.809%	5.368%
7-4,rep	09J10-3	8.075%	7.343%	72.412%	6.787%	5.385%
12-1	06J06-3	8.100%	7.310%	72.326%	6.729%	5.535%

Table 2-3b. Corrected Atom % (con't)						
sample	channel ID	46	47	48	49	50
12-2	06J06-3	8.142%	7.354%	72.378%	6.631%	5.495%
12-3	06J06-3	8.130%	7.322%	72.949%	6.194%	5.405%
12-3,rep	06J06-3	8.141%	7.375%	72.887%	6.242%	5.355%
12-4	06J06-3	8.169%	7.359%	71.648%	7.238%	5.586%
37-2	09J10-5	8.188%	7.257%	67.219%	11.421%	5.916%
37-3	09J10-5	8.147%	7.229%	66.838%	11.960%	5.825%
37-4	09J10-5	8.173%	7.258%	67.414%	11.390%	5.765%
10-2	09J10-6	8.196%	7.265%	67.908%	10.872%	5.759%
10-3	09J10-6	8.223%	7.296%	68.037%	10.745%	5.699%
4-2	09J10-2	8.057%	7.322%	72.811%	6.420%	5.391%
4-3	09J10-2	8.020%	7.270%	71.906%	7.184%	5.619%
4-4	09J10-2	7.883%	7.078%	72.823%	6.888%	5.327%
4-4,rep	09J10-2	8.151%	7.369%	71.919%	7.101%	5.459%
70-2	01J08-2	8.107%	7.319%	71.469%	7.150%	5.955%
70-3	01J08-2	8.138%	7.386%	71.373%	7.149%	5.954%
70-4	01J08-2	8.070%	7.295%	71.524%	7.064%	6.048%
3-2	01J08-8	8.128%	7.349%	72.054%	6.345%	6.125%
3-3	01J08-8	8.132%	7.389%	72.573%	6.143%	5.763%
11-2	01J08-1	8.077%	7.331%	72.480%	6.256%	5.855%
11-3	01J08-1	8.082%	7.344%	72.647%	6.173%	5.755%
11-4	01J08-1	8.095%	7.319%	72.109%	6.263%	6.215%
51-2	02J07-8	8.098%	7.335%	71.640%	7.027%	5.900%
51-3	02J07-8	8.059%	7.312%	71.364%	7.107%	6.158%
51-4	02J07-8	8.076%	7.324%	71.595%	6.794%	6.211%
23-2	09J10-7	8.217%	7.336%	69.880%	8.998%	5.570%
23-3	09J10-7	8.199%	7.325%	70.031%	8.887%	5.559%
23-4	09J10-7	8.171%	7.316%	70.094%	8.865%	5.555%
27-2	01J08-6	8.121%	7.346%	71.179%	7.790%	5.563%
27-3	01J08-6	8.140%	7.329%	71.086%	7.817%	5.627%
48-2	01J08-5	8.081%	7.329%	70.443%	8.247%	5.900%
48-3	01J08-5	8.106%	7.300%	70.214%	8.278%	6.102%
74-2	08J07-7	8.121%	7.300%	69.877%	8.950%	5.752%

Table 2-3b. Corrected Atom % (con't)						
sample	channel ID	46	47	48	49	50
74-3	08J07-7	8.117%	7.300%	69.584%	9.071%	5.928%
18-2	02J07-7	8.131%	7.322%	70.549%	8.520%	5.479%
18-3	02J07-7	8.129%	7.321%	70.571%	8.448%	5.531%
24-2	01J08-3	8.101%	7.342%	72.088%	6.732%	5.737%
24-3	01J08-3	8.099%	7.323%	71.521%	7.159%	5.897%
24-4	01J08-3	8.105%	7.279%	70.996%	7.717%	5.904%
21-2	02J07-5	8.226%	7.279%	68.149%	10.365%	5.981%
21-3	02J07-5	8.149%	7.298%	70.508%	8.363%	5.681%
21-4	02J07-5	8.100%	7.338%	71.925%	7.063%	5.575%
52-2	08J07-5	8.192%	7.255%	66.382%	12.359%	5.813%
52-3	08J07-5	8.184%	7.261%	66.584%	12.319%	5.653%
15-2	02J07-3	8.174%	7.307%	70.097%	8.735%	5.687%
15-3	02J07-3	8.147%	7.268%	68.871%	9.754%	5.959%
15-4	02J07-3	8.171%	7.303%	69.298%	9.543%	5.684%
13-2	02J07-4	8.135%	7.334%	70.966%	8.082%	5.482%
13-3	02J07-4	8.172%	7.312%	68.619%	10.244%	5.653%
13-4	02J07-4	8.149%	7.282%	68.309%	10.599%	5.662%
84-2	02J07-1	8.071%	7.290%	71.405%	7.214%	6.020%
84-3	02J07-1	8.048%	7.319%	71.402%	7.208%	6.023%
32-2	02J07-6	8.181%	7.302%	69.109%	9.738%	5.670%
32-3	02J07-6	8.202%	7.309%	69.011%	9.725%	5.753%
32-4	02J07-6	8.231%	7.312%	69.415%	9.358%	5.684%
59-2	08J07-8	8.129%	7.326%	71.445%	7.206%	5.893%
59-3	08J07-8	8.015%	7.328%	73.710%	5.547%	5.400%
50-2	02J07-2	8.175%	7.331%	70.521%	8.503%	5.470%
68-2	01J08-4	8.084%	7.282%	70.240%	8.071%	6.322%
68-3	01J08-4	8.046%	7.260%	70.534%	8.040%	6.121%
30-2	01J08-7	8.153%	7.356%	72.049%	6.869%	5.573%
30-3	01J08-7	8.074%	7.374%	73.328%	5.825%	5.400%
30-4	01J08-7	8.118%	7.352%	71.820%	7.129%	5.581%
80-2	08J07-6	8.163%	7.277%	68.470%	10.536%	5.553%
9-2	04J07-8	8.062%	7.309%	71.269%	7.553%	5.807%

Table 2-3b. Corrected Atom % (con't)						
sample	channel ID	46	47	48	49	50
9-3	04J07-8	8.099%	7.344%	71.867%	6.874%	5.816%
9-4	04J07-8	8.112%	7.311%	70.933%	7.613%	6.031%
46-2	04J07-7	8.155%	7.282%	69.873%	8.662%	6.028%
46-3	04J07-7	8.187%	7.305%	69.575%	9.055%	5.878%
46-4	04J07-7	8.163%	7.299%	69.505%	9.137%	5.895%
1-2	04J07-6	8.123%	7.272%	68.908%	9.724%	5.973%
1-3	04J07-6	8.158%	7.276%	69.084%	9.466%	6.015%
17-2	04J07-1	8.130%	7.300%	70.875%	7.851%	5.844%
17-3	04J07-1	8.097%	7.273%	70.646%	7.974%	6.010%
17-4	04J07-1	8.147%	7.320%	70.847%	7.842%	5.844%
25-2	04J07-4	8.248%	7.288%	68.418%	10.517%	5.528%
25-3	04J07-4	8.321%	7.266%	66.434%	12.320%	5.659%
25-3,rep	04J07-4	8.283%	7.257%	66.465%	12.355%	5.640%
25-4	04J07-4	8.308%	7.267%	66.398%	12.382%	5.646%
83-2	04J07-3	8.198%	7.284%	67.905%	11.047%	5.566%
83-3	04J07-3	8.233%	7.259%	67.251%	11.440%	5.817%
83-4	04J07-3	8.166%	7.251%	68.291%	10.735%	5.556%
6-2	04J07-2	8.040%	7.202%	69.099%	9.471%	6.187%
6-3	04J07-2	8.207%	7.297%	69.199%	9.545%	5.751%
55-2	04J07-5	8.187%	7.286%	67.537%	11.246%	5.743%
55-3	04J07-5	8.205%	7.283%	68.179%	10.622%	5.711%
71-2	01J08-4	8.095%	7.299%	71.569%	7.109%	5.929%
79-2	04J07-4	8.277%	7.292%	67.626%	10.997%	5.807%
79-3	04J07-4	8.311%	7.250%	66.812%	11.796%	5.831%
79-4	04J07-4	8.278%	7.292%	67.570%	11.178%	5.682%
42-1	09J10-4	8.134%	7.204%	67.859%	10.944%	5.859%
42-2	09J10-4	7.870%	7.183%	71.065%	7.495%	6.386%
42-3	09J10-4	8.190%	7.216%	67.438%	11.520%	5.635%
42-3,rep	09J10-4	8.206%	7.223%	67.477%	11.449%	5.645%
42-4	09J10-4	8.133%	7.245%	67.643%	11.268%	5.711%
42-5	09J10-4	8.096%	7.245%	68.727%	10.161%	5.771%
42-5,rep	09J10-4	8.165%	7.253%	68.822%	10.161%	5.599%

Table 2-3b. Corrected Atom % (con't)						
sample	channel ID	46	47	48	49	50
77-1	09J10-4	8.267%	7.267%	67.193%	11.591%	5.683%
77-2	09J10-4	8.266%	7.245%	67.341%	11.433%	5.715%
77-3	09J10-4	8.288%	7.255%	66.855%	11.723%	5.879%
77-4	09J10-4	8.262%	7.228%	66.744%	11.833%	5.934%
77-5	09J10-4	8.262%	7.240%	67.224%	11.435%	5.839%
Second Half-plane, channels 10G06, 11E07, 12C06						
67	11E07-7	7.979%	7.268%	70.085%	9.109%	5.560%
56	11E07-8	8.129%	7.359%	71.534%	7.607%	5.372%
35	11E07-3	8.185%	7.299%	68.254%	10.725%	5.536%
38	11E07-5	8.196%	7.290%	67.550%	11.453%	5.512%
62	11E07-1	7.990%	7.328%	72.903%	5.749%	6.030%
5	11E07-4	8.132%	7.268%	67.131%	11.928%	5.541%
8	11E07-2	8.147%	7.312%	69.812%	9.226%	5.503%
54	11E07-6	8.090%	7.304%	69.350%	9.750%	5.506%
33	12C06-3	8.126%	7.301%	69.434%	9.687%	5.451%
89	12C06-4	8.037%	7.292%	69.711%	9.464%	5.496%
78	12C06-5	8.028%	7.275%	69.439%	9.434%	5.824%
58	12C06-4	8.066%	7.297%	69.619%	9.528%	5.489%
28	12C06-6	8.089%	7.291%	69.318%	9.787%	5.514%
29	12C06-7	8.099%	7.326%	70.602%	8.511%	5.462%
65	12C06-2	8.148%	7.347%	70.261%	8.852%	5.391%
31	12C06-8	8.076%	7.286%	71.663%	7.521%	5.453%
22	12C06-1	8.168%	7.382%	71.788%	7.284%	5.377%
49	10G06-8	8.108%	7.361%	71.853%	7.315%	5.362%
88	10G06-5	8.148%	7.261%	66.941%	12.114%	5.536%
20	10G06-1	8.102%	7.340%	71.153%	8.017%	5.388%
47	10G06-4	8.161%	7.265%	67.332%	11.357%	5.885%
81	10G06-7	8.036%	7.267%	70.187%	8.936%	5.574%
16	10G06-6	8.055%	7.298%	68.277%	10.911%	5.460%
43	10G06-3	8.046%	7.299%	69.760%	9.387%	5.508%
Third Half-plane, channels 11N11, 12Q06						
40	11N11-1	8.149%	7.376%	71.613%	7.523%	5.339%

Table 2-3b. Corrected Atom % (con't)						
sample	channel ID	46	47	48	49	50
44	11N11-4	8.196%	7.284%	67.275%	11.798%	5.448%
90	11N11-5	8.127%	7.314%	69.318%	9.795%	5.447%
69	11N11-7	8.057%	7.282%	69.878%	9.185%	5.598%
66	11N11-2	8.097%	7.329%	69.686%	9.449%	5.438%
41	11N11-3	8.091%	7.340%	71.870%	7.201%	5.497%
61	11N11-8	8.064%	7.347%	72.592%	6.445%	5.551%
82	11N11-6	8.138%	7.311%	68.578%	10.535%	5.438%
45	12Q06-1	8.077%	7.337%	71.631%	6.990%	5.965%
53	12Q06-4	8.065%	7.305%	70.114%	8.972%	5.544%
87	12Q06-4	8.177%	7.325%	68.290%	10.721%	5.488%
63	12Q06-7	8.059%	7.306%	70.792%	8.310%	5.533%
73	12Q06-5	8.106%	7.251%	67.579%	11.151%	5.913%
39	12Q06-2	8.110%	7.357%	71.505%	7.687%	5.342%
36	12Q06-3	8.099%	7.324%	70.351%	8.740%	5.486%
64	12Q06-6	8.100%	7.333%	70.804%	8.261%	5.502%
57	12Q06-8	8.040%	7.320%	71.551%	7.499%	5.590%

Table 2-3c. Corrected Isotope Ratios									
sample	channel ID	$^{46}Ti/^{48}Ti$	error	$^{47}Ti/^{48}Ti$	error	$^{49}Ti/^{48}Ti$	error	$^{50}Ti/^{48}Ti$	error
86-1	06J06-4	0.11608	0.00092	0.10303	0.00077	0.12285	0.00097	0.08515	0.00384
86-1,rep	06J06-4	0.11575	0.00074	0.10304	0.00053	0.12532	0.00057	0.07972	0.00099
86-2	06J06-4	0.11606	0.00075	0.10416	0.00057	0.12736	0.00068	0.09236	0.00333
86-2,rep	06J06-4	0.11577	0.00082	0.10369	0.00049	0.12794	0.00067	0.08628	0.00129
86-2,rep	06J06-4	0.11367	0.00096	0.10274	0.00025	0.12617	0.00126	0.08704	0.00098
2-1	06J06-4	0.11761	0.00074	0.10482	0.00043	0.14047	0.00066	0.08309	0.00117
2-2	06J06-4	0.11551	0.00056	0.10322	0.00041	0.12314	0.00060	0.08107	0.00105
2-3	06J06-4	0.11771	0.00031	0.10473	0.00031	0.14153	0.00053	0.08780	0.00189
26-1	06J06-8	0.11173	0.00034	0.10139	0.00029	0.10471	0.00034	0.07735	0.00053
26-2	06J06-8	0.11157	0.00063	0.10084	0.00053	0.10506	0.00069	0.07707	0.00029
34-1	06J06-5	0.11975	0.00045	0.10605	0.00040	0.15808	0.00061	0.08116	0.00043
34-2	06J06-5	0.11499	0.00098	0.10366	0.00082	0.13163	0.00158	0.07755	0.00062
34-2,rep	06J06-5	0.11496	0.00104	0.10352	0.00061	0.13218	0.00147	0.07781	0.00085
34-3	06J06-5	0.11766	0.00051	0.10490	0.00050	0.14486	0.00071	0.07983	0.00033
34-4	06J06-5	0.11931	0.00042	0.10599	0.00042	0.16026	0.00064	0.08130	0.00040
34-4,rep	06J06-5	0.11996	0.00044	0.10637	0.00052	0.16093	0.00066	0.08188	0.00057
60-1	06J06-6	0.11681	0.00055	0.10468	0.00052	0.14467	0.00047	0.08201	0.00091
60-2	06J06-6	0.11644	0.00069	0.10474	0.00064	0.14957	0.00088	0.08237	0.00112
60-3	06J06-6	0.11337	0.00053	0.10195	0.00059	0.11117	0.00066	0.07862	0.00079
60-3,rep	06J06-6	0.11311	0.00056	0.10213	0.00064	0.11208	0.00057	0.07790	0.00136
14-1	06J06-7	0.11464	0.00037	0.10293	0.00033	0.11515	0.00048	0.08678	0.00104
14-2	06J06-7	0.11247	0.00114	0.10054	0.00092	0.12468	0.00138	0.08125	0.00227
14-2,rep	06J06-7	0.11550	0.00157	0.10357	0.00105	0.12748	0.00135	0.07505	0.00273
14-3	06J06-7	0.11249	0.00175	0.10138	0.00070	0.09502	0.00224	0.07825	0.00073
14-3,rep	06J06-7	0.11118	0.00067	0.10097	0.00052	0.09725	0.00055	0.07666	0.00086
14-4	06J06-7	0.11538	0.00070	0.10295	0.00061	0.12883	0.00147	0.08711	0.00266
72-1	09J10-8	0.11216	0.00173	0.10118	0.00083	0.09963	0.00191	0.08591	0.00058
72-1, rep	09J10-8	0.11117	0.00076	0.10081	0.00061	0.10232	0.00063	0.08895	0.00346
72-2	09J10-8	0.11092	0.00059	0.10047	0.00065	0.09893	0.00067	0.08129	0.00103
75-1	06J06-2	0.11207	0.00077	0.10138	0.00056	0.11063	0.00085	0.07793	0.00117
75-2	06J06-2	0.11590	0.00076	0.10375	0.00073	0.13116	0.00053	0.08427	0.00070
75-3	06J06-2	0.10978	0.00037	0.09937	0.00071	0.07968	0.00065	0.07401	0.00073

Table 2-3c. Corrected Isotope Ratios (con't)									
sample	channel ID	$^{46}Ti/^{48}Ti$	error	$^{47}Ti/^{48}Ti$	error	$^{49}Ti/^{48}Ti$	error	$^{50}Ti/^{48}Ti$	error
19-1	06J06-1	0.11024	0.00094	0.10007	0.00086	0.09312	0.00055	0.07729	0.00050
19-2	06J06-1	0.11271	0.00057	0.10152	0.00040	0.10410	0.00051	0.08267	0.00128
19-3	06J06-1	0.11071	0.00029	0.10073	0.00030	0.09450	0.00040	0.07821	0.00040
76-1	09J10-1	0.10932	0.00075	0.09930	0.00045	0.07954	0.00039	0.07354	0.00031
76-2	09J10-1	0.11211	0.00095	0.10101	0.00041	0.10466	0.00042	0.08262	0.00128
76-2,rep	09J10-1	0.11059	0.00260	0.09950	0.00264	0.10124	0.00203	0.08074	0.00268
76-3	09J10-1	0.11309	0.00051	0.10197	0.00051	0.10914	0.00032	0.08205	0.00066
76-3,rep	09J10-1	0.11373	0.00035	0.10218	0.00033	0.10936	0.00046	0.08277	0.00025
76-4	09J10-1	0.11207	0.00058	0.10139	0.00062	0.10772	0.00059	0.07835	0.00051
7-1	09J10-3	0.11531	0.00059	0.10349	0.00056	0.12892	0.00070	0.07970	0.00065
7-2	09J10-3	0.10855	0.00247	0.09933	0.00249	0.09152	0.00147	0.07876	0.00349
7-2,rep	09J10-3	0.10951	0.00137	0.09966	0.00103	0.09025	0.00094	0.07480	0.00197
7-3	09J10-3	0.11670	0.00104	0.10408	0.00087	0.15544	0.00093	0.08355	0.00087
7-4	09J10-3	0.11060	0.00064	0.10042	0.00076	0.09479	0.00036	0.07515	0.00040
7-4,rep	09J10-3	0.11015	0.00065	0.10032	0.00054	0.09442	0.00092	0.07534	0.00056
12-1	06J06-3	0.11062	0.00717	0.09998	0.00150	0.09373	0.00131	0.07754	0.00220
12-2	06J06-3	0.11112	0.00043	0.10052	0.00050	0.09230	0.00088	0.07692	0.00039
12-3	06J06-3	0.11008	0.00054	0.09930	0.00065	0.08555	0.00045	0.07507	0.00038
12-3,rep	06J06-3	0.11032	0.00067	0.10010	0.00060	0.08628	0.00038	0.07444	0.00055
12-4	06J06-3	0.11263	0.00032	0.10161	0.00036	0.10177	0.00046	0.07900	0.00046
37-2	09J10-5	0.12032	0.00047	0.10680	0.00037	0.17117	0.00046	0.08917	0.00084
37-3	09J10-5	0.12040	0.00063	0.10700	0.00054	0.18027	0.00054	0.08831	0.00253
37-4	09J10-5	0.11975	0.00078	0.10651	0.00040	0.17021	0.00035	0.08665	0.00121
10-2	09J10-6	0.11922	0.00035	0.10583	0.00035	0.16130	0.00056	0.08593	0.00108
10-3	09J10-6	0.11939	0.00041	0.10609	0.00032	0.15911	0.00040	0.08487	0.00111
4-2	09J10-2	0.10930	0.00060	0.09948	0.00060	0.08883	0.00050	0.07501	0.00107
4-3	09J10-2	0.11017	0.00103	0.10002	0.00055	0.10066	0.00070	0.07918	0.00080
4-4	09J10-2	0.10692	0.00200	0.09616	0.00163	0.09530	0.00177	0.07412	0.00157
4-4,rep	09J10-2	0.11195	0.00074	0.10137	0.00081	0.09947	0.00047	0.07691	0.00108
70-2	01J08-2	0.11204	0.00059	0.10131	0.00023	0.10079	0.00040	0.08443	0.00105
70-3	01J08-2	0.11263	0.00094	0.10237	0.00079	0.10092	0.00081	0.08452	0.00103
70-4	01J08-2	0.11145	0.00052	0.10090	0.00102	0.09950	0.00079	0.08567	0.00186

Table 2-3c. Corrected Isotope Ratios (con't)									
sample	channel ID	$^{46}Ti/^{48}Ti$	error	$^{47}Ti/^{48}Ti$	error	$^{49}Ti/^{48}Ti$	error	$^{50}Ti/^{48}Ti$	error
3-2	01J08-2	0.11142	0.00092	0.10090	0.00076	0.08872	0.00073	0.08612	0.00128
3-3	01J08-2	0.11069	0.00066	0.10072	0.00069	0.08528	0.00078	0.08046	0.00162
11-2	01J08-1	0.11008	0.00066	0.10007	0.00070	0.08696	0.00070	0.08185	0.00065
11-3	01J08-1	0.10988	0.00058	0.10001	0.00043	0.08561	0.00048	0.08026	0.00055
11-4	01J08-1	0.11089	0.00057	0.10041	0.00039	0.08750	0.00047	0.08732	0.00345
51-2	02J07-8	0.11165	0.00068	0.10128	0.00068	0.09882	0.00058	0.08345	0.00256
51-3	02J07-8	0.11155	0.00077	0.10137	0.00065	0.10033	0.00053	0.08742	0.00243
51-4	02J07-8	0.11142	0.00042	0.10121	0.00058	0.09561	0.00034	0.08789	0.00068
23-2	09J10-7	0.11614	0.00063	0.10385	0.00044	0.12973	0.00043	0.08075	0.00091
23-3	09J10-7	0.11565	0.00078	0.10347	0.00060	0.12785	0.00124	0.08043	0.00091
23-4	09J10-7	0.11514	0.00066	0.10325	0.00048	0.12741	0.00066	0.08030	0.00054
27-2	01J08-6	0.11270	0.00095	0.10211	0.00061	0.11026	0.00068	0.07918	0.00145
27-3	01J08-6	0.11311	0.00034	0.10200	0.00035	0.11079	0.00060	0.08020	0.00064
48-2	01J08-5	0.11331	0.00047	0.10293	0.00048	0.11795	0.00064	0.08486	0.00069
48-3	01J08-5	0.11403	0.00054	0.10285	0.00062	0.11878	0.00105	0.08806	0.00102
74-2	08J07-7	0.11480	0.00063	0.10335	0.00060	0.12905	0.00079	0.08341	0.00098
74-3	08J07-7	0.11522	0.00050	0.10379	0.00044	0.13133	0.00067	0.08632	0.00156
18-2	02J07-7	0.11385	0.00071	0.10267	0.00034	0.12167	0.00064	0.07869	0.00050
18-3	02J07-7	0.11378	0.00074	0.10263	0.00047	0.12061	0.00069	0.07941	0.00065
24-2	01J08-3	0.11100	0.00039	0.10076	0.00032	0.09409	0.00044	0.08063	0.00058
24-3	01J08-3	0.11186	0.00080	0.10130	0.00063	0.10084	0.00068	0.08354	0.00062
24-4	01J08-3	0.11276	0.00116	0.10143	0.00068	0.10951	0.00074	0.08425	0.00205
21-2	02J07-5	0.11923	0.00059	0.10566	0.00040	0.15322	0.00053	0.08892	0.00068
21-3	02J07-5	0.11417	0.00056	0.10240	0.00055	0.11950	0.00044	0.08164	0.00066
21-4	02J07-5	0.11124	0.00050	0.10093	0.00050	0.09893	0.00052	0.07853	0.00061
52-2	08J07-5	0.12191	0.00071	0.10812	0.00052	0.18757	0.00042	0.08872	0.00095
52-3	08J07-5	0.12140	0.00083	0.10788	0.00063	0.18639	0.00075	0.08603	0.00071
15-2	02J07-3	0.11519	0.00068	0.10313	0.00045	0.12554	0.00089	0.08220	0.00087
15-3	02J07-3	0.11684	0.00037	0.10441	0.00063	0.14269	0.00072	0.08767	0.00091
15-4	02J07-3	0.11647	0.00064	0.10425	0.00060	0.13874	0.00056	0.08311	0.00078
13-2	02J07-4	0.11323	0.00047	0.10224	0.00051	0.11474	0.00062	0.07827	0.00041
13-3	02J07-4	0.11764	0.00049	0.10542	0.00045	0.15040	0.00095	0.08348	0.00057

Table 2-3c. Corrected Isotope Ratios (con't)									
sample	channel ID	$^{46}Ti/^{48}Ti$	error	$^{47}Ti/^{48}Ti$	error	$^{49}Ti/^{48}Ti$	error	$^{50}Ti/^{48}Ti$	error
13-4	02J07-4	0.11783	0.00038	0.10547	0.00069	0.15632	0.00081	0.08398	0.00052
84-2	02J07-1	0.11165	0.00039	0.10100	0.00065	0.10178	0.00037	0.08542	0.00115
84-3	02J07-1	0.11134	0.00052	0.10141	0.00056	0.10171	0.00041	0.08547	0.00078
32-2	02J07-6	0.11693	0.00040	0.10453	0.00035	0.14197	0.00052	0.08313	0.00061
32-3	02J07-6	0.11739	0.00053	0.10477	0.00054	0.14198	0.00064	0.08447	0.00077
32-4	02J07-6	0.11712	0.00043	0.10421	0.00038	0.13582	0.00042	0.08296	0.00056
59-2	08J07-8	0.11238	0.00049	0.10145	0.00060	0.10162	0.00068	0.08358	0.00119
59-3	08J07-8	0.10741	0.00048	0.09835	0.00054	0.07581	0.00047	0.07422	0.00052
50-2	02J07-2	0.11450	0.00067	0.10285	0.00066	0.12148	0.00051	0.07859	0.00067
68-2	01J08-4	0.11369	0.00065	0.10257	0.00057	0.11576	0.00049	0.09120	0.00293
68-3	01J08-4	0.11268	0.00071	0.10182	0.00072	0.11484	0.00067	0.08793	0.00114
30-2	01J08-7	0.11177	0.00053	0.10101	0.00060	0.09606	0.00048	0.07837	0.00067
30-3	01J08-7	0.10876	0.00045	0.09949	0.00043	0.08003	0.00057	0.07461	0.00055
30-4	01J08-7	0.11165	0.00082	0.10127	0.00094	0.10000	0.00109	0.07873	0.00077
80-2	08J07-6	0.11776	0.00107	0.10514	0.00091	0.15503	0.00097	0.08218	0.00033
9-2	04J07-8	0.11174	0.00043	0.10145	0.00065	0.10677	0.00054	0.08256	0.00058
9-3	04J07-8	0.11131	0.00029	0.10110	0.00051	0.09636	0.00044	0.08200	0.00123
9-4	04J07-8	0.11296	0.00070	0.10196	0.00050	0.10813	0.00062	0.08615	0.00045
46-2	04J07-7	0.11529	0.00020	0.10311	0.00062	0.12489	0.00080	0.08741	0.00121
46-3	04J07-7	0.11623	0.00043	0.10388	0.00062	0.13112	0.00049	0.08560	0.00055
46-4	04J07-7	0.11601	0.00058	0.10389	0.00069	0.13245	0.00067	0.08593	0.00063
1-2	04J07-6	0.11644	0.00070	0.10440	0.00051	0.14218	0.00067	0.08782	0.00095
1-3	04J07-6	0.11664	0.00054	0.10420	0.00059	0.13805	0.00045	0.08822	0.00119
17-2	04J07-1	0.11331	0.00058	0.10189	0.00038	0.11160	0.00062	0.08355	0.00045
17-3	04J07-1	0.11321	0.00097	0.10186	0.00119	0.11372	0.00084	0.08619	0.00131
17-4	04J07-1	0.11359	0.00074	0.10221	0.00049	0.11151	0.00074	0.08358	0.00058
25-2	04J07-4	0.11909	0.00060	0.10539	0.00057	0.15486	0.00047	0.08187	0.00026
25-3	04J07-4	0.12372	0.00069	0.10820	0.00056	0.18683	0.00070	0.08630	0.00054
25-3,rep	04J07-4	0.12309	0.00091	0.10802	0.00081	0.18728	0.00132	0.08598	0.00081
25-4	04J07-4	0.12359	0.00062	0.10828	0.00055	0.18788	0.00079	0.08615	0.00069
83-2	04J07-3	0.11926	0.00061	0.10612	0.00049	0.16391	0.00083	0.08305	0.00036
83-3	04J07-3	0.12092	0.00075	0.10678	0.00050	0.17138	0.00074	0.08764	0.00122

Table 2-3c. Corrected Isotope Ratios (con't)									
sample	channel ID	$^{46}Ti/^{48}Ti$	error	$^{47}Ti/^{48}Ti$	error	$^{49}Ti/^{48}Ti$	error	$^{50}Ti/^{48}Ti$	error
83-4	04J07-3	0.11811	0.00080	0.10505	0.00041	0.15837	0.00074	0.08244	0.00031
6-2	04J07-2	0.11493	0.00150	0.10312	0.00137	0.13809	0.00134	0.09073	0.00328
6-3	04J07-2	0.11716	0.00072	0.10432	0.00036	0.13897	0.00074	0.08420	0.00165
55-2	04J07-5	0.11974	0.00067	0.10673	0.00057	0.16776	0.00081	0.08616	0.00098
55-3	04J07-5	0.11888	0.00039	0.10568	0.00065	0.15696	0.00087	0.08487	0.00092
71-2	01J08-4	0.11172	0.00071	0.10089	0.00059	0.10008	0.00034	0.08393	0.00070
79-2	04J07-4	0.12089	0.00055	0.10668	0.00059	0.16384	0.00073	0.08701	0.00072
79-3	04J07-4	0.12287	0.00052	0.10735	0.00040	0.17788	0.00051	0.08843	0.00118
79-4	04J07-4	0.12101	0.00062	0.10676	0.00040	0.16666	0.00069	0.08519	0.00058
42-1	09J10-4	0.11840	0.00121	0.10502	0.00085	0.16248	0.00118	0.08748	0.00115
42-2	09J10-4	0.10939	0.00192	0.10000	0.00129	0.10626	0.00121	0.09105	0.00364
42-3	09J10-4	0.11997	0.00134	0.10586	0.00106	0.17211	0.00123	0.08467	0.00088
42-3,rep	09J10-4	0.12012	0.00087	0.10590	0.00097	0.17094	0.00128	0.08476	0.00100
42-4	09J10-4	0.11876	0.00097	0.10596	0.00114	0.16783	0.00067	0.08554	0.00113
42-5	09J10-4	0.11636	0.00137	0.10429	0.00091	0.14896	0.00119	0.08507	0.00077
42-5,rep	09J10-4	0.11719	0.00089	0.10425	0.00083	0.14874	0.00104	0.08243	0.00064
77-1	09J10-4	0.12152	0.00035	0.10699	0.00051	0.17379	0.00083	0.08569	0.00068
77-2	09J10-4	0.12125	0.00063	0.10643	0.00053	0.17105	0.00061	0.08598	0.00094
77-3	09J10-4	0.12245	0.00047	0.10736	0.00046	0.17665	0.00043	0.08910	0.00155
77-4	09J10-4	0.12227	0.00068	0.10714	0.00036	0.17861	0.00138	0.09008	0.00097
77-5	09J10-4	0.12141	0.00055	0.10654	0.00058	0.17138	0.00061	0.08800	0.00065
Second Half-plane, channels 10G06, 11E07, 12C06									
67	11E07-7	0.11245	0.00071	0.10259	0.00048	0.13094	0.00070	0.08038	0.00049
56	11E07-8	0.11225	0.00039	0.10177	0.00053	0.10713	0.00042	0.07609	0.00034
35	11E07-3	0.11845	0.00055	0.10580	0.00052	0.15831	0.00042	0.08218	0.00058
38	11E07-5	0.11985	0.00054	0.10676	0.00053	0.17082	0.00067	0.08267	0.00045
62	11E07-1	0.10826	0.00114	0.09944	0.00090	0.07945	0.00064	0.08381	0.00966
5	11E07-4	0.11965	0.00047	0.10710	0.00032	0.17901	0.00088	0.08363	0.00042
8	11E07-2	0.11527	0.00052	0.10361	0.00048	0.13314	0.00047	0.07987	0.00058
54	11E07-6	0.11523	0.00071	0.10419	0.00058	0.14165	0.00058	0.08044	0.00039
33	12C06-3	0.11560	0.00037	0.10403	0.00036	0.14056	0.00034	0.07954	0.00046
89	12C06-4	0.11388	0.00071	0.10349	0.00058	0.13677	0.00067	0.07988	0.00113

Table 2-3c. Corrected Isotope Ratios (con't)									
sample	channel ID	$^{46}Ti/^{48}Ti$	error	$^{47}Ti/^{48}Ti$	error	$^{49}Ti/^{48}Ti$	error	$^{50}Ti/^{48}Ti$	error
78	12C06-5	0.11420	0.00094	0.10365	0.00055	0.13687	0.00051	0.08498	0.00147
58	12C06-4	0.11445	0.00098	0.10370	0.00075	0.13789	0.00066	0.07988	0.00100
28	12C06-6	0.11526	0.00057	0.10406	0.00063	0.14225	0.00097	0.08060	0.00073
29	12C06-7	0.11331	0.00053	0.10266	0.00043	0.12145	0.00042	0.07838	0.00049
65	12C06-2	0.11456	0.00040	0.10345	0.00048	0.12693	0.00059	0.07774	0.00053
31	12C06-8	0.11132	0.00074	0.10058	0.00100	0.10574	0.00047	0.07710	0.00045
22	12C06-1	0.11239	0.00050	0.10174	0.00038	0.10222	0.00034	0.07589	0.00024
49	10G06-8	0.11146	0.00039	0.10135	0.00038	0.10257	0.00044	0.07561	0.00022
88	10G06-5	0.12024	0.00041	0.10730	0.00028	0.18231	0.00065	0.08378	0.00050
20	10G06-1	0.11248	0.00049	0.10206	0.00042	0.11351	0.00044	0.07672	0.00035
47	10G06-4	0.11973	0.00041	0.10674	0.00042	0.16993	0.00049	0.08855	0.00103
81	10G06-7	0.11309	0.00061	0.10243	0.00036	0.12828	0.00104	0.08047	0.00077
16	10G06-6	0.11653	0.00129	0.10575	0.00079	0.16099	0.00091	0.08102	0.00072
43	10G06-3	0.11392	0.00048	0.10352	0.00046	0.13557	0.00051	0.08000	0.00042
Third Half-plane, channels 11N11, 12Q06									
40	11N11-1	0.11240	0.00040	0.10190	0.00033	0.10583	0.00052	0.07553	0.00040
44	11N11-4	0.12033	0.00070	0.10711	0.00049	0.17668	0.00059	0.08205	0.00041
90	11N11-5	0.11581	0.00046	0.10438	0.00047	0.14236	0.00048	0.07961	0.00035
69	11N11-7	0.11389	0.00083	0.10309	0.00050	0.13243	0.00086	0.08117	0.00082
66	11N11-2	0.11477	0.00058	0.10405	0.00050	0.13661	0.00054	0.07906	0.00043
41	11N11-3	0.11121	0.00067	0.10104	0.00047	0.10094	0.00036	0.07750	0.00052
61	11N11-8	0.10973	0.00041	0.10012	0.00045	0.08945	0.00026	0.07748	0.00034
82	11N11-6	0.11721	0.00053	0.10547	0.00046	0.15476	0.00054	0.08035	0.00033
45	12Q06-1	0.11138	0.00049	0.10134	0.00024	0.09831	0.00032	0.08437	0.00158
53	12Q06-4	0.11362	0.00044	0.10307	0.00041	0.12893	0.00049	0.08011	0.00067
87	12Q06-4	0.11827	0.00052	0.10611	0.00036	0.15817	0.00042	0.08142	0.00050
63	12Q06-7	0.11245	0.00077	0.10210	0.00063	0.11826	0.00079	0.07919	0.00087
73	12Q06-5	0.11849	0.00044	0.10614	0.00051	0.16624	0.00079	0.08865	0.00137
39	12Q06-2	0.11203	0.00054	0.10179	0.00041	0.10830	0.00036	0.07569	0.00039
36	12Q06-3	0.11371	0.00042	0.10299	0.00034	0.12516	0.00042	0.07901	0.00031
64	12Q06-6	0.11301	0.00043	0.10246	0.00047	0.11754	0.00035	0.07874	0.00043
57	12Q06-8	0.11100	0.00083	0.10120	0.00052	0.10559	0.00051	0.07916	0.00118

Notes, Table 3

- Sample data are listed in order of analysis, except for #'s 42 and 77 in the first half-plane.
- Errors stated are equivalent to one standard error.
- Corrected values in Table 3b and 3c refer to corrections for mass bias based on numerous measurements of a natural Ti standard during this study.

Analysis Notes, Table 3

Sample	Comments
86-1	poor run, less that optimal signal
86-2, rep	significant Cr
86-3	significant Ca
86-3, rep	significant Cr
2-1	significant Ca
2-2	significant Ca
34-2	poor run, weak signal
14-2, rep	weak, short-lived mass spec run
75-1	poor, unstable run
75-3	poor run, insufficient sample provided
7-2, 7-4, 12-1, 12-2	7-2 & 7-4 poor runs, insufficient signal weak, short-lived mass spec analysis; samples 7 & 12 noticeably high in Cr, during sample preparations and during mass spec analysis.
4-2	mostly blank, insufficient sample provided
4-4	poor run
70-4	high V at start of mass spec analysis
11-3	high Ca & Cr at start of run
11-4	high Ca, Cr, & V at start
15-3	15-3 & 15-4 high in Ca & Cr at start of run
13-3	high Ca & Cr
13-4	high Ca & Cr at start
84-2	high Ca, Cr, & V at start of run
32-3	sample 32 subsample separates high
32-4	in Ca & Cr at start of mass spec runs
59-3	least amount Ca & Cr observed in any sample
9-2	high V & Cr t start of run
9-4	high Cr at start
1-3	high V at start of run
6-2	poor run, weak signal
42 & 77	samples 42 & 77 digested with $HC1O_4$; ^{44}Ca and ^{52}Cr not analyzed
62	high in V; little sample amount provided

89	high Cr at start
28	relatively weak, short-lived run
31	high V at start
22	high Ca at start of run
88	high Cr at start of run
47	high Ca & Cr at start
81	high Cr & V at start, short-lived run
16	weak run, high Cr
69	somewhat weak run

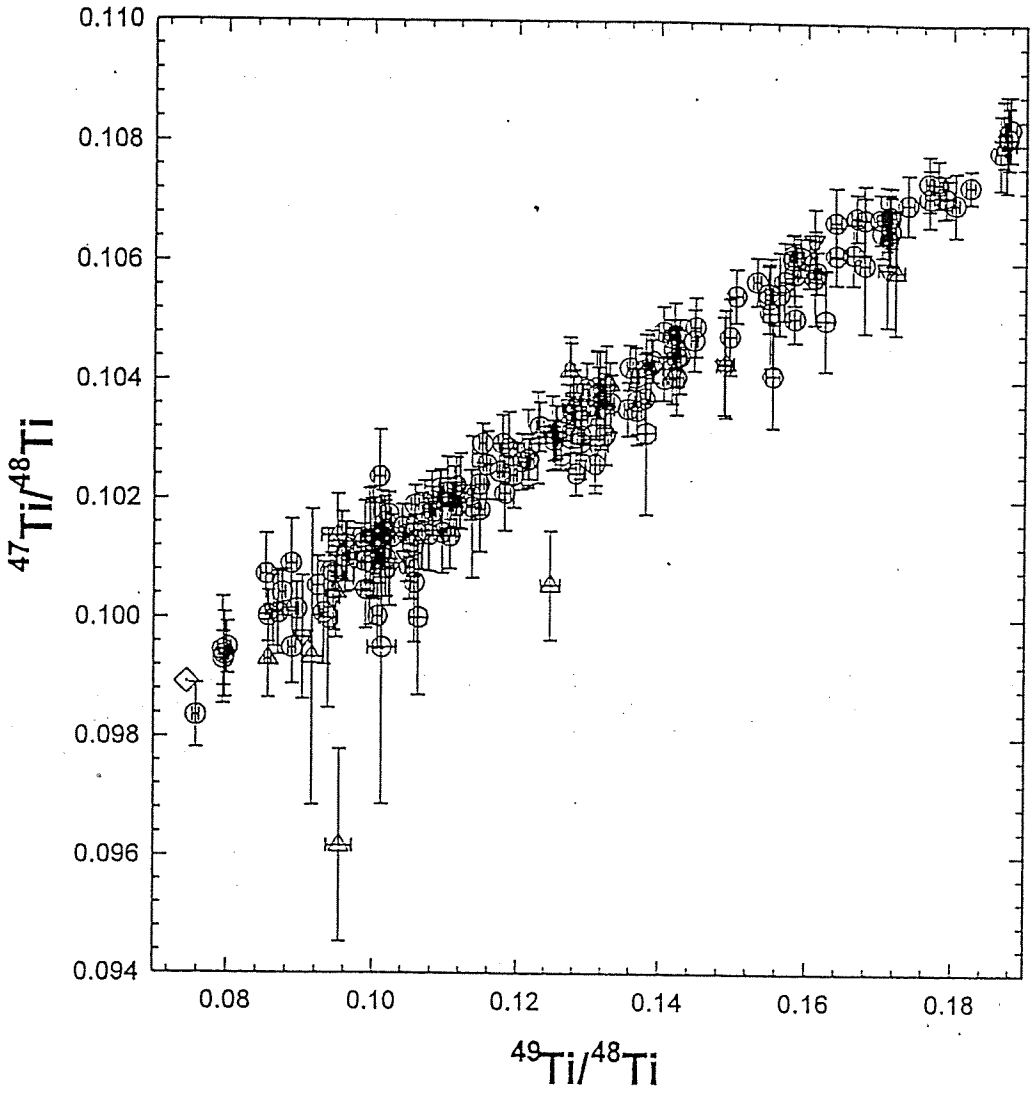

Figure 2.8-1. Variation plot of all Ti isotope ratios analyzed in all Trawsfynydd samples and subsamples. The diamond-shaped symbol refers to the composition of natural Ti. The upward-pointing triangle symbols refer to samples selected for re-analysis on the basis of displacement from the main trend or relatively larger errors.

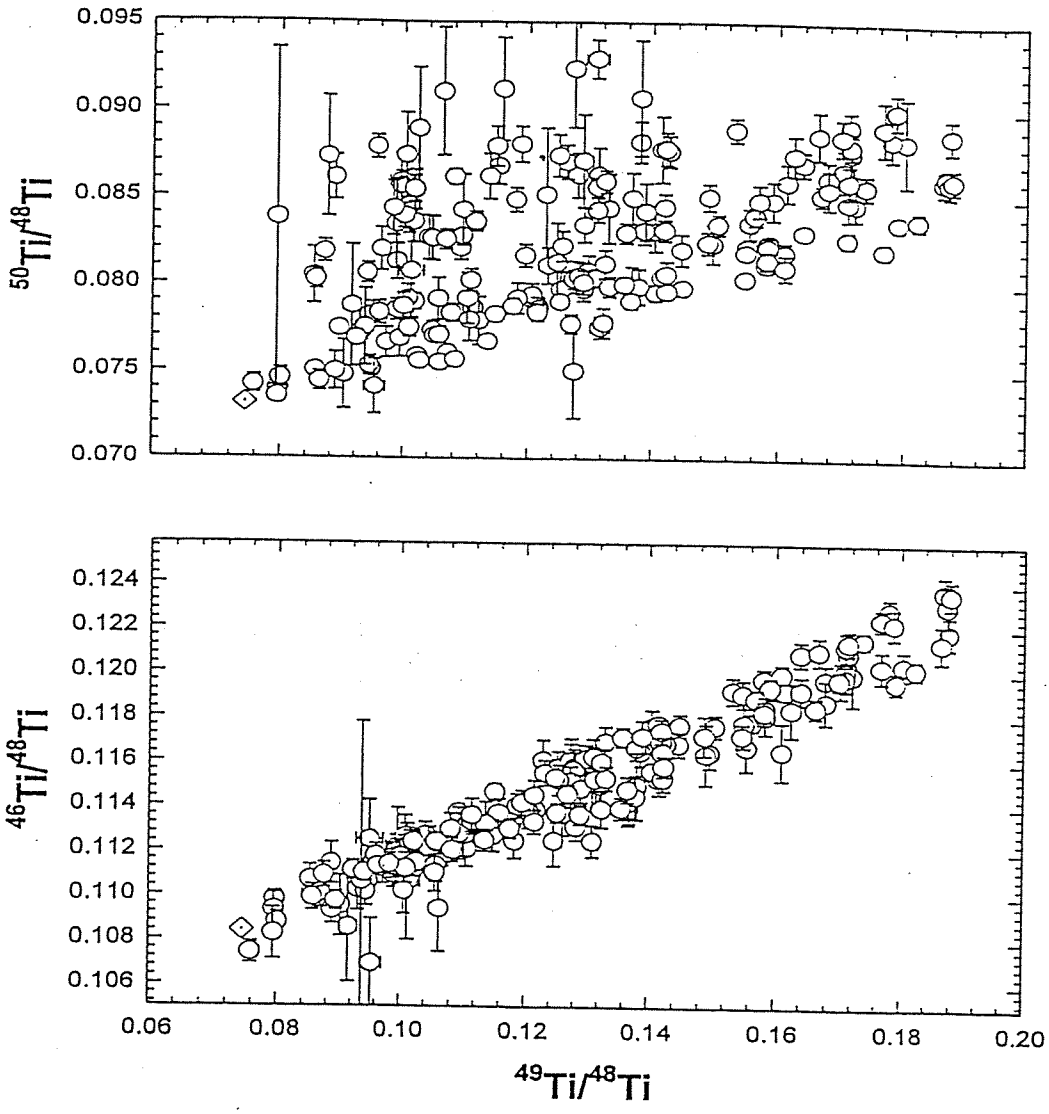

Figure 2.8-1 (con't). Variation plots of Ti isotope ratios for all Trawsfynydd samples and subsamples. Natural Ti is represented by a diamond symbol; samples selected for reanalysis and replicate results are not distinguished on these plots as in the previous plot.

2.9 Discussion: Intra-sample variability/heterogeneity, results from Ti isotopes in subsamples of the first half-plane

All subsamples for each core sample of graphite in the first half-plane, or 'J' plane were analyzed in a continuing effort to evaluate small fluence gradient effects on the altered Ti isotope ratios across a single sample. Very few subsample trends displayed this, and in most cases, one or more subsamples from each group differed greatly and appeared to be biased toward natural Ti isotopic compositions.

Results for selected groups of subsamples are shown in Figure 2.9-1 on an isotope ratio variation plot. Each pair or group of subsamples in this diagram displayed an increase in $^{49}Ti/^{48}Ti$ ratios with distance from the fuel channel, and this increase was expected to be a maximum of 2-3% in this ratio measured from one end of the sample to the other. The variation in $^{47}Ti/^{48}Ti$ ratios is much less and fluence variations on this ratio are largely indistinguishable beyond analytical uncertainty (Figure 2.9-1). Sample #24 subsamples contrast with the other groups, however, in that the ranges of isotope ratios measured show the expected variation trend, but the apparent differences from one end of the sample to the other are much larger than expected. Thus, it appears that results for two of the three subsamples in #24, in addition to results discussed earlier for #86, are unreliable and may also reflect bias by natural Ti blank contributions.

A few examples of spatial variations in Ti isotope ratios measured in subsamples are displayed in Figure 2.9-2. Results for sample 34 show no discernible trend, except that isotope ratio values for the subsamples closest and further from the channel may reflect the magnitude of an expected variation, but the two intermediate samples are biased toward natural Ti. This bias is seen in all 4 isotope ratios, even those ratios that vary less with neutron fluence exposure. Isotope ratios in sample 24 seem to show the correct variation in all 4 isotope ratios except that shown by $^{49}Ti/^{48}Ti$ ratios is too extreme and greater than expected. Results for sample 46 may be closer to expected trends, although the $^{49}Ti/^{48}Ti$ ratios again may vary more than expected. This is also true for sample 86, as mentioned earlier. Among the 48 samples taken for an extensive study of the 'J' half-plane, samples for which there were two or more subsamples available did not display any reasonable trends in Ti isotope ratios reflecting fluence variation exposures across the sample, with only a few exceptions. Thus, the attempt to measure and evaluate this expected small-scale fluence variation within single samples, which was aimed at improving the accuracy of this method, was not very successful.

The major conclusion from these results is that the heterogeneity in the distribution of impurity Ti in intergranular inclusions, domains, or intra crystalline substitutions is greater than anticipated. Preliminary estimates of minimum representative sizes for subsamples were based on a few bulk trace element analyses conducted on unirradiated archived samples of graphite obtained from British Nuclear that are thought to be representative of the graphite moderator materials used in the construction of the reactors at Trawsfynydd (Tables 2-4 & 2-5). These analyses were performed by instrumental neutron activation analysis (INAA) and the data reported depend on (1) the detection limits of the elements, (2) the presence of a useful analyte peak with a moderate half-life after activation, and (3) the abundances in the graphite samples.

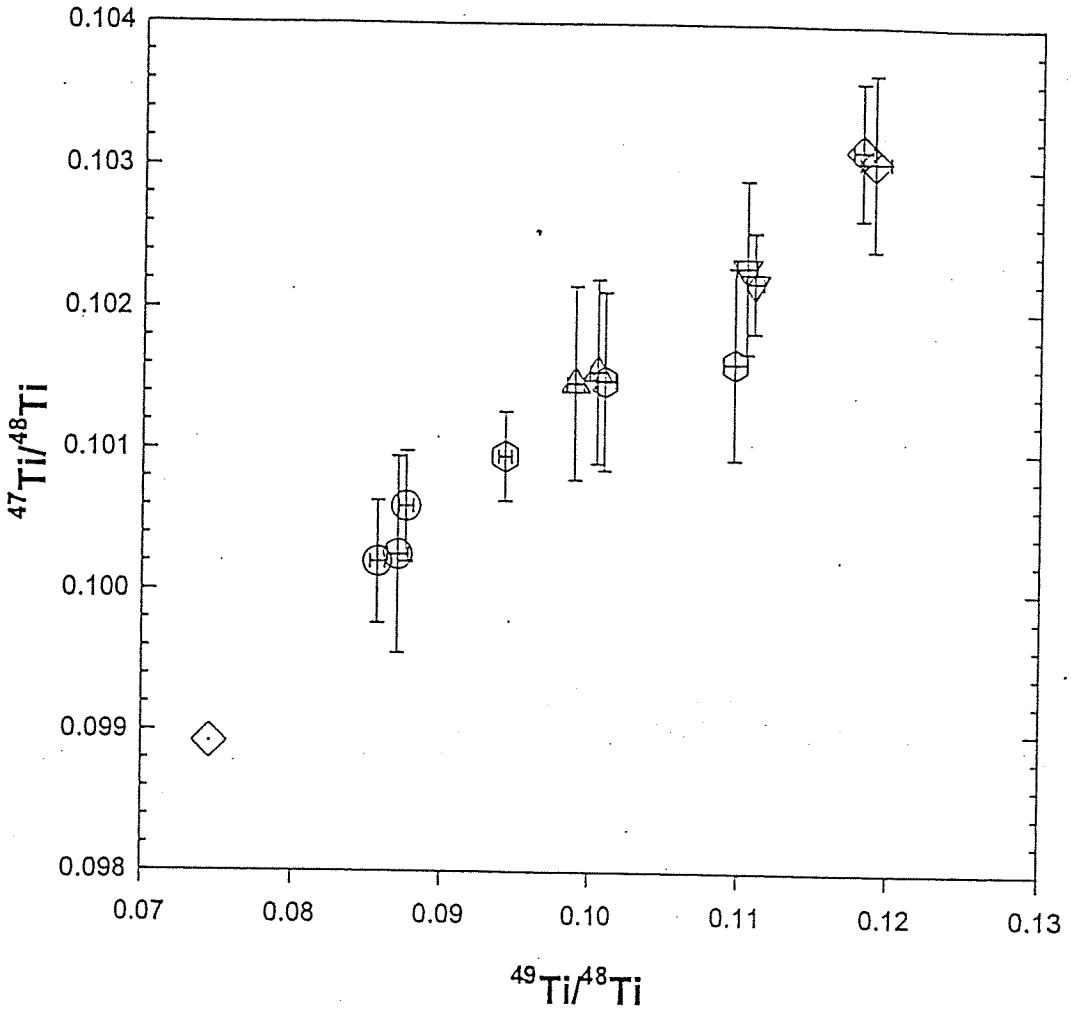

Figure 2.9-1. Titanium isotope ratios in selected subsample groups. Sample analyses are displayed with error bars representing 1 SE (standard error). Natural Ti is represented by a diamond-shaped symbol, sample #11 by circles, sample #51 by upward triangles, sample #24 by hexagons, sample #27 by downward triangles, and sample #48 by diamonds.

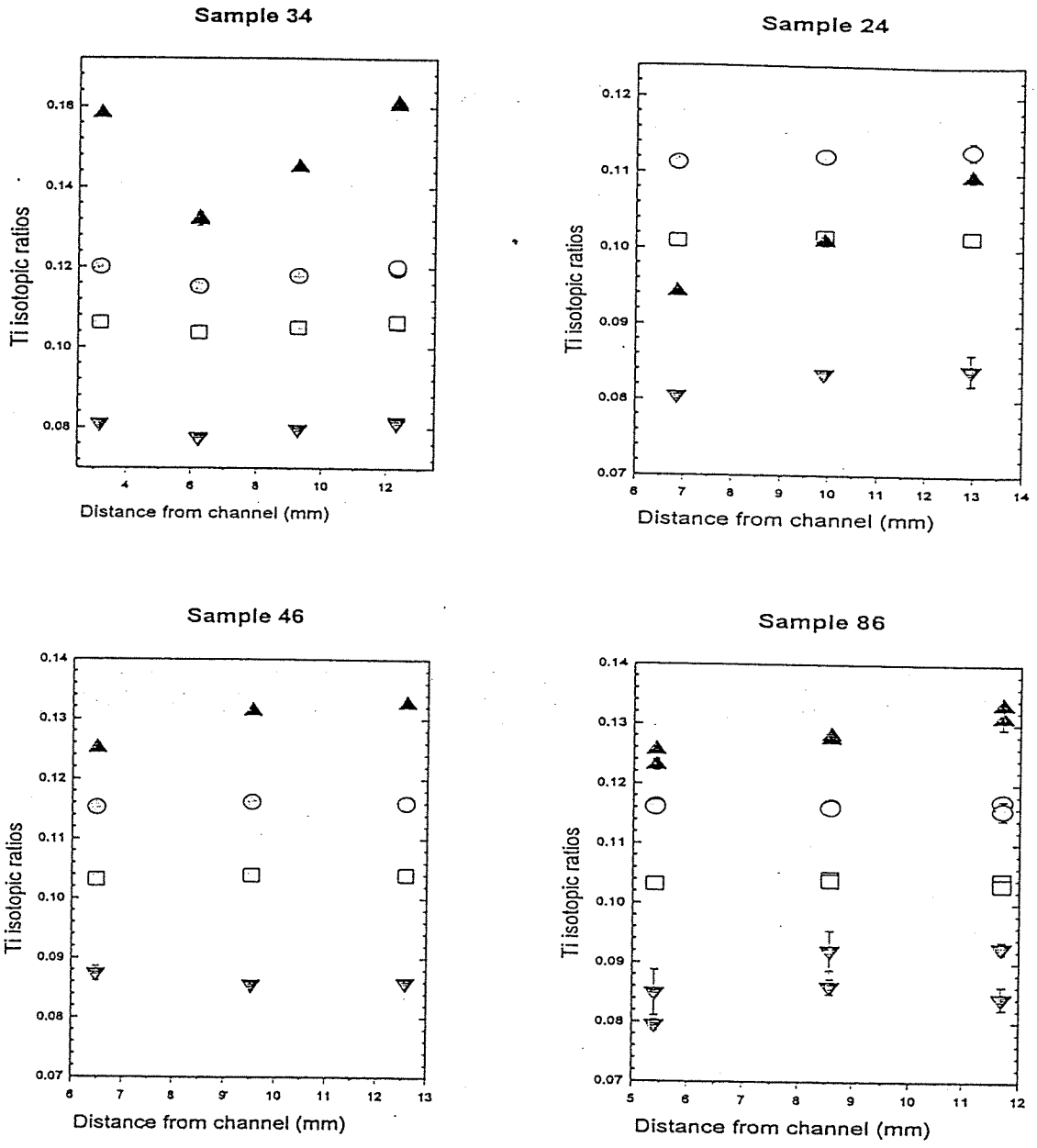

Figure 2.9-2. Variations in Ti isotope ratios in subsamples with distance from the fuel channel. In this and the following three plots, $^{49}Ti/^{48}Ti$ ratios are represented by upward triangles, $^{46}Ti/^{48}Ti$ ratios by circles, $^{47}Ti/^{48}Ti$ ratios by squares, and $^{50}Ti/^{48}Ti$ ratios by downward pointing triangles. For most results error bars are smaller than the symbol size. Overlapping symbols in samples 34 and 86 represent results of replicate analyses.

Table 2-4. Results of NAA analyses of archived unirradiated Trawsfynydd graphite samples

Elements	Sample 7422	Sample 7453	Sample 7480	Sample 7483	Sample 7507	Sample 7514
Au	-	0.001	-	0.00038	0.00113	-
Ce	0.162	0.106	0.0585	0.1725	0.1205	0.0615
Co	0.0212	0.0102	0.0086	0.0067	0.0064	0.0091
Cr	0.54	0.322	0.188	0.231	0.102	0.225
Eu	0.0033	0.0024	0.0071	0.0062	0.0052	0.0013
Hf	0.0045	0.0650	-	0.0063	0.0155	0.0123
La	0.094	0.066	0.025	0.090	0.057	0.043
Lu	0.00123	0.00089	0.00047	0.00099	0.00078	0.00061
Na	0.153	0.156	-	0.018	0.091	0.090
Sc	0.0233	0.0147	0.0116	0.0167	0.0372	0.081
Sm	0.0167	0.0060	0.0196	0.0319	0.0349	0.0037
Th	0.0049	0.0225	-	0.0052	0.01075	0.0026
U	0.0057	0.0159	0.0300	0.0136	-	0.0070
Yb	0.0034	0.0038	0.0024	0.0036	0.0025	-
Elements	Sample 7562	Sample 8468	Sample 8473	Sample 8479	Sample 8518	Sample 8529
Au	-	0.0025	-	0.0077	-	0.0044
Ce	0.0745	0.0805	0.257	0.101	0.099	0.138
Co	0.0166	0.0245	0.0125	0.0187	0.0159	0.0288
Cr	0.269	0.3355	0.1325	0.188	0.397	0.610
Eu	0.0034	0.0039	0.0045	0.0020	0.0036	0.0026
Hf	0.0043	0.0166	0.0151	0.0000	0.0036	0.0183
La	0.045	0.049	0.129	0.061	0.054	0.088
Lu	0.00086	0.00073	0.00125	-	-	-
Na	0.232	0.135	0.229	0.539	0.046	0.072
Sc	0.0128	0.0117	0.0274	0.0214	0.0118	0.0157
Sm	0.0096	0.0103	0.0086	0.0092	0.00784	0.0054
Th	0.0057	0.0139	0.01555	0.0050	0.0037	0.0140
U	0.0377	0.0083	0.0105	0.0030	0.0085	0.0160
Yb	0.0026	0.0025	-	0.0043	0.00257	0.0029

(Hyphen indicates elements not detected).

Table 2-5. Results of NAA analyses of archived unirradiated Trawsfynydd graphite samples.

Sample	As	Ba	Cl	Dy	Eu	La	Mn	Na	Sm
7422	0.23	3.40	0.186	0.0091	2.690	0.108	0.0126	0.124	0.014
7453	0.013	0.74	0.999	0.0057	1.945	0.076	0.0071	0.107	0.006
7480	0.038	8.05	0.558	0.0059	7.117	0.032	0.0021	0.045	0.031
7483	0.029	2.09	0.797	0.0120	6.415	0.106	0.0019	0.035	0.029
7507	n.d	4.18	1.502	0.0169	5.733	0.094	0.0127	0.053	0.035
7514	0.011	1.55	0.036	0.0040	1.299	0.047	0.0050	0.053	n.d
7517	0.0265	5.170	0.866	0.0073	8.25	0.124	0.0065	0.110	0.1163
7562	0.0152	2.808	0.820	0.0048	2.98	0.046	0.0190	0.173	0.0036
7571	0.256	4.150	0.792	0.0068	3.09	0.063	0.0030	0.054	0.0043
7575	0.0107	1.616	0.569	0.0047	1.72	0.08	0.0033	0.094	0.0043
8468	0.0110	1.573	0.838	0.0037	4.04	0.045	0.0089	0.091	0.0087
8473	0.0651	3.533	0.737	n.d.	1.54	0.152	0.0036	0.033	0.0064
8479	0.0218	4.93	0.90	0.0806	2.233	0.058	0.0227	0.664	0.0121
8485	0.0132	2.44	0.59	0.0062	1.767	0.064	0.0083	0.054	0.0071
8490	0.0200	4.24	0.66	0.0120	2.655	0.139	0.0087	0.136	0.0103
8510	0.0167	3.04	0.60	0.0055	3.00	0.049	0.0046	0.055	0.0082
8518	0.0086	1.57	0.29	0.0039	2.948	0.052	0.0023	0.033	0.0087
8529	0.0026	2.07	0.48	0.0055	1.293	0.080	0.0065	0.066	0.0058

Though Ti is very difficult to analyze by INAA, Cr is feasible, and results for Cr, Mn, and other trace elements provided an initial idea of variability or heterogeneity in the samples (Tables 2-4 & 2-5). These results and practical considerations both from machining concerns and minimum amounts required for mass spec analysis led to estimates of ideal sizes for subsamples. Depending on the density of the graphite, subsamples consisted of a maximum of 200 mg, though samples were not weighed prior to microwave leaching because the goal was only to measure isotope ratios, and not exact bulk concentrations, of impurity elements.

During development of digestion methods and ion exchange separations, blank contributions were occasionally evaluated by ICPMS analysis. The ICPMS analysis results were not quantitative due to many interferences in the mass range of the transition metals, but still indicated differences in impurity levels among the high-purity acids as described earlier, and also differences in various acid digestion mixtures. Although bulk Ti and Cr impurity contents in the irradiated graphite samples were not available, these earlier ICPMS results supported the decision to use only HF, rather than a mixture of perchloric acid and HF, in microwave leaching

procedures adopted following the mass spectrometric analysis results for samples 42 and 77 as described earlier. ICPMS results also indicated that precleaning the HF using an anion exchange procedure should also help to reduce Ti blanks.

The calibrated ^{46}Ti spike proved useful in later blank determinations because this approach, termed isotope dilution analysis, is more sensitive and quantitative. Assuming that the isotopic composition of the Ti blank is natural, and knowing the concentration of the spike and the amount added, the ratio of $^{46}Ti/^{48}Ti$ measured can be used in the previous mixing equation to determine the amount of natural or blank Ti present. This method also requires that Ti from both the spike and sample or blank be thoroughly mixed together or equilibrated. We compared digestions using perchloric acid + HF with those only using HF for microwave leaching. Appropriate amounts of acids were added to the microwave vessels, and a typical digestion or leaching program was performed. An aliquot of Ti spike was added to each afterward, evaporated to dryness under a heat lamp, and analyzed on the mass spectrometer for Ti isotope ratio determinations, using the same filament materials, etc. The Ti spike was added afterward to avoid loss of volatile $TiCl_4$ before complete mixing of the spike and sample Ti. The results were surprising in that the HF digestions had higher and variable blank levels ranging from 5 to 14 ng/ml Ti, and digestions with perchloric+HF mixtures had blanks of 2 to 3 ng/ml Ti. The latter result may be partly explained by loss of volatile $TiCl_4$ during digestion and before addition of the spike, as suggested by an average blank level of 7 ng/ml measured in perchloric acid taken from a fresh bottle. Several weeks after completion of the last graphite analyses, high blank levels of up to 18 ng/ml were found in a lot of stored, precleaned HF. It is not certain that these levels are typical of those in the freshly prepared precleaned HF used during the sample preparation, because HF taken immediately from a new, unopened bottle contained a Ti blank level of only 1 ng/ml. This level and that determined above in the perchloric acid, though consistent with earlier ICPMS results, are significantly higher than vendor-certified values described earlier (HF ~0.02 ng/ml, $HClO_4$ ~0.4 ng/ml).

These observations suggest several possible sources of blank Ti, and these include:

1) airborne particulate sources of Ti as suggested by higher than certified blank levels in the high-purity reagent acids, the general variability of blank levels, for example, in the HF-only digestion analyses, and high levels in HF that had been precleaned by ion exchange;

2) contact with labware and leaching of Ti from container materials, as suggested by surprisingly high levels in precleaned HF that had been stored for some time, even in Teflon;

3) volatile loss of $TiCl_4$ from perchloric acid or mixtures with perchloric acid during microwave digestions or evaporation steps;

4) particles or shavings from white polyethylene caps of vials used to collect powdered graphite during machining.

Source (1) may be the most important contribution, because all blank preparations and preparation of irradiated graphite samples included open-vial evaporation steps on a hot plate or under a heat lamp in a radiological fume hood with relatively high air flow. This is also suggested by a blank determination wherein the vial remained open for a longer time than those for other blank tests. The contribution of environmental or airborne Ti during this study may also have been variable, with some samples affected more than others. Some airborne particulate contributions may also have occurred during initial machining and sample preparation in the glovebox. Separation and analysis of Ti, since it is a common element in the Earth's crust and in the environment, may thus require the same level of stringent clean-lab controls for preparation of samples analyzed for Pb-isotopic compositions. Previous studies cited from the literature (cf., refs) featured the isotopic analysis of microgram or higher amounts of Ti extracted from meteorites which may contain Ti at levels up to several hundred ppm. Many samples of graphite analyzed in this study may have contained sub-ppm levels of Ti, and it is not surprising that blank or natural Ti has affected the isotopic compositions measured in the samples.

Sources (2) and (3) may be less important. High-quality, chemically-inert Teflon labware was used whenever possible. One exception was the use of polyethylene disposable sample transfer pipets, though these were also subjected to the same cleaning before use as the Teflon labware. It is also possible that precleaning the HF by ion exchange was not as effective as originally thought: since the large column used for this procedure was not made of Teflon, some leaching and contribution of blank Ti may have occurred during the HF precleaning. Loss of volatile Ti from samples may have occurred only in the first two sets of graphite subsamples (samples 42 and 77), and in perchloric acid blanks.

The importance of source (4) was recently tested by leaching about 1 g of the white plastic vial cap material in an HF-only microwave digestion. Opaque white plastics are often colored by addition of TiO_2. The plastic did not just leach but melted within the Teflon vessel, not surprisingly, since the digestion program allowed temperatures up to 200° C. The HF leachate was spiked and analyzed for Ti isotopic compositions. The analyzed ratios were very close to natural, i.e., the sample was severely underspiked, and the leachate probably contained relatively high ppm levels of blank Ti. It is possible that small particles of white plastic fell into the powdered graphite samples during glovebox preparations, and this would also be a variable blank contribution.

2.10 Spatial Relationships of Ti Isotopes

Titanium isotope ratios should vary in relationship to the position of the graphite samples in the reactor core. At a later stage in this project, the core height and position for each sample was made available. In the following figures, Ti isotope ratios are plotted versus the relative core position to recognize any obvious anomalous analyses.

Many samples in the 1st half plane, or 'J' plane, which was the most extensive sampling effort, form curved profiles as expected. The data plotted in Figure 2.10-1 are only a subset of the entire data set for this half plane, and were selected on the basis of run precision and the most altered

isotope ratios among the results for a group of subsamples. The highest isotope ratios at the midpoint and on either side of the midpoint are related to relative neutron fluence exposure between the different fuel channels. The best profiles are seen in samples taken from the two outermost channels, 02J07 and 01J08. However, in channel 01J08, two samples from the same sampling height have very different isotope ratios. These are samples 68 and 71, which represent closely adjacent fuel channel 'duplicate' samples as discussed earlier. Other isotope ratios at different sampling heights from this same fuel channel and others, which more closely overlap, represent only analytical replicates. Samples just left of the apparent midpoint for channels 06J06, 09J10, and 04J07 also represent results for closely adjacent fuel channel 'duplicate' samples. The differences in isotope ratios between these duplicates further support the magnitude of small-scale heterogeneity in Ti impurities in the graphite.

The subsamples prepared for samples from the second and third half planes were combined to increase the amount of sample material processed for analysis, and to improve chances of success in overcoming occasional blank contamination. Results for these samples are also plotted as a function of core height and relative distance from the reactor midplane in Figures 2.10-2 and 2.10-3. Even though larger sample amounts were used to extract Ti, anomalous isotope ratios which depart from an idealized curve are still observed. This suggests that even the combined subsamples in some cases did not contain enough Ti to overcome blank contributions resulting in a bias toward natural Ti isotopic ratios. The combined samples for the second and third half planes did not always each have the same number of subsamples (see Table 2-1). For example, sample 62 from channel 11E07 may be biased toward natural (Fig. 10-2), due to limited material available: only a partial subsample was possible (Table 2-1). Other samples for which only one subsample was available include #38 (channel 11E07) and #43 (channel 10G06), which display departures from possible profiles (fig. 10-2). For the two fuel channel duplicate samples from near the midplane of channel 12C06, sample #89 consisted of only one subsample, and #58 consisted of two subsamples. Results for both of these samples compare the best analytically among all the fuel channel duplicates analyzed (Table 2-2), even though both deviate a similar amount from an ideal profile for the channel, as seen in Figure 2.10-2. There is also a lack of correlation between sample size and deviation from a profile in results for the third half plane. For example, sample #41 is the greatest outlier for channel 11N11, but the amount used in the analysis included 4 subsamples. The two fuel channel duplicates taken from near the midpoint of channel 12Q06 differ greatly from one another in Ti isotope ratios and also deviate from the profile.

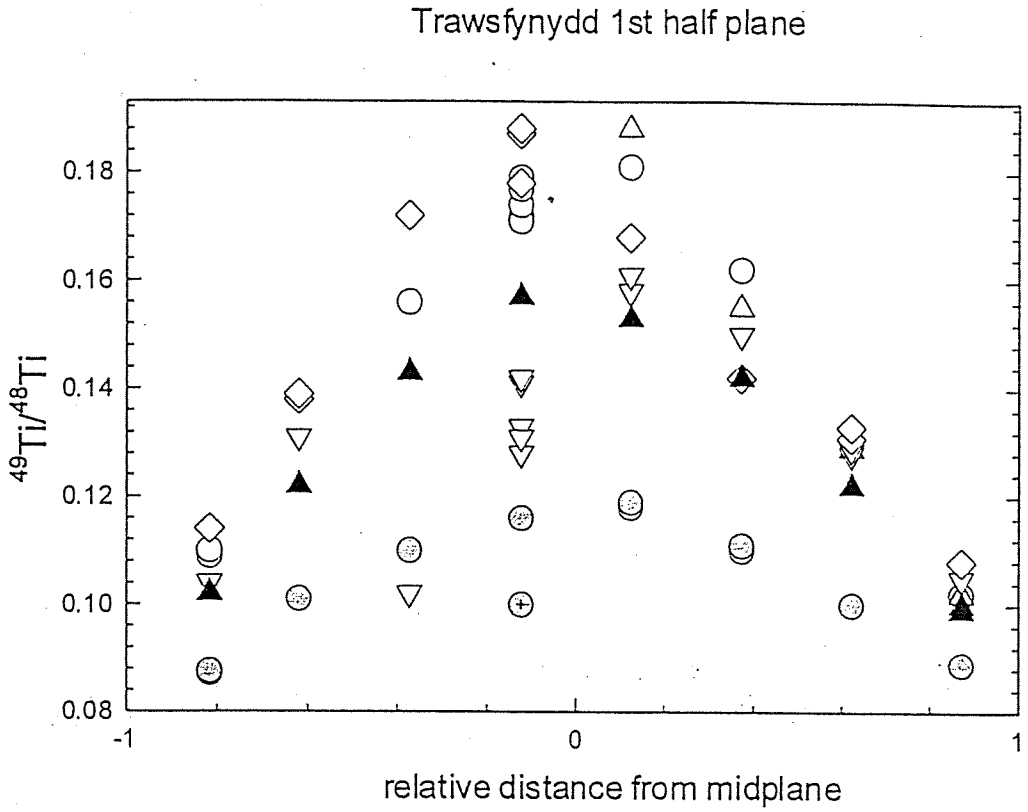

Figure 2.10-1. $^{49}Ti/^{48}Ti$ isotope ratios measured in graphite samples from the 'J' half plane of the Trawsfynydd Unit 2 reactor plotted as a function of core height or relative distance from the reactor midplane. Samples from different fuel channels are represented by different symbols: channel 09J10, open circles; channel 08J07, upward-pointing triangles; channel 06J06, downward-pointing triangles; channel 04J07, open diamonds; channel 02J07, solid upward-pointing triangles; channel 01J08, shaded circles. The sample in the latter fuel channel profile with a plus symbol added is sample #71, which is a fuel channel 'duplicate' sample as discussed in the text.

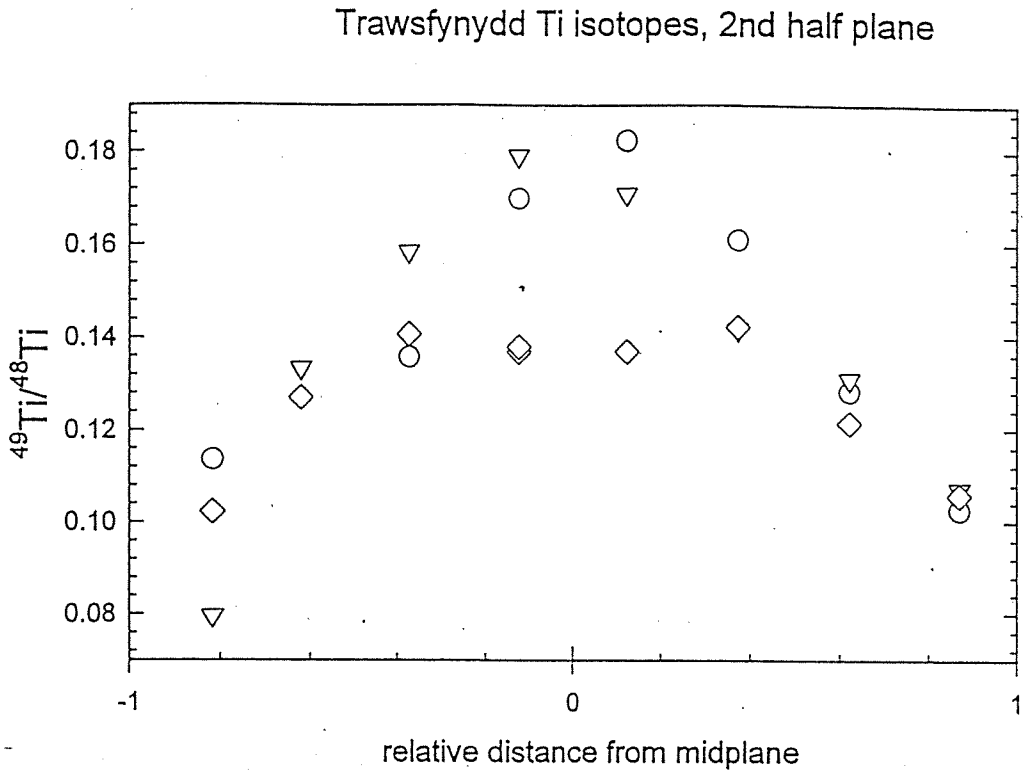

Figure 2.10-2. $^{49}Ti/^{48}Ti$ ratios measured in graphite samples from the 2nd half plane of the Trawsfynydd Unit 2 reactor plotted as a function of core height. Samples from different fuel channels are represented by different symbols: channel 10G06, circles; channel 11E07, down-pointing triangles; channel 12C06, open diamonds.

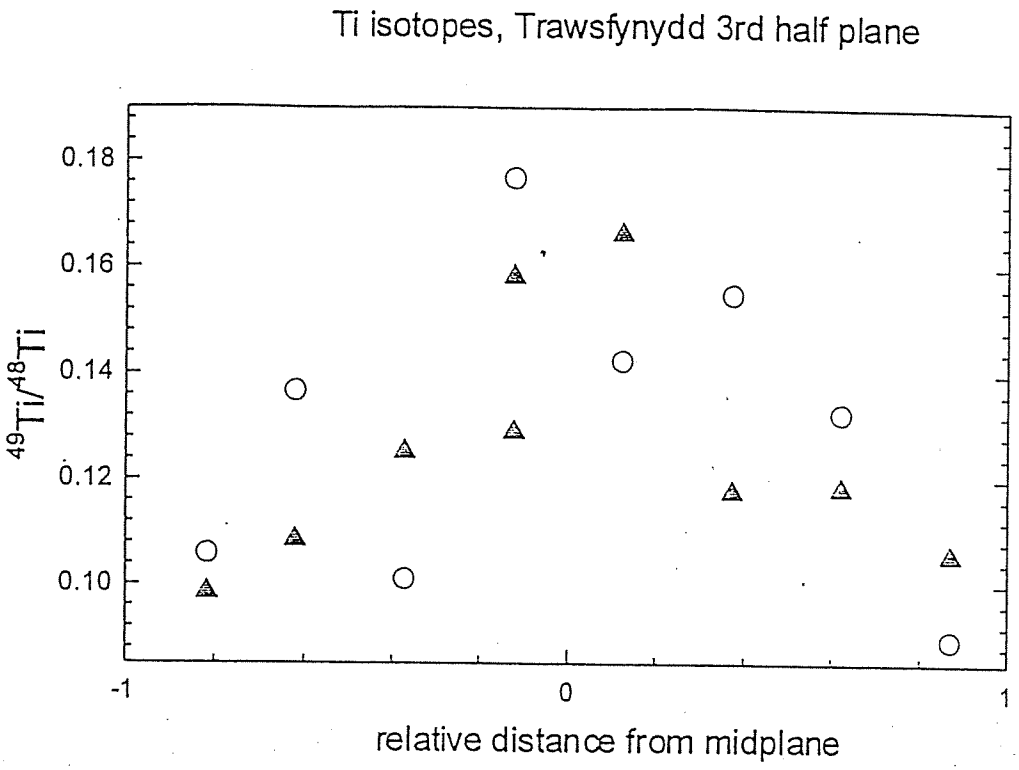

Figure 2.10-3. $^{49}Ti/^{48}Ti$ ratios measured in graphite samples from the third half plane of the Trawsfynydd Unit 2 reactor plotted as a function of core height. Samples from different fuel channels are represented by different symbols: channel 11N11, open circles; channel 12Q06, shaded triangles.

2.11 Rationale for Data Screening, Analytical Basis

Several factors have been considered in choosing the best results for further modeling and neutronics calculations. An underlying principle is that the only possible contaminant in laboratory preparation and analysis is natural Ti, which has a fixed and well-known isotopic composition. Unless significant cross-contamination between different samples occurred during machining or laboratory preparation including microwave leaching/digestion, ion exchange separations, and mass spectrometric analysis, it is virtually impossible to achieve a Ti isotope ratio which would be more altered than expected. Thus, this bias affects sample results in only one direction, which simplifies data screening somewhat.

Bias toward natural Ti isotopic compositions is observed on two scales in this study: on a small sample-size scale, based on results from subsample analyses, and on a fuel channel or reactor scale, based on deviations from profiles suggested by the majority of sample results and shown in Figures 2.10-1, 2.10-2, and 2.10-3. The first and most significant screening step consisted of close examination of the results of subsample analyses. For two or more subsamples taken from a single sample, the data for the sample with the most altered (furthest from natural) Ti isotope ratios were selected. In some cases, analytical replicates for these most altered ratios were performed and these were included.

The problem of deviations from profiles suggested in Figures 2.10-1, 2.10-2, and 2.10-3 involves some subjective decisions. In some fuel channels where only one sample result appears to deviate, such as sample #71 in channel 01J08 (Figure 2.10-1), this data point is clearly anomalous. In other fuel channel profiles such as that for channel 12Q06 (Figure 2.10-3), at least 2 and possibly up to 4 samples may be deviant and this requires a more sophisticated approach such as curve-fitting.

2.12 Suggested Further Work & Improvements

The chief cause of isotopic ratios in some samples which are less altered than expected or which do not conform to trends suggested by other analyses, is a bias toward natural Ti isotopic compositions. The amount of bias depends on the ratio of sample Ti to blank Ti, and in this study, samples near the midplane of the reactor were most vulnerable because these samples were likely to contain the most altered Ti ratios. The same mixing equation presented earlier for Ti spike calibration and isotope dilution measurements can be used to estimate the amount of blank Ti required to significantly bias the altered Ti ratios in a sample. An alternative approach can be taken for samples which fall below a suggested fluence profile, and either the amount of blank or sample Ti may be assumed or calculated.

Further work may improve the sample/blank ratio, and also the detection limits and sensitivity of mass spectrometer measurements. Based on blank results earlier, two major means of lowering blanks, and increasing sample/blank ratios, is (1) scaling down the separation chemistry and using less reagents, and (2) controlling airborne particulate contributions during sample preparation. To some degree, we cannot effectively change uncertainties due to insufficient

impurity element contents in graphite samples. One way to improve the feasibility of analyses when initiating the study of a new suite of graphite samples is to perform prescreening analyses of the irradiated samples to obtain measurements of impurity element bulk contents, and work could be restricted only to samples judged to contain sufficient abundances of trace impurity elements. Prescreening analyses by X-ray fluorescence (XRF) spectroscopy, an old and well-established method, would be helpful, and could be performed on 'hot' irradiated samples on a short time-scale. Detection limits vary for different elements, but extend to sub-ppm values. Sample preparation and mounting methods for XRF analysis could be developed such that the analysis procedure is nondestructive and does not substantially contaminate or bias the samples, and the samples can then be retrieved and processed for isotopic analysis by TIMS.

Further improvements may be possible on the 3-stage mass spectrometer described earlier from which it was possible to obtain desirable ion current measurements from comparatively smaller amounts of Ti or Cr than that required in the single stage mass spectrometer used for analyses in this study. This development can potentially reduce the size of the graphite sample required. Given the problem of apparent random heterogeneous distribution of impurity elements, the question of how representative the sample amount is, may arise. The main emphasis on isotopic compositional data largely circumvents this question, assuming as always that all portions of a specific impurity element in the sample have been affected by neutron fluence exposure to the same degree. Alternative analytical methods could be investigated such as ion microprobe isotopic analyses of individual Ti- and Cr- bearing impurity inclusions in graphite, though this requires that the instrument be set up and dedicated for the study of irradiated samples under current radiological controls.

3.0 Neutronics Calculations

3.1 Introduction

The primary goal of the neutronics calculations was to translate the measured titanium isotopic ratios for each sample into an estimate of plutonium produced in the fuel elements that were irradiated adjacent to each sample. Due to the flux profile variation across the core it would be expected that less plutonium would be produced in core locations near the core periphery. A second activity was to estimate, prior to analytical measurement, the titanium isotopic ratios for each graphite sample. The calculations of titanium isotopic ratios and plutonium production were conducted without prior knowledge of the analytical results. All information used in the analysis was derived from the Trawsfynydd trepanning report (Reference 2) with the exception of additional information on the graphite densities from AJ Wickham of Nuclear Electric.

A cylindrical pin cell model in the WIMS-E 5A code (Reference 8) was used for this series of neutronics calculations. The model details are discussed in section 3.2. The calculations were performed on HP workstations using version 115 of WIMS. Due to the complexity and number of the WIMS input models required for the analysis, a spreadsheet was developed to generate the WIMS input. Material properties and burnup information were placed in the spreadsheet and separate WIMS inputs cases were then generated for each sample site. The results from the WIMS calculations were then placed into another spreadsheet for graphical display and data manipulation. The overall flow path of the data is shown in Figure 3-1.

Of the total 90 samples taken, 80 locations were modeled with WIMS. The four control rod sample sites were not modeled. At six locations two samples were taken 180 degrees apart at the same elevation. These six duplicate samples have the same model characteristics as the primary samples and did not require separate calculations. Each analysis has location specific power histories and graphite densities.

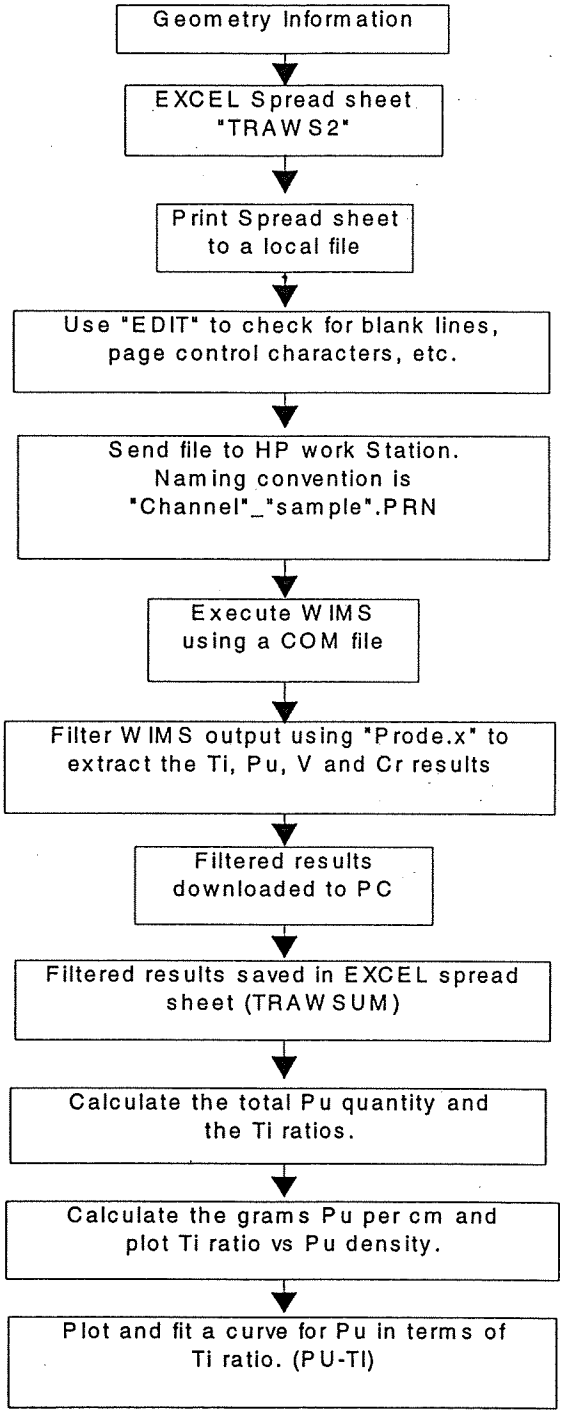

Figure 3-1. Data Flow Path for WIMS Calculations

3.2 Model Description

Data for the geometry, burnup and sample locations were obtained from the Trawsfynydd trepanning report (Reference 2). The pin cell model has cylindrical material regions of fuel, cladding, coolant and moderator. Unirradiated fuel pins are naturally enriched uranium metal clad in Magnox. Carbon dioxide is used as coolant and graphite is the moderator. The power generation and graphite densities were found to have significant impact on the titanium isotope ratios and thus the resulting plutonium generation relationship.

3.2.1 Burnup and Power

Individual fuel cycle burnup histories were modeled for each sample location. The local fuel burnup was estimated by using a linear interpolation of the mean fuel element irradiation history adjacent to the sample locations. No attempt was made to adjust the power profile for the fuel gaps between fuel elements (the total inventory is adjusted after the WIMS calculations to account for the axial fuel gaps).

The axial location (height) of each sample location was taken from the Trawsfynydd trepanning report. These values are listed in Table 3-1. The mean irradiation value was assumed to be at the fuel element midpoint (also listed in Table 3-1).

Table 3-1. Sample and Element Heights

Sample Number	Height above Base (m)	Fuel Element	Midpoint Height (m)
8	7.181	9	7.317
7	6.267	8	6.497
6	5.353	7	5.677
5	4.437	6	4.857
4	3.524	5	4.037
3	2.610	4	3.217
2	1.695	3	2.397
1	0.981	2	1.577
--	--	1	0.757

The fuel element discharge irradiation values and dates from the Trawsfynydd trepanning report were used with a few exceptions. Based on expected axial profile shapes and adjacent fuel element values, there were a few numbers in the table which appear to be in error. Channel 04J07 element 2 was assumed to have a mean element irradiation of 3333 $MWd.te^{-1}$ instead of 3383 $MWd.te^{-1}$. This change was based on making the values for this channel the same as in channels 06J06, 09J10, 11E07 and 11N11 which all have the same axial profile for the first fuel cycle.

Element 7, channel 06J06 discharged on 23/10/73 was assumed to be 3844 $MWd.te^{-1}$ instead of 2844 $MWd.te^{-1}$. The higher burnup makes the axial shape of the burnup values consistent with the other fuel cycles.

The remaining change made to the burnup data was for channel 09J10 element 6 discharged on 17/3/80. The 3505 $MWd.te^{-1}$ value was changed to 5303 $MWd.te^{-1}$. The modified value was estimated based on the axial shape of the fuel burnup. It was surmised that the first two digits were transposed in the document.

Eight end fuel elements were "retained for second cycle" and have an "X" for the mean element irradiation for the second to the last fuel cycle. The burnup in these elements was assumed to be proportional to the burnup in the adjacent fuel elements. The WIMS models assumed that the fuel was discharged and fresh fuel used in the last cycle and does not account for the higher burnup fuel in the channel.

A xenon burn-in step of 11.856 MWd was used to obtain a calculated xenon content for the calculation. Other burnup steps were at 237.13 MWd with the exception of the final step which was adjusted to obtain the proper total burnup of the fuel.

At burnup values which correspond to each fuel reload, fresh fuel was reinserted into the model. Thus, the fuel reloads were explicitly modeled. The total plutonium content for a channel was obtained by summing the plutonium content of all the fuel elements.

3.2.2 Geometry

The WIMS model has four concentric cylindrical material regions; fuel, cladding, coolant and moderator. The model has 19 regions, one each for the fuel, clad and coolant and 13 for the graphite. The model uses a cylindricized geometry which maintains the total moderator volume for a fueled location in the Trawsfynydd reactor.

The inner most region is modeled as uranium metal fuel with the radius adjusted for thermal expansion (i.e., 1.422 cm). A mean fuel temperature is calculated based on height at each axial location and the axial temperature profile provided in the Trawsfynydd trepanning report. The fuel density was reduced to account for the radial expansion at operating temperatures. Multiple fuel materials were used to account for the fuel reloads. All initial fuel materials were of the same type and enrichment (i.e., natural enrichment).

An annular clad region was modeled with magnesium, aluminum and beryllium (Magnox) with a clad thickness of 0.3915 cm. The radial expansion of the fuel and cladding displaces the carbon dioxide coolant and was neglected due to the low density of carbon dioxide. The cladding composition use was 99.19% magnesium, 0.80%aluminum, and 0.01%beryllium. The Trawsfynydd trepanning report give a range of composition densities for Magnox.

The inner graphite radius was modeled as 4.7625 cm. Multiple graphite regions were modeled to calculate the radial variations of the titanium transmutation/ burnup within the pincell. Twelve different graphite densities were used to account for the graphite loss as a function of exposure and temperature. Sensitivity studies on graphite mesh thickness were conducted to ensure the mesh spacing in the graphite did not impact the titanium calculations. Titanium isotope ratio variations within a pincell were homogenized and variations within a pincell were not used.

3.2.3 Cross Section Set

A WIMS 5a library set with 69 groups was used. Modifications to the library were necessary to allow for the generation and depletion of titanium isotopes.

3.2.4 Graphite Properties

A sensitivity study on the graphite density indicated that this had a significant impact on the titanium isotope ratios. The graphite density is reduced due to material loss to the carbon dioxide coolant. This effect is dependent on temperature, time at power and coolant properties. Thus, the moderator density decreases with reactor age. An empirical relation with temperature and power was developed based on the information in The Trawsfynydd trepanning report. The graphite density (material) was modified such that the maximum change in the density is less than 0.01 g/cm^3. This corresponds to changing the density at about every 3000 MWd/Mt of burnup.

Thermal expansion of the graphite was not incorporated since it has little effect on neutronics calculations. Impurities in the graphite were included as an equivalent boron concentration (1.63 ppm for grade A graphite). The equivalent boron concentration was calculated based on the impurities levels listed for Grade A graphite in the Trawsfynydd trepanning report.

3.3 Calculation Results

Two objectives of the WIMS calculations were a) to estimate the titanium isotope ratios in the graphite sample locations and b) estimate the local plutonium production based on the titanium isotope ratios. Titanium isotope ratio results from the WIMS calculation are compared to the measured sample data results in two ways. The first comparison is a direct pointwise comparison of the titanium isotope ratios and the second is a spacial comparison. Plutonium production values were not provided for comparison in this calculation.

3.3.1 Titanium Isotope Ratios

Relative isotopic ratios for all five titanium isotopes were evaluated. The ratio of each isotope with respect to the others is based on the initial ratio and the irradiation history. Since all isotopes received the same irradiation history and the initial ratios are known, a consistency check between different titanium isotope ratios was performed. Titanium 48 was used as the basis for the comparisons. The isotopic ratios of 48 to 49 are used for the majority of the comparisons due to their sensitivity in the fluence range of interest.

3.3.1.1 Pointwise Comparison to Analytical Data

Comparison of the calculated titanium isotope ratios with the analytical data on a point by point basis is shown in Figure 3-2. An ideal data fit would have all of the points on a line with slope equal to one (45 degrees). As can be seen on the figure, some of the data points show that the measured (sample) data have higher titanium 49 to 48 ratio (i.e., the measured data is closer to natural titanium) than is predicted by the WIMS calculation. The data shows a bias that is constant with interference (or contamination) from unirradiated titanium.

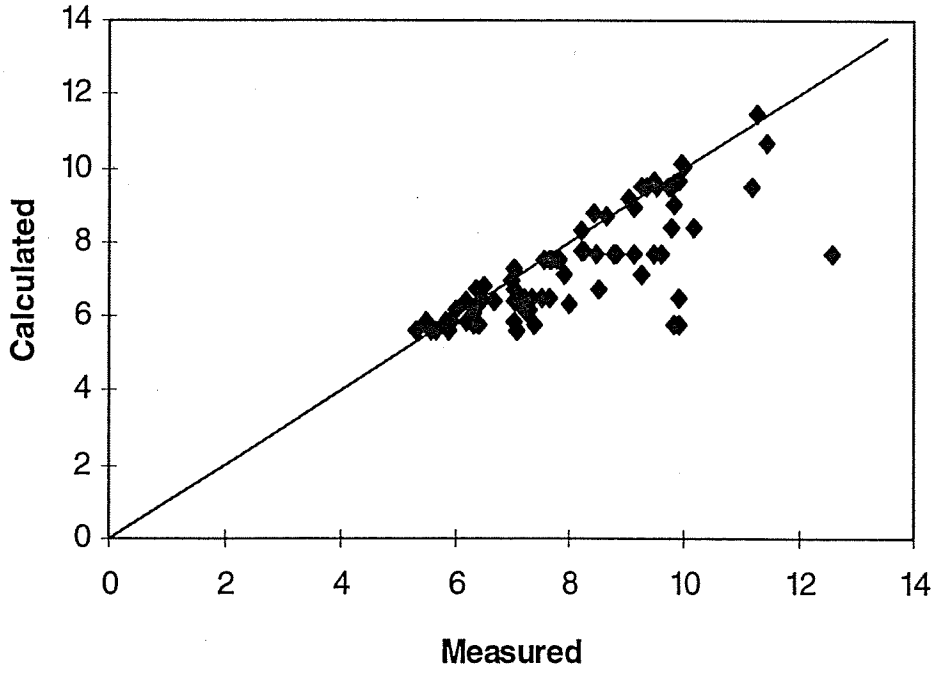

Figure 3-2. Measured vs Calculated Ti49/48 Ratios

3.3.1.2 Spatial Shapes

Titanium isotope ratios are expected to be dependant on the integrated local power (neutron source) and the graphite density (spectrum of the neutron source). Thus, the spacial shape of the titanium isotope ratios are expected to follow the reactor's power profile. Radial and axial profiles of the titanium isotope ratio were calculated. These profiles are compared to the measured data as discussed below. Local perturbations in the reactor (such as control rods or other localized neutron absorbers) are not modeled in the calculation.

The axial plots of the titanium isotope ratios are given in Figures 3-3 through 3-12 for each sampled channel. Physics of the reactor requires the profiles to be relatively smooth. Thus, the large deviation of some of the sample points toward natural titanium ratios would indicate these data points have been compromised.

Interestingly, the plots uniformly show a bias at the lower end of the core, where the measured titanium 48/49 ratio is higher (less altered) than the calculated value. Such a consistent bias implies that the power at the lower end of the core is less than reported by Nuclear Electric.

Radial profiles for the primary plane are shown in Figures 3.13 through 3.20. The profiles are plotted for each axial sample elevation (z). The bias described above is also visible on the outer radius locations. As indicated in the pointwise comparison, the measured data is consistent with or less altered than the calculated values.

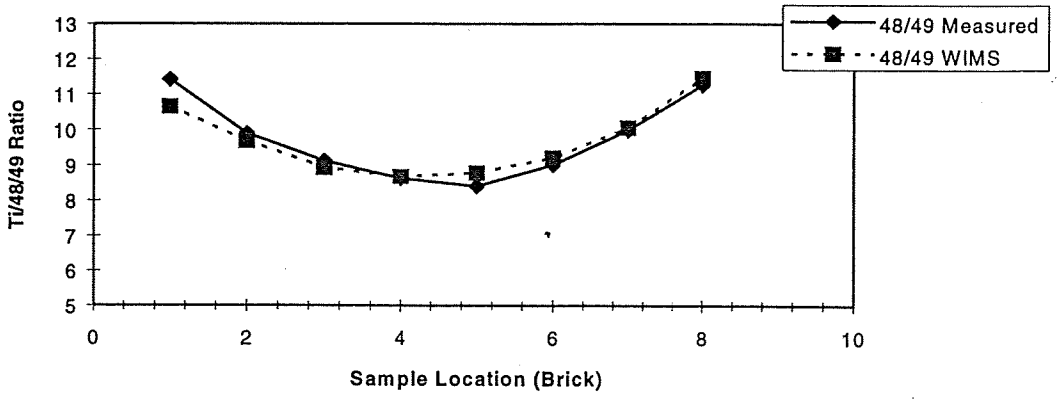

Figure 3-3. Axial Ti 48/49 Ratios for 01J08/7

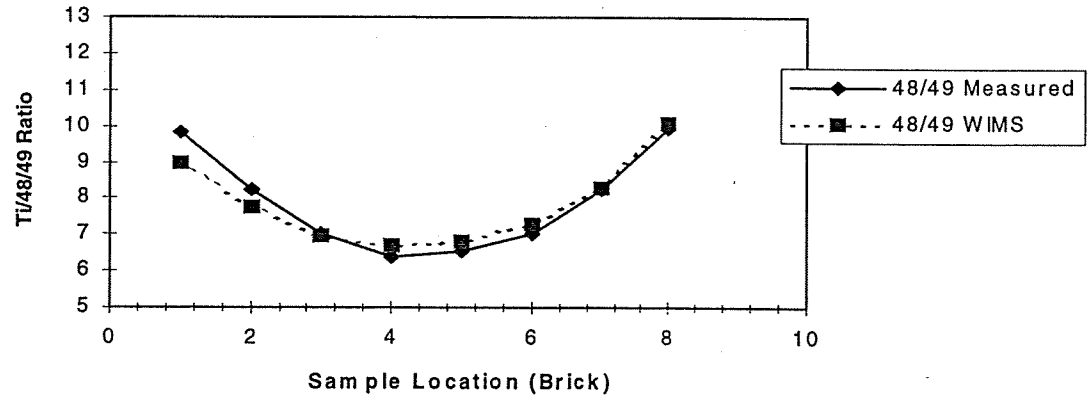

Figure 3-4. Axial Ti 48/49 Ratios for 02J07

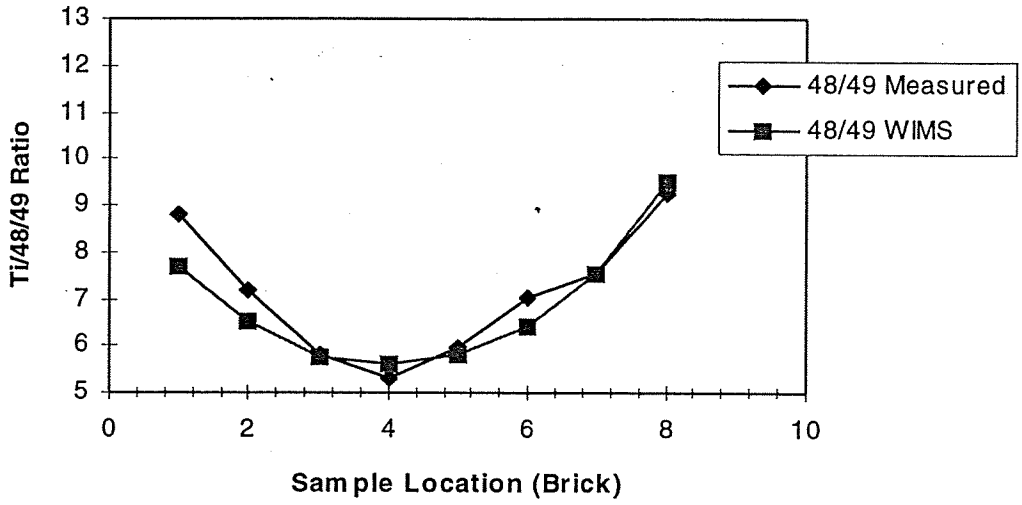

Figure 3.5. Axial Ti 48/49 Ratios for 04J07

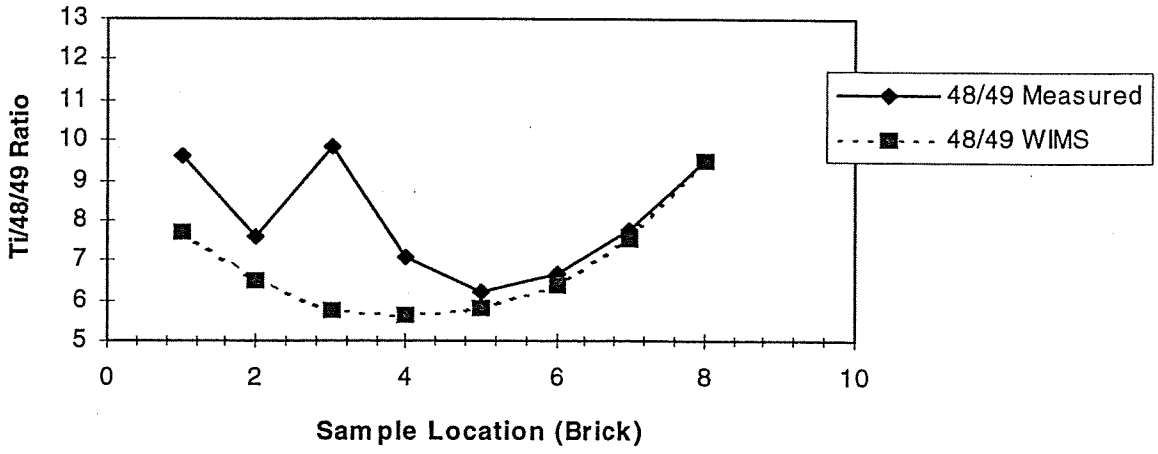

Figure 3.6. Axial Ti 48/49 Ratios for 06J06

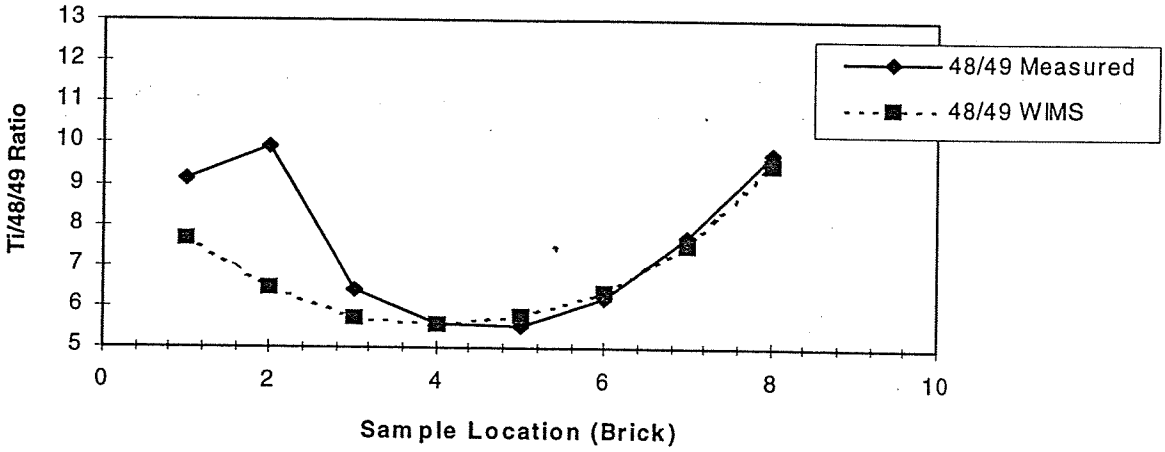

Figure 3.7. Axial Ti 48/49 Ratios for 09J10

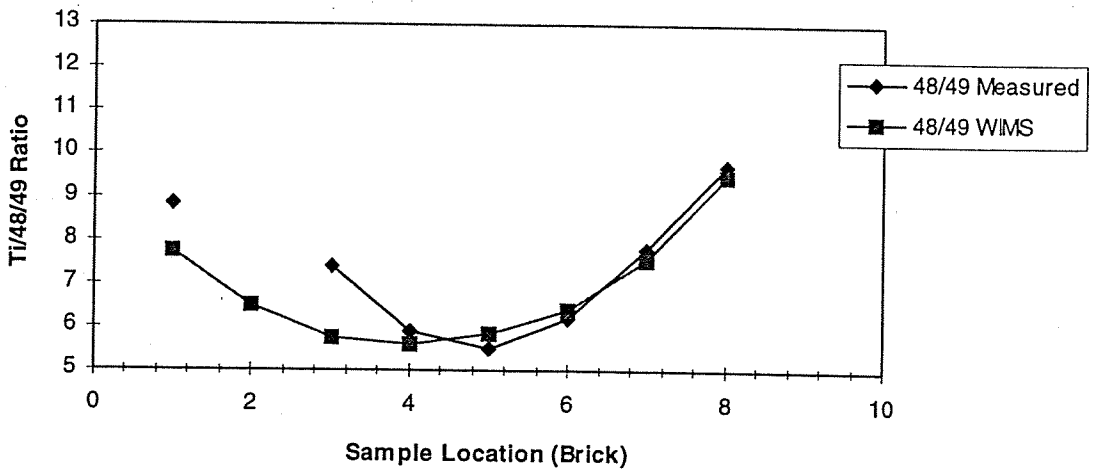

Figure 3.8. Axial Ti 48/49 ratios for 10G06

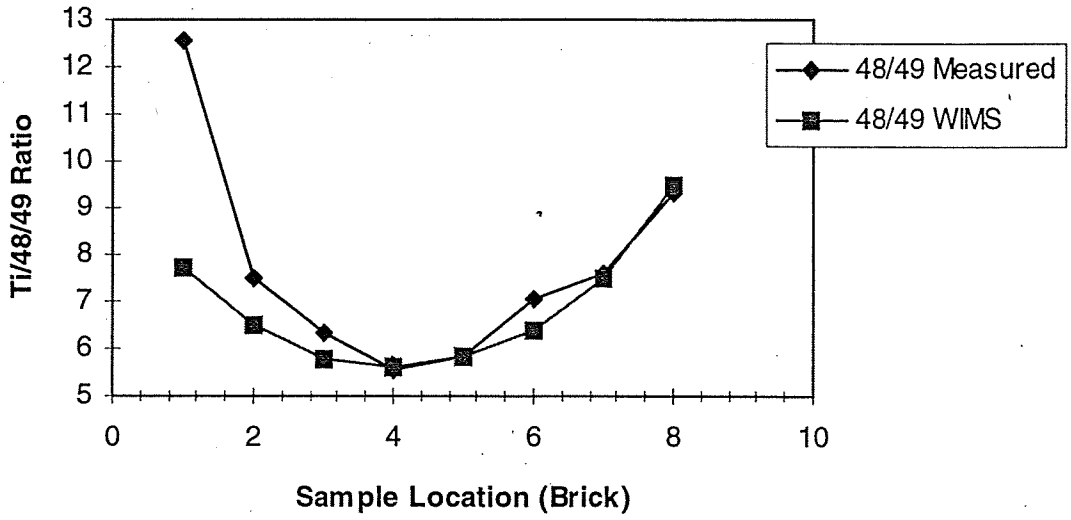

Figure 3.9. Axial Ti 48/49 Ratios for 11E07

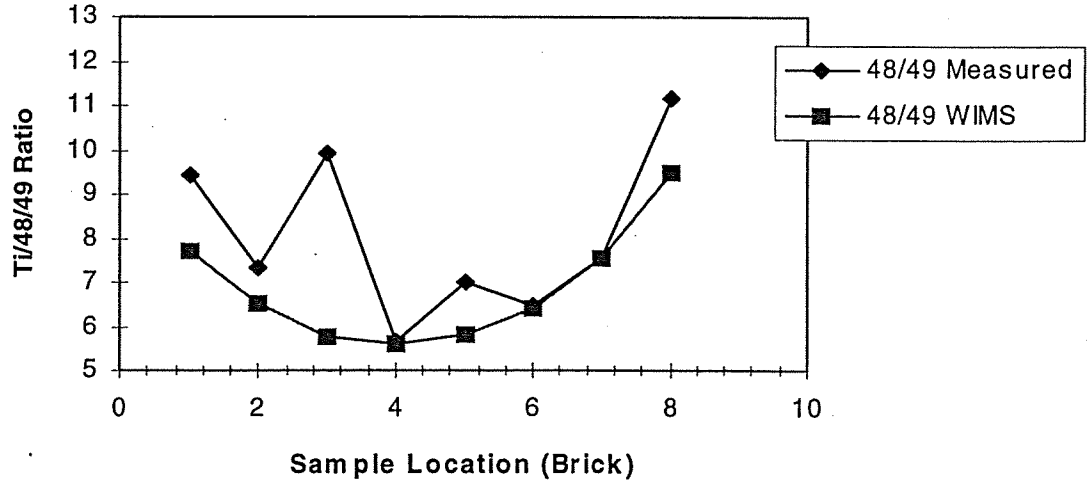

Figure 3.10. Axial Ti 48/49 Ratios for 11N11

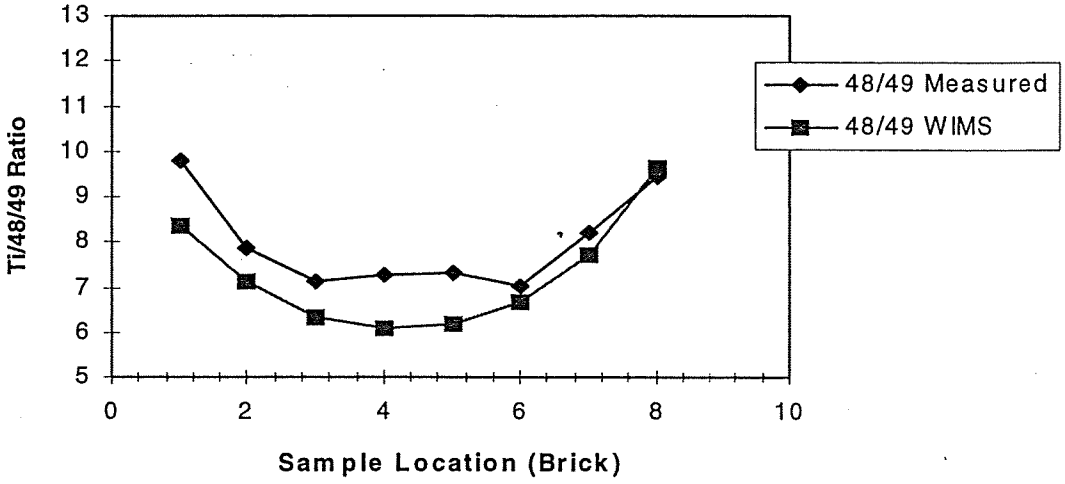

Figure 3.11. Axial Ti 48/49 Ratios for 12C06

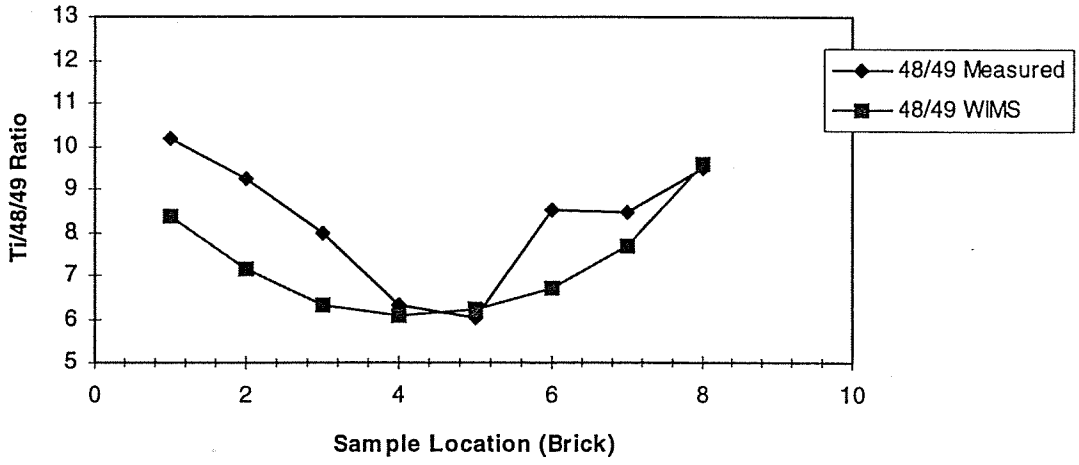

Figure 3.12. Axial Ti 48/49 Ratios for 12Q06

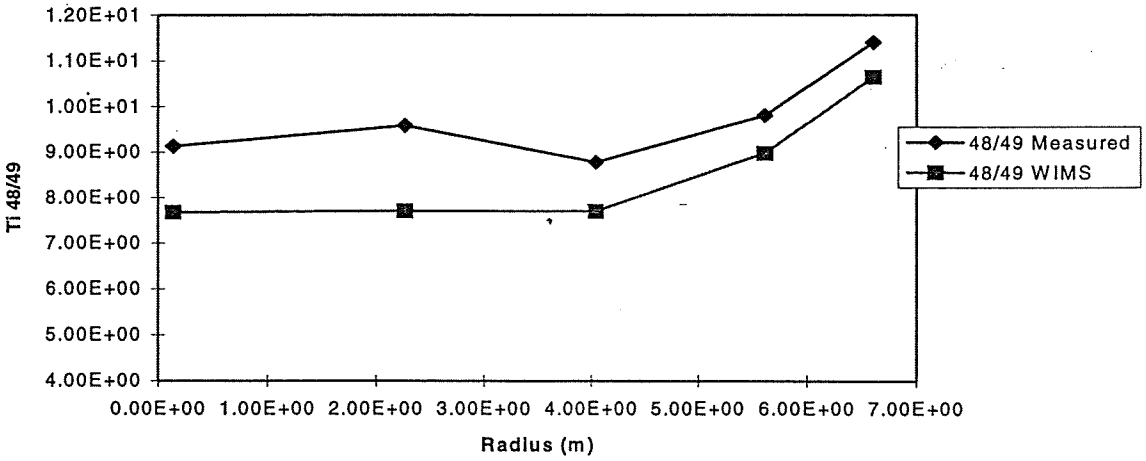

Figure 3.13. Radial Profile of Ti 48/49 Ratio at z=0.981 m

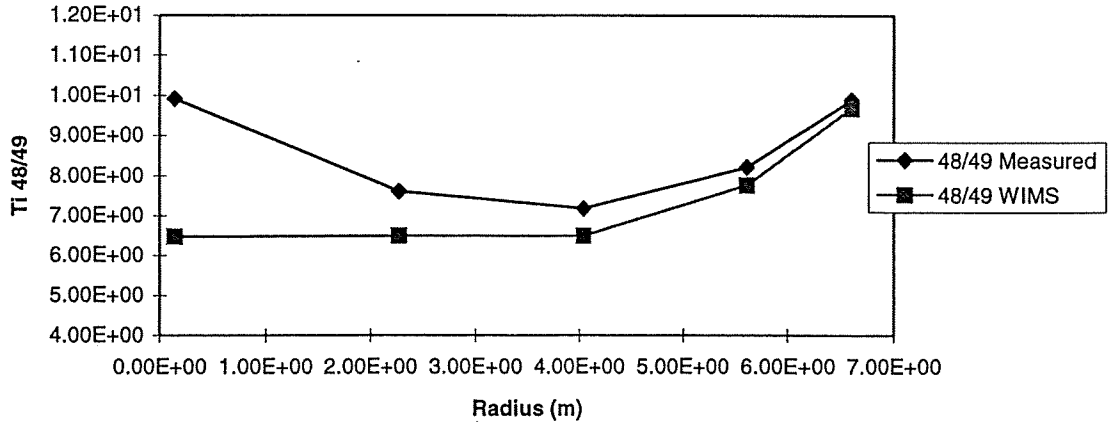

Figure 3.14. Radial Profile of Ti 48/49 Ratio at z=1.695 m

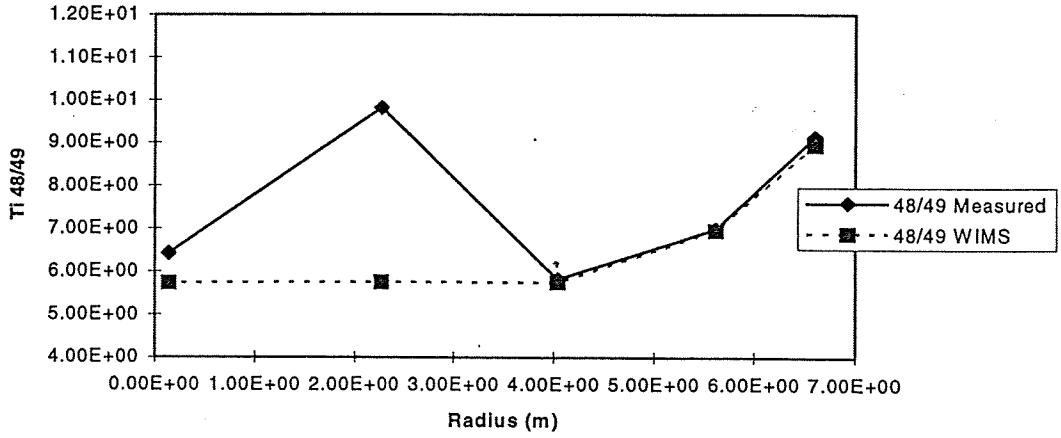

Figure 3.15. Radial Profile of Ti 48/49 Ratio at z=2.610 m

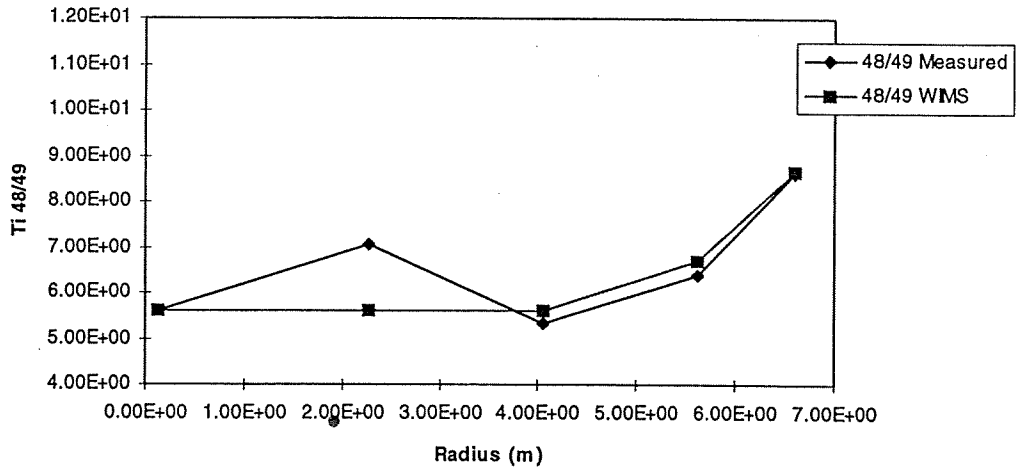

Figure 3.16. Radial Profile of Ti 48/49 Ratio at z=3.524 m

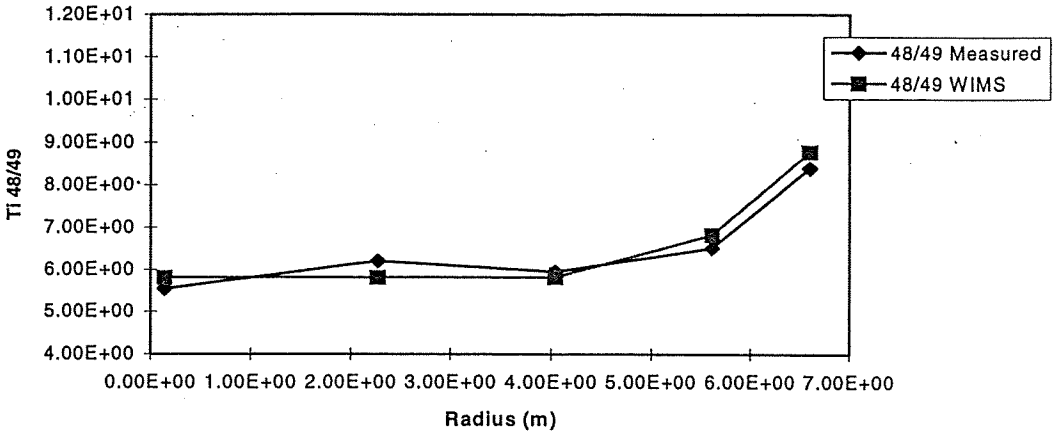

Figure 3.17. Radial Profile of Ti 48/49 Ratio at z=4.437 m

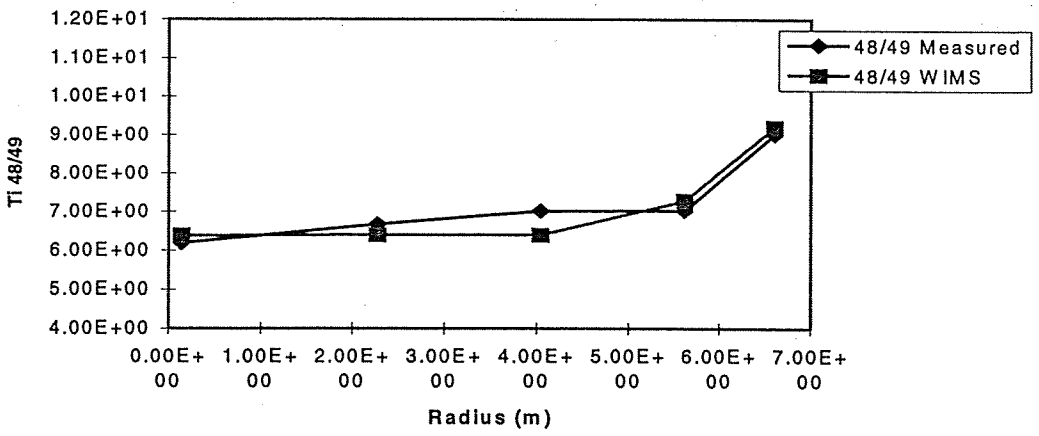

Figure 3.18. Radial Profile of Ti 48/49 Ratio at z=5.353 m

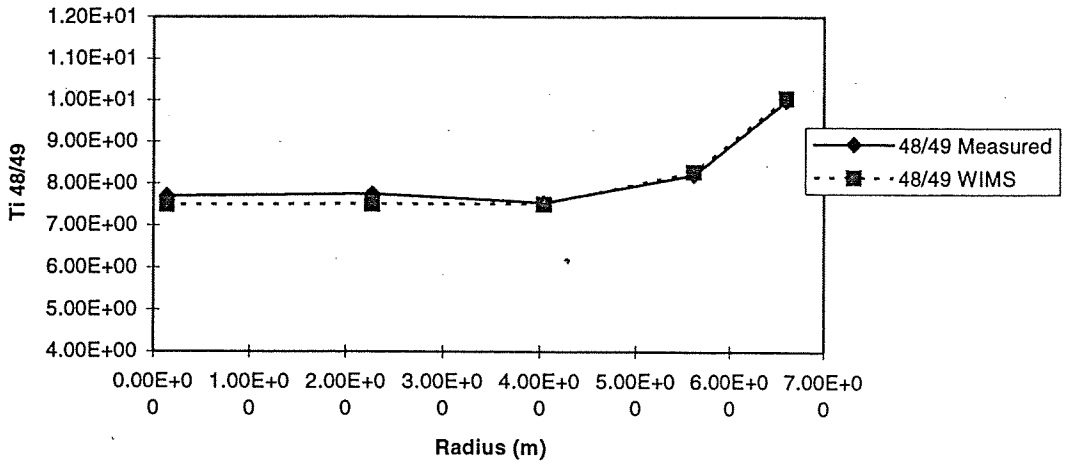

Figure 3.19. Radial Profile of Ti 48/49 Ratio at z=6.367 m

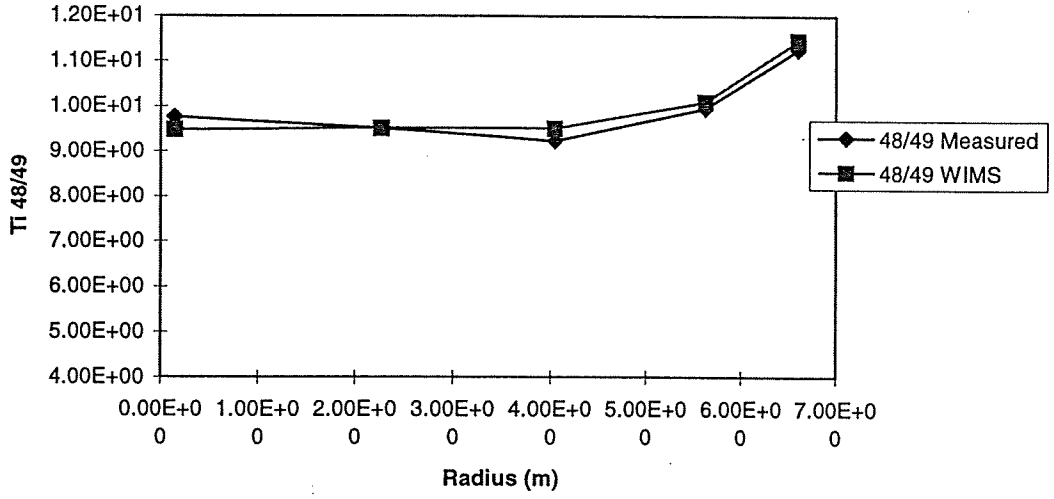

Figure 3.20. Radial Profile of Ti 48/49 Ratio at z=7.181 m

3.3.2 Plutonium Production

Figures 3.21 and 3.22 have the summary results from the WIMS Trawsfynydd plutonium production calculation. The curves represent the calculated correlation of the Titanium 48/49 ratio in the graphite with the plutonium production in the adjacent fuel. The results from the outer fuel channel (channel 01J08) were significantly different from the other channels, due to the much different fuel management strategy for peripheral channels, and a separate titanium isotope ratio/Plutonium correlation was generated. The equations and lines drawn were obtained by standard trend line analysis.

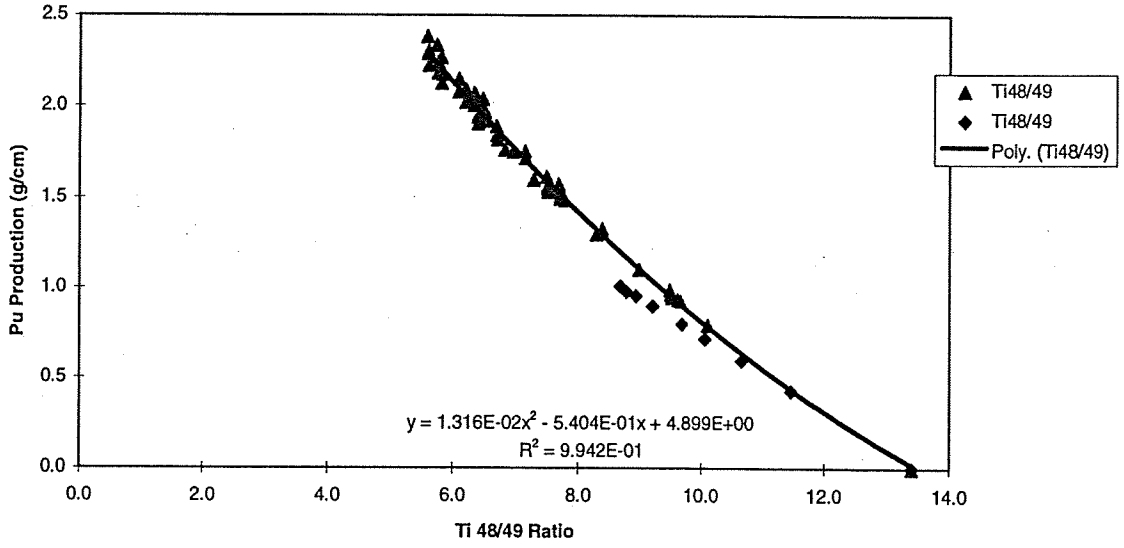

Figure 3.21. WIMS Result for Traws

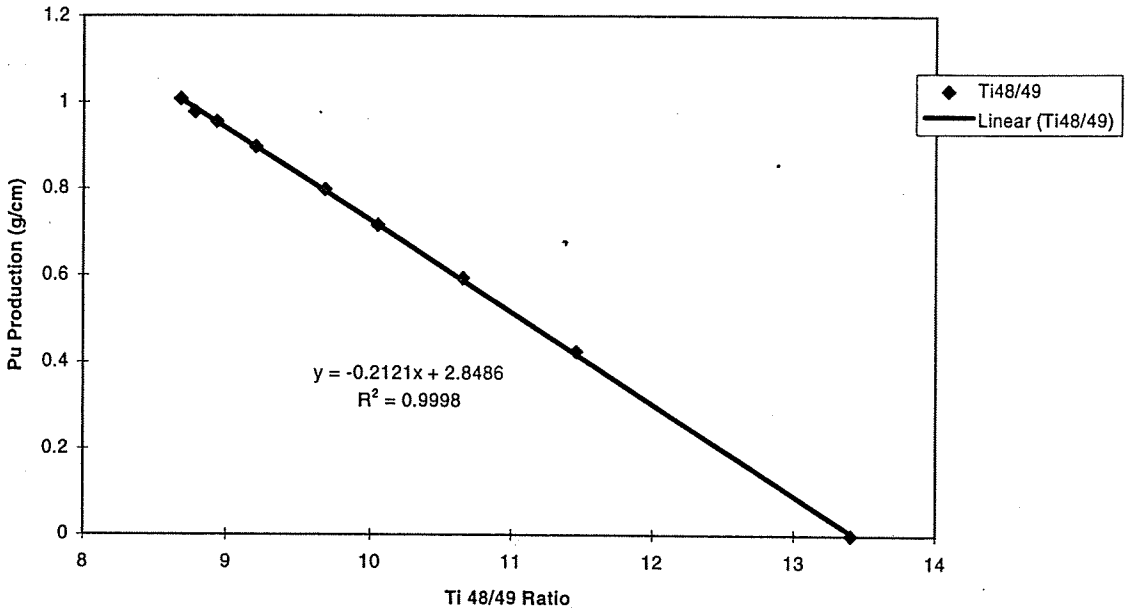

Figure 3.22. WIMS Result for Traws Outer Fuel Channels

3.3.2.1 Sensitivities

Titanium atom densities were calculated by WIMS at various distances from the fuel. Atom densities for titanium isotopes 46, 47, 48, 48 and 50 were included in the calculation. The titanium isotope ratio (48/49) was determined by dividing the average atom density of titanium 48 by that for titanium 49. An average of the number densities in the first 3.3 cm of the graphite was used. There are 11 graphite layers, each 0.3 cm thick in the WIMS model. The WIMS model includes burnup and transmutation of the titanium, but does not include scandium (a potential precursor to titanium 46).

Vanadium and chromium atom densities were also calculated, but were not used.

Plutonium isotopes 238, 239, 240, 241 and 242 were included in the results. The combined mass of all of the plutonium isotopes was calculated and reported. The plutonium atom density values, calculated by WIMS, were converted to grams/cm using the plutonium's atomic weight and the cross sectional area of the fuel. The fuel diameter used was 2.858 cm giving an area of 6.41526 cm^2.

3.3.2.2 Plutonium Production Profiles

The Ti48/49 ratio shows a strong correlation with the plutonium production. The relationship is not direct, but related through the neutron fluence. Using the trend line analysis, the plutonium production in the adjacent fuel channels can be estimated from the titanium 48/49 ratio (Ti(48/49)) with equation **(1)**.

$$Plutonium(g/cm) = 0.01316 * Ti(48/49)^2 - 0.5404 * Ti(48/49) + 4.899 \quad \textbf{(1)}$$

The titanium isotope ratio is unitless. The plutonium production is in grams per centimeter of active fuel. Although the active core height of the core is 7.361 m, the total active fuel length is 9*73.5cm or 6.615 m. The difference in the lengths is due to the gaps in the fuel between fuel assemblies. The smaller active length (6.615 m) is the appropriate length to use to calculate a channel production value.

Equation **(1)** fits the WIMS data (excluding channel 01J08) with an R^2 of 0.9942.

Plutonium production estimate for channel 01J08 with respect to a titanium 48/49 ratio is shown in equation **(2)**.

$$Plutonium(g/cm) = -0.2121 * Ti(48/49) + 2.8486 \quad \textbf{(2)}$$

Equation **(2)** fits the WIMS data for channel 01J08 with an R^2 of 0.9998.

3.3.2.3 Total Plutonium Production Estimates

The equations in section 3.3.2.2, in conjunction with the measured titanium ratios for each sample location, provide local plutonium production estimates for fuel adjacent to each sample location. Using the statistical aggregation method in section 4.0, the local plutonium production estimates can be translated to an estimate of the cumulative plutonium production for the reactor as a whole. This aggregation method and cumulative global plutonium production estimate is provided in section 4.0.

4.0 Regression Production Estimates

In this section, the local production estimates described in Section 3.0 are aggregated together to form a total production estimate. Iteratively weighted regression is used to produce the estimates presented in this section. The method fits a 3-dimensional "fluence field" to the local production estimates, and then integrates over the volume of the reactor to get an average production estimate. The average production estimate (measured in g/cm) can then be multiplied by the effective length of the fuel rods to produce a total production estimate.

The regression methodology employed in this section is nearly the same as that described in Reference 1, with one important difference. In the previous study (Reference 1), the errors were assumed to be Gaussian with a fixed sigma, so ordinary least-squares (OLS) regression was used. However, the errors in the Ti49/48 ratios seem to be decidedly skewed, so weighted regression has been utilized to account for this difficulty.

Section 4.1 gives a description of the measurement error distribution that applies to the Ti49/48 ratios, while Section 4.2 describes how this error distribution has been used in the regression procedure to obtain the proper production estimates. (It should be noted that the Ti49/48 error distribution and local production error distributions are essentially the same, because local production is related to the Ti49/48 measurements through a transformation that is essentially linear.

The last section describes the results of the regression fit. The regression fit produces much more than a total production estimate; it produces a 3-dimensional production field that can be compared to the measurements at each sampled location. This comparison (residual analysis) can tell whether the regression model is reasonable, and also describe the correct measurement error structure.

4.1 Error Structure Associated With Local Predictions

Laboratory measurement replicates, have produced a measurement RSD (relative standard deviation) that is about 0.5%, a respectably small value. This RSD does not include variations due to sample preparation, sample contamination, or insufficient Ti, so the 0.5% figure actually represents mass spectrometer instrument variability. The total analysis variability could be larger than this.

The sample data collected from Traws II strongly indicates that instrument variability is indeed overwhelmed by other errors. More specifically, the data indicates that sample contamination may be the dominant source of error. When we use the term, sample contamination, we refer to the case when the ratio, unirradiated/irradiated Ti is relatively high. This condition may be caused by 1) significant background contamination, or 2) insufficient graphite sample size. We will not distinguish between the two possible causes of this high ratio, because both causes result in the same consequences for the error distribution.

4.1.1 Contamination Errors associated with Ti

If un-irradiated Ti contamination is a significant source of error in the Ti49/48 measurements, we would expect the errors to be highly skewed. In fact, if it were the only source of error, all errors in the Ti49/48 ratio would be negative.

Let C represent the fraction of un-irradiated Ti that is contaminating the sample, R_M the measured 49/48 ratio, R_T the "true" ratio associated with irradiated Ti, and finally, R_B the unirradiated background ratio ($R_B = 0.0745$). Then the measured and correct ratio are approximately related through the interpolation formula:

$$R_M = (1 - C)\, R_T + CR_B \qquad (3)$$

It so happens that the Traws II samples have been divided into sub-samples, which allow us to obtain some information on the distribution of C. Let the indices ij represent a measurement from location I in the reactor on sub-sample j. Then the measurements are described by the equation:

$$R_{Mij} = (1 - C_{ij})\, R_{Ti} + C_{ij} R_B \qquad (4)$$

Our objective is to actually estimate the distribution of the contamination error which is defined as $R_{Mij} - R_{Ti}$. However, one can see from the equation above that the distribution of C_{ij} and this contamination error are closely related:

$$R_{Mij} - R_{Ti} = (R_B - R_{Ti})\, C_{ij} \qquad (5)$$

so the error distribution can be obtained from the contamination distribution simply by multiplying by a constant.

To produce an empirical distribution of the C_{ij} one needs to use equation 4 to solve for the C_{ij}, but there are too many unknowns in the equation to accomplish this. An estimate for R_{ti} is required. A crude estimate for the true ratio is:

$$\hat{R}_{Ti} = \max_j R_{Mij} \qquad (6)$$

This must be considered a very crude estimate because at the majority of locations, the number of sub-samples is only 2, with a few locations having 3 and 4 sub-samples. Given the small number of sub-samples, this simple estimator will underestimate R_T, and consequently the magnitude of

C will be underestimated. In other words, the contamination distribution that we have produced may be too optimistic.

Applying this scheme to all locations where sub-samples exist produces the empirical CDF presented in Figure 4.1.A. In this Figure the points C_j have been used to produce an empirical cumulative distribution function (the solid line), along with a beta distribution fit to this data. The beta fit yields parameters of $\alpha = (0.4, 1.46)$ for the distribution:

$$f(C) = \frac{\Gamma(\alpha_1+\alpha_2)}{\Gamma(\alpha_1)\Gamma(\alpha_2)} C^{\alpha_1-1}(1-C)^{\alpha_2-1} \qquad (7)$$

Figure 4.1.B illustrates the corresponding density. As one can see from these results, the mean contamination seems to be about 20%, but there is a substantial chance of much larger contamination. From the CDF, one can deduce that the contamination is above 60% on 20% of the samples.

As stated earlier, the method used may underestimate the magnitude of the contamination, so the results presented here confirm that contamination is an important problem. This error structure causes big problems with ordinary regression, which cannot deal with an error structure that is biased to one side.

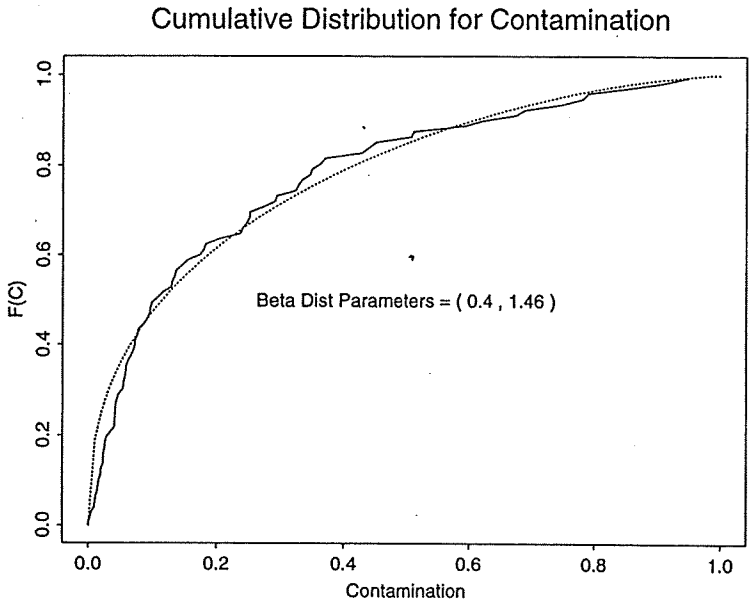

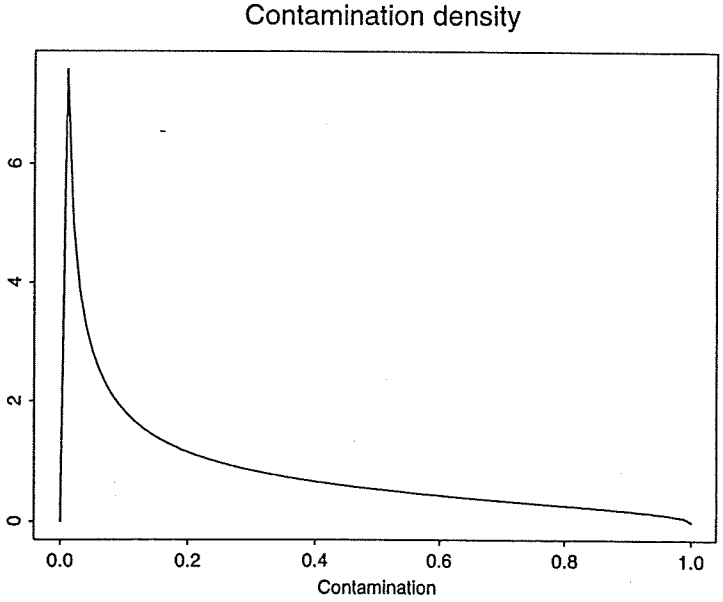

Figures 4.1.A and 4.1.B. Contamination Error Distribution for Ti48/49 Ratios

4.1.2 Total Error Distribution for Ti 49/48 Ratio Measurements

The distribution developed in the last section describes only one component of the total measurement error. The total measurement error should consist of contamination error plus Gaussian instrument/sample preparation error. This error is computed for each sample, and is about 0.5%. Figure 4.2 presents the distribution of relative standard deviations computed from measurement replicates. As one can see from the plot, the RSD's range up to about 1.5%.

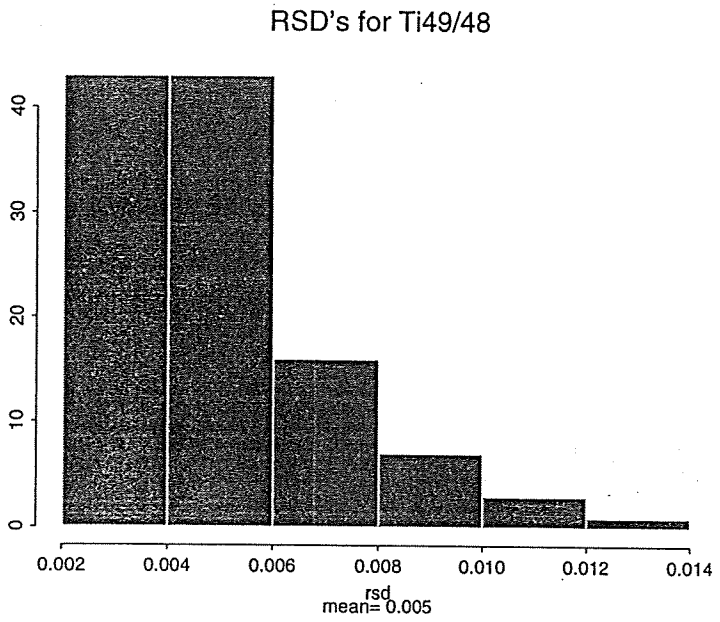

Figure 4.2. Measurement Error RSD's Calculated from Replicates

The RSD's presented in the figure may be too optimistic, because they do not include sample preparation variability. We will therefore take the mean value for the RSD's and multiply it by a factor of 5 and will therefore assume that the instrument+sample preparation RSD is 2.5%. This results in a total measurement error distribution that is a convolution of the contamination distribution with a normal distribution having a standard deviation of 0.003=0.125 x 0.025, (0.125 is the mean of the data). This result is presented in Figure 4.3.

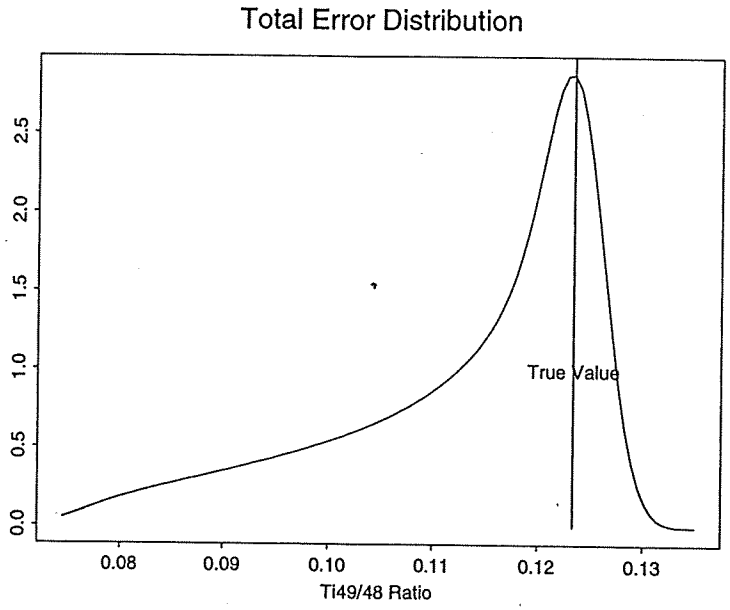

Figure 4.3 Assumed Distribution of Total Measurement Error for Ti49/48 Ratios

4.2 Regression Model for Aggregation

The field, $\Phi(r, z, \theta)$ describes the fluence at the polar coordinates (r, z, θ) in the reactor (r and z measured in cm, θ in degrees). The regression model attempts to determine this field by fitting a functional form of this field to data. The "data" that this regression model uses is not the Ti49/48 ratios, but the local production estimates (g/cm) that have been computed from the ratios (see section 3.0 for details). Thus, the fitted field is really a production field and not a fluence field.

The regression procedure fits the field $\Phi(r, z, \theta)$ to the data using the model:

$$Y_{k\ell} = \Phi\,(r_k, z_k, \theta_k) + e_{k\ell} \qquad (8)$$

where $Y_{k\ell}$ represents a local production estimate at location k and ℓ identifies replicate measurements. The last term in the model, $e_{k\ell}$ represents the error associated with measurement $Y_{k\ell}$, which is distributed according to Figure 4.3.

4.2.1 Regression Model Details

The field is assumed to be the linear combination of the following eigenfunctions:

$$\Phi(r, z, \theta) = \sum_{i,j} \beta_{ij} F_i(r) G_j(z) \qquad (9)$$

The parameters β_{ij} are to be determined by regression and each eigenfunction is built from univariate eigenfunctions that have been multiplied together. The radial component of the eigenfunctions is described by:

$$F_i(r) = \cos\left(\frac{\pi (2i-1)}{2R_0} r\right) \qquad (10)$$

for $I = 1,2,3$, while the axial component, the functions have the forms:

$$G_j(z) = \begin{cases} \cos\left(\frac{\pi j}{2Z_0} z\right) & \textit{odd index} \\ \frac{z}{Z_0} \cos\left(\frac{\pi (j-1)}{2Z_0} z\right) & \textit{even index} \end{cases} \qquad (11)$$

for $j = 1,2,3$. Since both I and j range over 1,2,3, a total of 9 "eigen-functions" are used in the above regression model. Previous studies (Reference 1) have shown that this number of components is sufficient to adequately determine this 3-dimensional field. Figure 4.4 illustrates the eigen-function components used in the regression model.

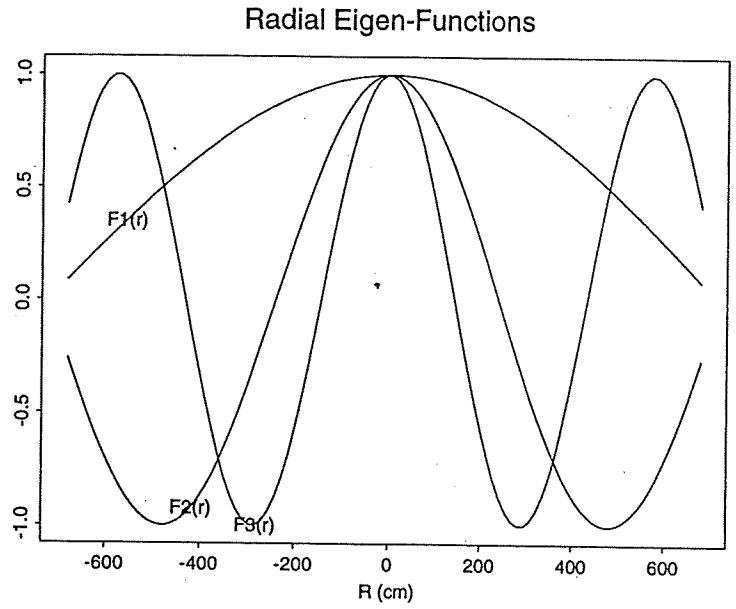

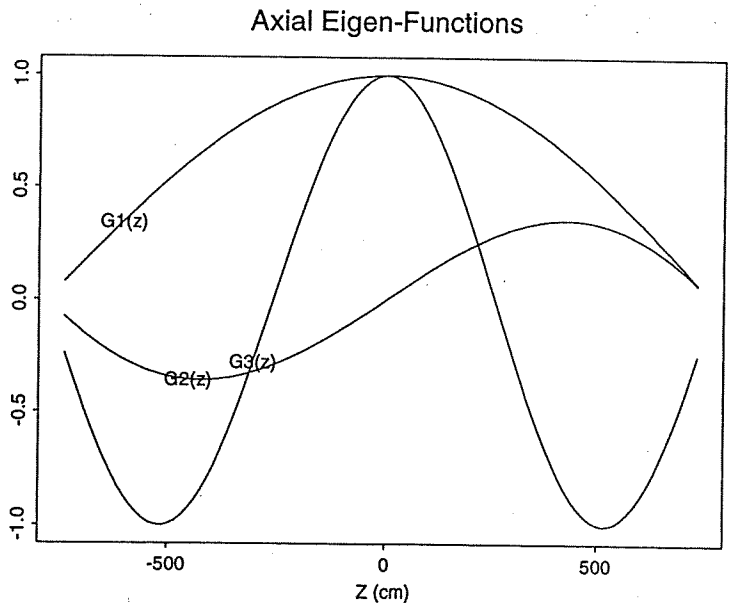

Figure 4.4. Plots of Eigen-function Components

Total production is calculated by integrating the field over the volume of the reactor, and then multiplying by the appropriate conversion factor to convert to the correct units.

4.2.2 Regression Model Weights

The error term $e_{k\ell}$ present in Equation 8 should be distributed as illustrated in Figure 4.3, which is heavily skewed to the left. Ordinary least squares can not deal with a skewed distribution, so we have chosen to use a iteratively-weighted regression, which can accommodate this distribution. According to the methods described in Reference 9, if the errors e have the distribution $f(e)$, the regression weights should have the form:

$$W(e) = -\frac{f'(e)}{ef(e)} \qquad (12)$$

The weights, $W(e)$, depend on the individual errors, e. The weight function corresponding to the distribution $f(e)$ of Figure 4.3 is presented in Figure 4.5. As one would expect, the weight function dramatically downweights errors on the left side of the distribution. Because the error distribution $f(e)$, and hence the calculated weight $W(e)$ is only approximately known, the actual weight used in the regression has been simplified to the step-function represented in Figure 4.5. This weight function assigns unit weight to all points greater than -σ and zero weight to any points less than -σ.

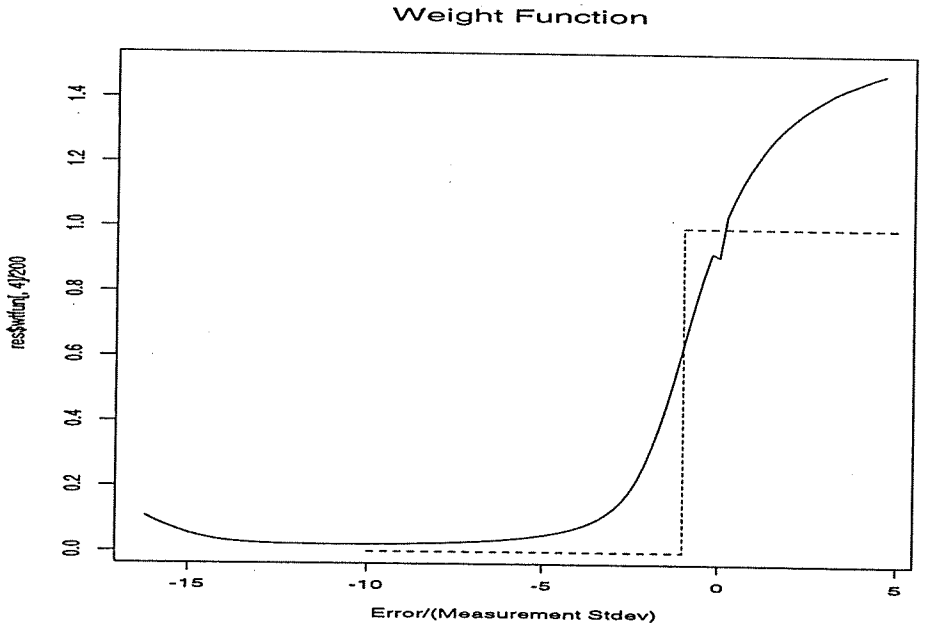

Figure 4.5. Weight Function Derived From the Error Distribution

This simple weighting function has been used to fit a production field, $\Phi(r,z,\theta)$ to the data. With this weight function, the fit tends to envelop the actual measurements. That is, most of the measurements are below the fitted curve.

4.3 Regression Results

A total of 89 locations in the reactor were measured, spread across three half planes. These locations provide more than enough information to adequately determine the 9 parameters present in the regression model (7). The regression fit produces the estimates presented in Table 4-1 and the residual distribution in Figure 4.6.

Table 4-1. Weighted and OLS Regression Results

Index		β Estimates	
I, (r)	*j, (z)*	Weighted	OLS
1	1	2.91	2.67
2	1	-0.88	-0.74
3	1	0.40	0.38
1	2	0.03	0.39
2	2	-0.01	0.11
3	2	0.04	0.01
1	3	-0.12	-0.09
2	3	0.04	0.09
3	3	0.05	0.02
Mean local Pu Production		1.466	1.327
SD (Mean)		0.031	0.025

(g/cm)

As one would expect, the weighted regression produces a larger average production value (1.466 g/cm) than ordinary least squares (1.327 g/cm). The nine regression parameters exhibit generally the same pattern in the weighted and OLS fits. The largest difference occurs with eigenvector $G_2(z)$. The OLS fit gives more weight to terms that involve this function. Since $G_2(z)$ is asymmetric, the OLS fit displays asymmetries in the z direction.

4.3.1 Residual Analysis

The Figures 4.7 through 4.10 display the production data and regression fits. The fit from the weighted regression is represented as a solid line while the OLS fit is represented as a dotted line. Each plot represents a specific (r,θ) location in the reactor. As one would expect, the weighted regression fit tends to envelope the data from above and is also greater than the OLS fit. These residual plots show locations where the data fits the curves poorly. Several isolated points are dramatically lower than the predicted, indicating contamination error (For example the points at [z =-300, r=360, θ=20], [z =-300, r=370, θ=150], or [z =-300, r=230, θ=270]). Some fuel channels seem to demonstrate more than isolated contamination. For example, the channel at (r=520, θ=150) indicates large contamination in 4 our of 8 sampling locations. Only one fuel channel exhibits a clear case of model misfit. All but one of the measurements taken on channel (r=660, θ=270) are higher than the fitted curve by a significant margin. Since this channel is nearest the core edge, this misfit is likely due to the significant difference in the fuel management which is employed for peripheral fuel channels.

4.3.2 Estimate of Total Production

Total production is calculated by taking the average production estimate (see Table 4-1) and multiplying this average by the effective fuel rod length and number of fuel rods. In other words;

$$TotalProduction = AverageX EffectiveFuelRodLengthX FuelRods$$

The effective fuel rod length is 0.90X736cm=662.4cm. When these multiplications are performed, one obtains a total production estimate of 3.633 metric tons (associated with weighted regression). This compares with a OLS estimate of 3.288 metric tons, which is biased low if the assumptions concerning contamination error are correct. The OLS standard error would also be too small. The least squares error estimate is 2% (RSD) for Pu production. The RSD obtained from regression describes only uncertainty due to "random" measurement error -- the reactor calculations may also introduce systematic biases. According to Reference 1, the reactor calculations, are expected to introduce another 6.5% of error into the estimate, so the total RSD is 6.8%. These results are summarized in Table 4-2:

Table 4-2. Pu Production Estimates and Errors

		Pu Estimate (MT)	Random Errors SD(Est) RSD	Systematic Errors RSD	Total RSD
Weighted Regression	Generic Reactor	3.633	0.076 2%	6.5%	6.8%
	Traws II	3.633	0.0776 2%	4.8%	5.2%
Ordinary Least Squares	Generic Reactor	3.288	0.061 2%	6.5%	6.8%*

*Note this RSD does not account for the bias in OLS.

Table 4-2 also indicates the impact on the systematic errors, due to reactor calculations, of increasing knowledge about the sampled reactor. The systematic errors for a generic reactor, about which little is known, is approximately 6.5% whereas the detailed knowledge about Traws II reduced the systematic error to 4.8%. The cumulative Pu production from Traws II is estimated as 3.633 metric tons with a relative standard deviation of 5.2%. Therefore, the best estimate for pre-production in Traws II is 3.633 MT ± 10.4%.[1] The ordinary least squares results presented in Table 4-2 are presented to allow a comparison to the weighted results. As can be seen, the OLS produces a result that is about 1.5 times the standard deviation below the preferred answer.

[1](± 2 σ bound)

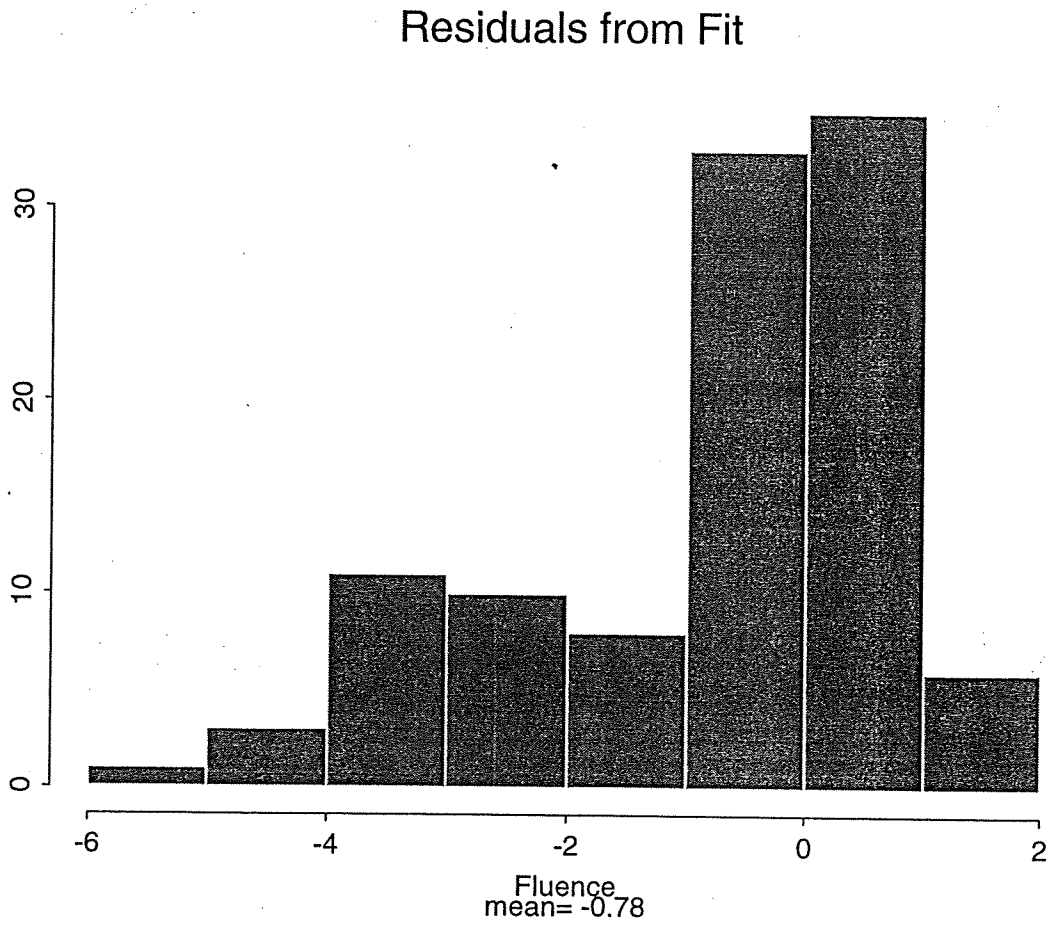

Figure 4.6. Residual Plots

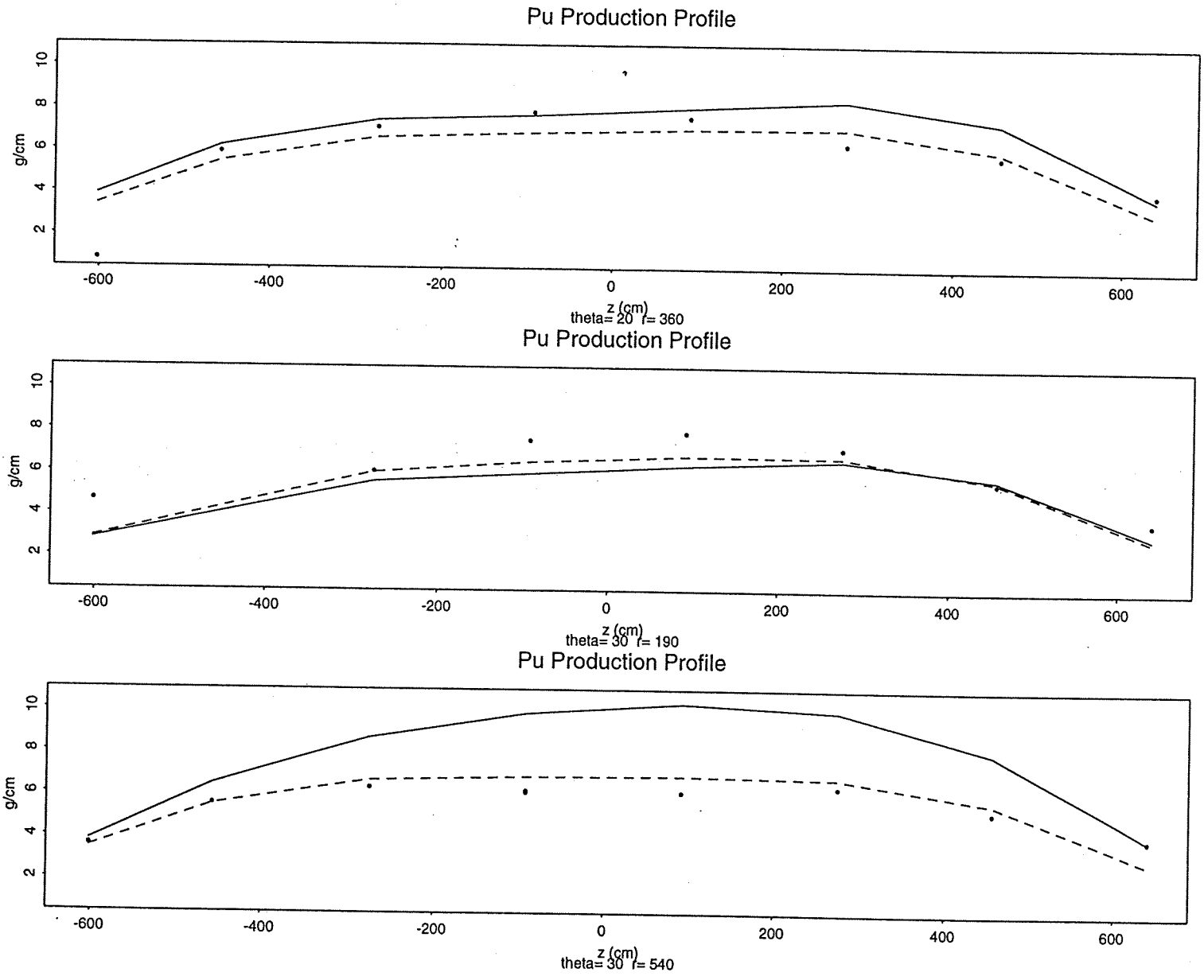

Figure 4.7. Residual Plots

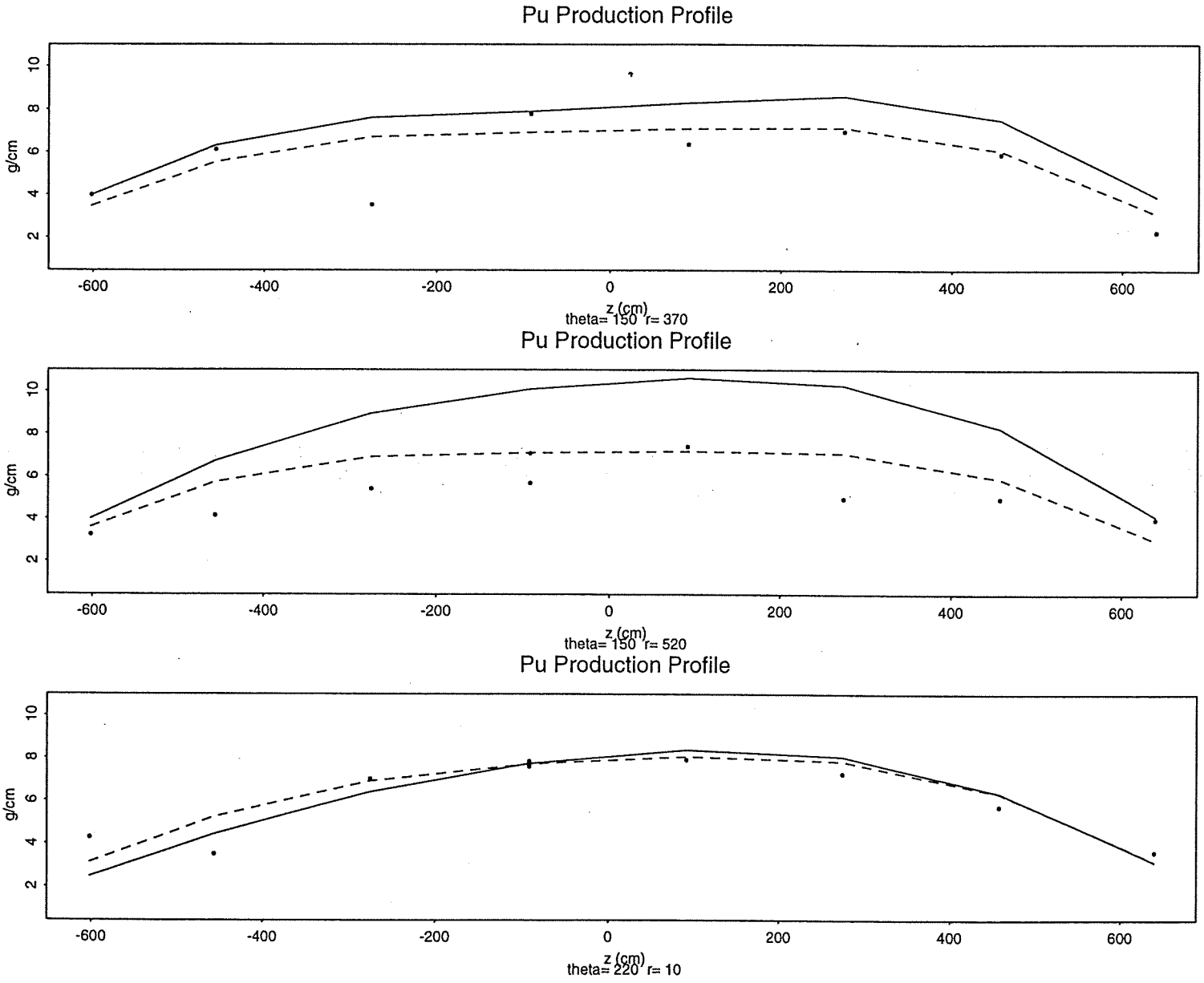

Figure 4.8. Residual Plots

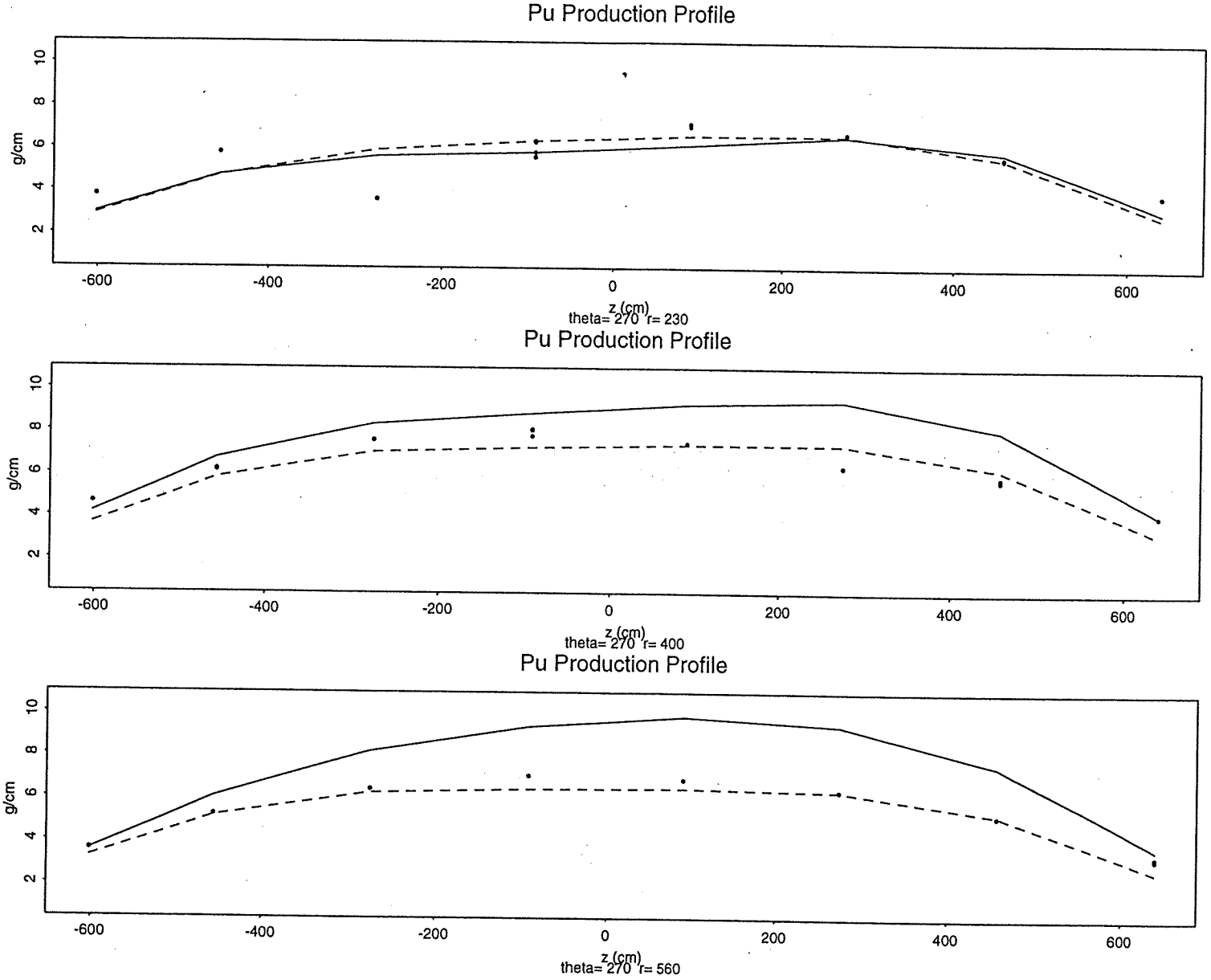

Figure 4.9. Residual Plots

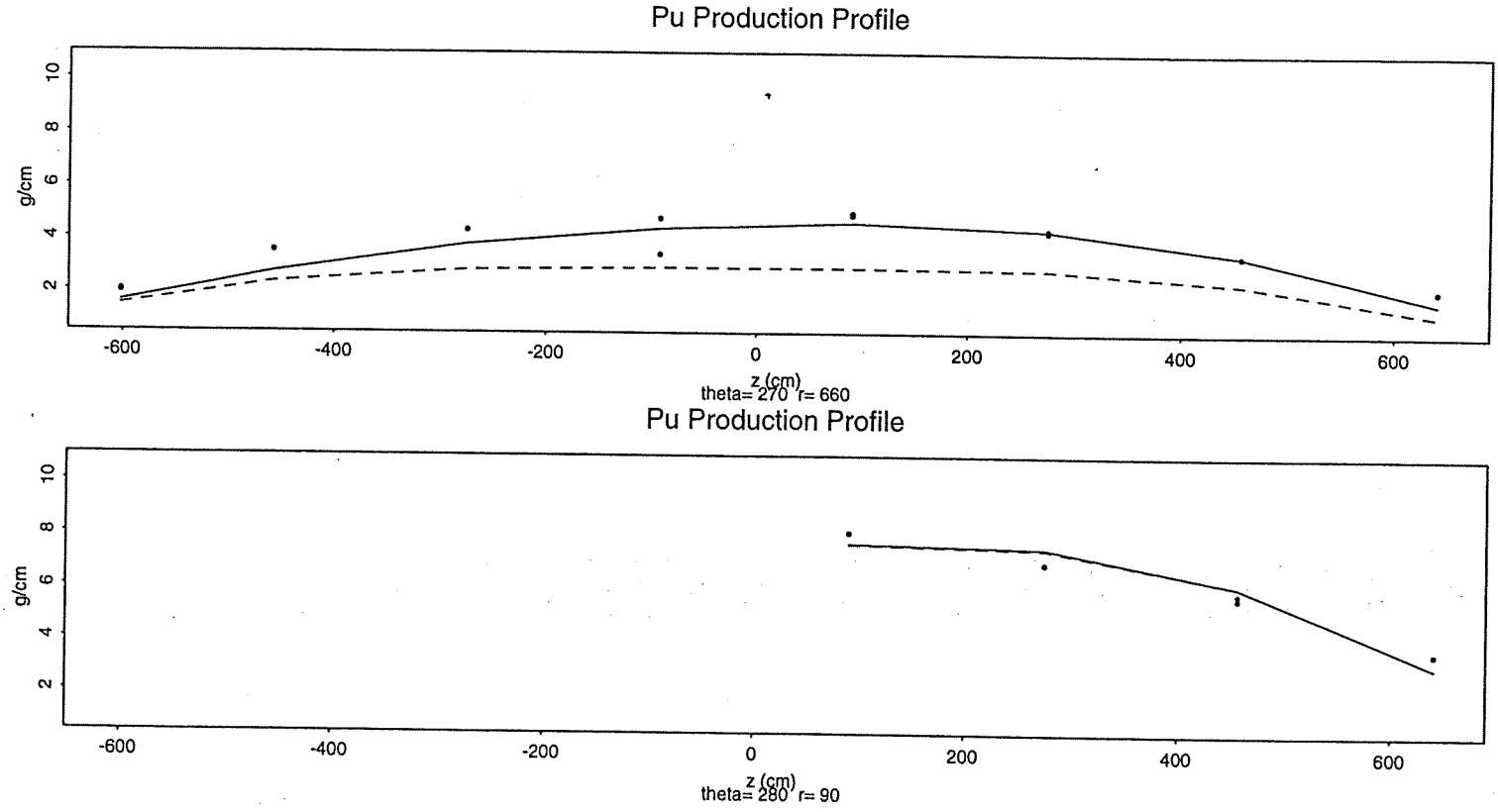

Figure 4.10. Residual Plots

References:

1. Talbert, R.J., B.D. Reid; et. al. 1995. Girm Accuracy Calculations , PNL-RTC-0693, Rev 1, Pacific Northwest Laboratory, Richland, Washington.

2. Wickham, A..J. 1995. Graphite Trepanning from Trawsfynydd Reactor 2 and Associated Activities in Support of USDOE/PNL Nuclear Archeology Programme, ED/EXT/REP/0019/95, Issue 1, August 1995.

3. Birck, J.L., and C.J. Allegre. 1984. Chromium Isotopic Anomalies in Allende Refractory Inclusions, Geophys. Res. Letts. 11, 943-946.

4. Nieder, F.R., D.A. Papanastassiou, and G.J. Wasserburg. 1980. Endemic Isotopic Anomalies in Titanium, Astrophys. J. 240, L73-L77.

5. Niemeyer, S., and G.W. Lugmair. 1981. Ubiquitous Isotopic Anomalies in Ti From Normal Allende Inclusions, Earth Planet. Sci. Letts. 53, 211-225.

6. Papanastassiou, D.A. 1986. Cr isotopic Anomalies in the Allende Meteorite, Astrophys. J. Lett. 308, L27-L30.

7. Patchett, P.J., and M. Tatsumoto. 1980. A Routine High-Precision Method for Lu-Hf Isotope Geochemistry and Geochronology, Contrib. Min. Petr. 75, 263-268.

8. Askew, J. R., and M. J. Roth. 1982. WIMS-E, A Schemefor Neutronics Calculations. AEEW-R 1315, Winfrith, United Kingdom Atomic Energy Authority, Dorchester, England.

9. Huber, P.J. 1981. Robust Statistics, Wiley, New York..